Motion of charged particles in ABC magnetic fields

Alejandro Luque*
Departament de Matemàtica Aplicada i Anàlisi
Universitat de Barcelona
08007 Barcelona (Spain)

Daniel Peralta-Salas†
Instituto de Ciencias Matemáticas
Consejo Superior de Investigaciones Científicas
28049 Madrid (Spain)

April 1, 2013

Abstract

In this paper we study the motion of a charged particle under the action of ABC magnetic fields. In particular, we analyze bifurcation diagrams and stability of the equilibrium points, existence of periodic and quasi-periodic trajectories near these equilibria, analytic integrability and existence of chaotic invariant sets. Our approach makes use of diverse tools from the theory of Hamiltonian systems, like Birkhoff normal form, KAM theory, Morales-Ramis theory and splitting of separatrices. Two interesting consequences of our study are the existence of confinement regions of charges near some magnetic lines and that ABC fields give rise to non integrable and chaotic motions. The analysis of the motion of a charge in ABC fields can be interpreted as a toy model for the motion of plasma charged particles in a tokamak, thus showing the potential interest of this work in applications.

Keywords: Newton-Lorentz equation, magnetic field, Hamiltonian dynamical system, elliptic equilibrium point, quasi-periodic solution, analytic integrability, Melnikov potential.

*luque@maia.ub.es
†dperalta@icmat.es

Contents

1 Introduction

The study of the motion of charged particles in magnetic fields has a long tradition in several areas of physics, such as condensed matter theory [17], accelerator physics [32], magnetobiology [20] and plasma physics [37]. The equation of motion of a (non-relativistic) unit-mass, unit-charge particle at the position $q \in \mathbb{R}^3$ in the presence of a magnetic field $\mathbf{B}$ is given by the Newton-Lorentz law:

$$\ddot{q} = \dot{q} \wedge \mathbf{B}(q)\,, \tag{1}$$

where the dot over q denotes, as usual, the time derivative, and $\wedge$ stands for the standard vector product in $\mathbb{R}^3$. In general, these equations cannot be integrated analytically and the trajectories are very complicated and have nothing to do with the magnetic lines, so it is usual to consider adiabatic approximations like the guiding centre [34, 46]. However, if we want to obtain global results (for all time) or the field is far from being uniform, this approximation is of little help, as illustrated with some planar examples in [47].

In spite of the importance of the previously mentioned contexts, there are not many rigorous results on the motion of charges in concrete magnetic fields. Of course, trajectories can be obtained explicitly in the special case of a uniform field [24], but this situation is rather exceptional. Even in the case of perturbations of uniform magnetic fields it is very hard to prove the existence of helicoidal trajectories, which has only been achieved for some particular cases [6]. An important property of the Newton-Lorentz equation (1) is that it can be written equivalently in a Hamiltonian way whenever there is a globally defined vector potential $\mathbf{A}$ such that $\mathbf{B} = \operatorname{curl} \mathbf{A}$. If this is the case, the Hamiltonian function is

$$H(q,p) := \frac{1}{2}(p - \mathbf{A}(q))^2 .$$

This Hamiltonian nature of the equations of motion allows us to apply modern techniques from Hamiltonian systems. This approach was pioneered by Braun [5], and further developed in [7, 45], to prove the existence of quasi-periodic trajectories and confinement regions in magnetic fields with rotational symmetry. These results were applied to analyze the motion of charges in the magnetic field created by a dipole, the so-called *Störmer problem*, which is a toy model to describe the dynamics of charged particles in the Earth magnetosphere. Recently, a more realistic description of the motion of a charged particle around a rotating magnetic planet (the generalized Störmer problem) has been presented in [23]. On the other hand, an extensive rigorous study of the motion of a charge in the presence of magnetic fields created by current filaments can be found in [1]. In this reference, the authors proposed a magnetic trap using a circular wire and illustrated that chaotic motions can arise for integrable magnetic fields, even though analytic justification was not given but just numerical evidence. We would also like to mention the works [35, 36], which introduce a wide set of techniques from Hamiltonian systems to study the interaction of two charges in the presence of a constant magnetic field.

In this paper we are interested in the motion of charges in ABC magnetic fields. These fields arise in the theory of magnetic dynamos (see [18] and references therein) and were introduced independently by Arnold [3] and Childress [11] in the 1960's. The well-known family of *ABC magnetic fields* depends on three real parameters, A, B and C, and reads in Cartesian coordinates $q = (x, y, z)$ as

$$\mathbf{B}_{ABC} = (A \sin z + C \cos y, B \sin x + A \cos z, C \sin y + B \cos x) .$$

ABC magnetic fields are steady solutions of the magnetohydrodynamics equations of force-free type, that is $\operatorname{curl} \mathbf{B_{ABC}}$ is collinear with $\mathbf{B_{ABC}}$ at any point, thus implying that the field exerts no force on the current distribution generating it. Force free fields are very important in applications and model diverse physical systems, as stellar atmospheres [8], the solar corona [15] and relaxed states of toroidal plasmas [43, 44]. Most of the literature on ABC magnetic fields is focused on the study of the qualitative properties of their magnetic lines: non integrability using Ziglin theory [50, 51] and differential Galois theory [31], chaos through splitting of separatrices [9, 22], and existence of hyperbolic closed lines [9]. In spite of its relevance in plasma physics, we are not aware of any rigorous study of the motion of charged particles in ABC magnetic fields, even though the motion of a charge in simple force-free fields has been analyzed in [47, 48, 49]. These works exploit the fact that the motion is integrable, a property that is not shared by general ABC fields.

Our goal in this paper is to study in detail several aspects of these equations of motion, such as the existence of stable equilibria, quasi-periodic trajectories, analytic first integrals and chaotic invariant sets, thus filling an important gap in the literature. This study has a double interest. On the one hand the analysis of the motion of a charge in ABC fields can be interpreted as a toy model for the motion of plasma charged particles in a tokamak. On the other hand it is an excellent framework, not constructed ad hoc but modeling a physical system, where many tools from dynamical systems can be applied, e.g. bifurcation theory, normal forms, KAM theory, Morales-Ramis theory, splitting of separatrices, etc.

The contents of this paper are organized as follows. In Section 2 we introduce the equations of motion of a charge under the action of an ABC magnetic field and show how these equations can be reduced to a 2 degrees of freedom Hamiltonian system when $C = 0$ (this is the so-called laminar ABC dynamo). Since we use a fairly wide set of techniques and tools, we also include a summary of results in this section. The dynamics near a degenerate curve of equilibrium points of the reduced system is studied in Section 3.1. In particular we show the existence of quasi-periodic trajectories in a neighborhood of the curve using a suitable set of coordinates that allows us to apply Moser's twist theorem. The isolated equilibria are considered in Section 3.2. Concretely, we analyze the linear stability and bifurcation diagrams in terms of the parameter B (cf. Section 3.2.1), we compute the stable, center and unstable manifolds near the equilibria using semi analytic methods (cf. Section 3.2.2) and we prove the existence of quasi-periodic trajectories in a neighborhood of the equilibria by computing the Birkhoff normal form up to fourth order (cf. Section 3.2.3). In Section 4 we study non integrability and chaos of the motion in ABC magnetic fields. Concretely, in Section 4.1 we show, using Morales-Ramis theory, that there does not exist an additional analytic first integral for a particular set of parameters and in Section 4.2 we prove that the dynamics is chaotic for small enough values of B and C through splitting of separatrices. Finally, in Section 5 we summarize the main contributions of this work and comment on some interesting open problems. For the sake of completeness, and due to the fact that probably it is not well known to most of the readers, we have included two appendixes with concise explanations of the Taylor method for the integration of vector fields (Appendix A) and the symbolic manipulation of multivariate power series and automatic differentiation (Appendix B).

2 Equations of motion and summary of results

As explained in Section 1, the family of ABC magnetic fields depends on three real parameters, A, B and C, and reads in Cartesian coordinates $q = (x, y, z)$ as

$$\mathbf{B}_{ABC} = (A \sin z + C \cos y, B \sin x + A \cos z, C \sin y + B \cos x) .$$

It is straightforward to check that $\mathbf{B}_{ABC}$ is divergence-free and force-free because $\operatorname{curl} \mathbf{B}_{ABC} = \mathbf{B}_{ABC}$, and so the ABC field admits the globally defined vector potential $\mathbf{A}_{ABC} = \mathbf{B}_{ABC}$. Since the dependence of the ABC magnetic field and its vector potential with the variables

x, y, z is 2π-periodic, it is customary to consider that these fields are defined in the 3-torus $\mathbb{T}^3 = \mathbb{R}^3/(2\pi\mathbb{Z})^3$ so that $(x, y, z) \in \mathbb{T}^3$. Notice that, after an appropriate rescaling, there is no loss of generality in taking $A = 1 \geq B \geq C \geq 0$ (see e.g. [10, Section 6.3.2]), so we shall assume it in what follows.

The Newton-Lorentz equation of motion (1) for the ABC magnetic field can be described as a 3DOF Hamiltonian system defined in the phase space $\mathbb{T}^3 \times \mathbb{R}^3 \ni (x, y, z, p_x, p_y, p_z)$ by the Hamiltonian function:

$$H = \frac{1}{2}(p_x - C\cos y - \sin z)^2 + \frac{1}{2}(p_y - B\sin x - \cos z)^2 + \frac{1}{2}(p_z - B\cos x - C\sin y)^2 . \quad (2)$$

For the sake of future reference let us write the associated system of ODEs:

$$\begin{aligned}
\dot{x} &= p_x - \sin z - C\cos y\,, \\
\dot{y} &= p_y - B\sin x - \cos z\,, \\
\dot{z} &= p_z - C\sin y - B\cos x\,, \\
\dot{p}_x &= (p_y - \cos z)B\cos x - (p_z - C\sin y)B\sin x\,, \\
\dot{p}_y &= (p_z - B\cos x)C\cos y - (p_x - \sin z)C\sin y\,, \\
\dot{p}_z &= (p_x - C\cos y)\cos z - (p_y - B\sin x)\sin z\,.
\end{aligned} \quad (3)$$

The set of equilibria (or critical points) of system (3) consists in a 3-dimensional submanifold

$$\mathcal{N} := \{(q, p) \in \mathbb{T}^3 \times \mathbb{R}^3 : p = \mathbf{A}_{ABC}(q)\} \quad (4)$$

that is diffeomorphic to $\mathbb{T}^3$, and which corresponds to initial conditions with zero velocity. The submanifold $\mathcal{N}$ is the global minimum of the Hamiltonian H, cf. Eq. (2), and it is easy to check that the level sets of H near this set are diffeomorphic to $\mathbb{T}^3 \times \mathbb{S}^2$. This is a very degenerate scenario in which the study of the stability of equilibria is a very difficult task and requires to consider a problem of singular perturbation. As we explain next, in this work we analyze the local behavior of the dynamics near $\mathcal{N}$ in a particular case.

A specially significant situation is when $C = 0$. This is the so-called laminar ABC dynamo [42], where the ABC magnetic field does not depend on the y direction:

$$\mathbf{B}_{ABC} = (\sin z, B\sin x + \cos z, B\cos x)\,.$$

An elementary computation shows that $F(x, z) := B\sin x + \cos z$ is a first integral of $\mathbf{B}_{ABC}$. The regular level sets $F^{-1}(c)$ are magnetic surfaces diffeomorphic to 2-dimensional tori that support periodic or quasi-periodic magnetic lines depending on the value of c. The magnetic field is hence completely integrable. The equations of the motion in (3) can be reduced to a 2DOF Hamiltonian system, after noticing that p_y is a first integral and fixing its value to $p_y = L$, to yield

$$H(x, z, p_x, p_z) = \frac{1}{2}(p_x - \sin z)^2 + \frac{1}{2}(p_z - B\cos x)^2 + V(x, z)\,, \quad (5)$$

where the effective potential $V(x,z)$ is defined as

$$V(x,z) := \frac{1}{2}(L - B\sin x - \cos z)^2\,, \tag{6}$$

with $(x,z,p_x,p_z) \in \mathbb{T}^2 \times \mathbb{R}^2$. This Hamiltonian function depends on two parameters $0 \le B \le 1$ and $L \in \mathbb{R}$, and in fact there is no loss of generality in assuming that $L \ge 0$ (otherwise we make the change of variables $t \to -t$, $x \to -x$ and $z \to \pi - z$). The motion in the configuration space $\mathbb{T}^3$ is obtained from the solutions $(x(t), z(t))$ of the Hamiltonian system defined by Eqs. (5) and (6) by integrating the following first order ODE

$$\dot{y} = L - B\sin x - \cos z\,,$$

with $y \in \mathbb{S}^1$. The equations of motion in the phase space $(x,z,p_x,p_z) \in \mathbb{T}^2 \times \mathbb{R}^2$ read as:

$$\begin{aligned} \dot{x} &= p_x - \sin z\,,\\ \dot{z} &= p_z - B\cos x\,,\\ \dot{p}_x &= (L - \cos z)B\cos x - Bp_z\sin x\,,\\ \dot{p}_z &= -(L - B\sin x)\sin z + p_x\cos z\,. \end{aligned} \tag{7}$$

In what follows we shall denote by X_H the vector field defined by Eq. (7). Let us compute the equilibrium points of this system, i.e. the critical points of X_H. An easy computation shows that there are four isolated equilibrium points and a set of degenerate equilibria. Indeed, the isolated points P_i with their corresponding energies $H_i := H(P_i)$ are:

$$\begin{aligned} P_1 &= \big(\frac{\pi}{2}, 0, 0, 0\big)\,, & H_1 &= \frac{1}{2}(L - B - 1)^2\,,\\ P_2 &= \big(\frac{\pi}{2}, \pi, 0, 0\big)\,, & H_2 &= \frac{1}{2}(L - B + 1)^2\,,\\ P_3 &= \big(\frac{3\pi}{2}, 0, 0, 0\big)\,, & H_3 &= \frac{1}{2}(L + B - 1)^2\,,\\ P_4 &= \big(\frac{3\pi}{2}, \pi, 0, 0\big)\,, & H_4 &= \frac{1}{2}(L + B + 1)^2\,. \end{aligned}$$

Note that the energies H_i are different for generic values of the parameters B and L. The motion in the full configuration space $\mathbb{T}^3$ that corresponds to these isolated equilibria P_i is given by the ODE $\dot{y} = \pm\sqrt{2H_i}$ (the sign is determined by the sign of the function $L - B\sin x - \cos z$ at the point P_i), indicating that the charge moves uniformly along the closed magnetic lines $(\pi/2, y, 0)$, $(\pi/2, y, \pi)$, $(3\pi/2, y, 0)$ and $(3\pi/2, y, \pi)$, respectively, and hence they are periodic trajectories in the non-reduced system. We observe that when $B = 1$ the closed curves $(\pi/2, y, \pi)$ and $(3\pi/2, y, 0)$ in $\mathbb{T}^3$ are vanishing points of the magnetic field.

Moreover, for any value of L satisfying $L < B + 1$ there is a 1-dimensional set of critical points which is given by:

$$\Gamma_L := \{(x,z,p_x,p_z) \in \mathbb{T}^2 \times \mathbb{R}^2 :\ L - B\sin x - \cos z = 0, p_x = \sin z, p_z = B\cos x\}\,. \tag{8}$$

Actually, this set degenerates to the point P_1 if $L = B + 1$. The energy of this set is clearly $H(\Gamma_L) = 0$. It is elementary to check that Γ is a smooth curve (possibly disconnected) for all values of B and L except for $L = -B + 1$, which is a self-intersecting curve associated to the separatrix of the saddle point $(\frac{3\pi}{2}, 0)$ of the function $B \sin x + \cos z$ in $\mathbb{T}^2$. Notice also that the set Γ_L corresponds to a set of equilibria in the full configuration space $\mathbb{T}^3$ (since $\dot{y} = 0$ on Γ_L), so obviously we have the identity of sets

$$\mathcal{N} \cap \{p_y = L\} = \Gamma_L \times \mathbb{S}^1$$

in the phase space $\mathbb{T}^3 \times \mathbb{R}^3$, where the inclusion of Γ_L in $\mathbb{T}^3 \times \mathbb{R}^3$ is done in the natural way, i.e. by identifying $\mathbb{T}^2 \times \mathbb{R}^2$ with $\{y = 0, p_y = L\} \subset \mathbb{T}^3 \times \mathbb{R}^3$, and $\mathcal{N}$ is the manifold introduced in Eq. (4).

We shall see in Section 3.1 that we can prove the existence of certain families of quasi-periodic solutions close to $\Gamma_L = H^{-1}(0)$ assuming that L is small. Concretely, we obtain the following result (the statement will be more precise in Theorem 3.2)

Theorem 2.1. *Given a value of* $0 < B < 1$*, we assume that the parameter* L *satisfies* $L = \mathcal{O}(\varepsilon)$*,* $L < 2B$ *and* $L < 1 - B$*. Then, if* ε *is sufficiently small, the set* Γ_L *consists of two smooth closed curves, and there are two points on each curve such that there exist quasi-periodic solutions (2-dimensional invariant tori) for the reduced Hamiltonian* (7) *in an* ε*-neighborhood of each point.*

The four stable points of Theorem 2.1 correspond to the local minima of the modulus $|\mathbf{B}_{ABC}|$ on Γ_L. For this reason, the regions of invariant tori can be interpreted as magnetic bottles, since the motion takes place around local minima of the magnetic field strength. Along the proof of Theorem 2.1, which is modeled upon ideas pioneered by Braun [1, 5], we introduce suitable scalings and transformations so that the problem is reduced to a vector field that is Hamiltonian with respect to a symplectic form which is a perturbation of the canonical one. The assumption $L = \mathcal{O}(\varepsilon)$ allows us to express the equations of motion as a perturbation of an integrable Hamiltonian that consists in a rotation and a pendulum. We will discuss how this construction provides additional information of the dynamics that could be useful to characterize other kinds of motions near the set of equilibria Γ_L.

To complete the local study of the equilibrium solutions of the reduced system, we consider the local analysis of the isolated equilibria P_i. In Section 3.2 we study their linear stability and we use semi-analytical methods to characterize the dynamics close to them. Although our main interest is to characterize the elliptic region of the point P_1, in this section we present computations of local invariant manifolds and normal forms in a wide set of cases (we follow [21]). With such computations we aim to illustrate that the implementation can be performed with a significant generality, since all cases are studied with the same algorithm. We also expect that the presented computations inspire questions and dynamical mechanisms to applied and experimental researchers. From the analytical viewpoint we prove in Section 3.2 (using classical results, e.g. [12, 38]) the following:

Theorem 2.2. *Let us consider* $0 < B \leq 1$ *and the set*

$$\mathcal{L}(B) := \left\{ L > \frac{2(1+B)(\sqrt[4]{B} - \sqrt[4]{B^3})^2}{(1-B)^2}, L \neq B+1 \right\}.$$

Then, the equilibrium point P_1 *is elliptic for any value of* $L \in \mathcal{L}(B)$ *and there is an open and dense set (to be specified) of values of* L *in* $\bigcup_{0<B\leq 1} \mathcal{L}(B)$ *for which* P_1 *is Lyapunov stable and there exists a large Cantor set of quasi-periodic trajectories in any small neighborhood of this point.*

From a different point of view, in Section 4 we illustrate the complexity of the dynamics of charges under ABC magnetic fields. On the one hand, we use Morales-Ramis theory [33] to prove the non-existence of an additional first integral in a particular case where the magnetic field is integrable. In section 4.1 we present the next result:

Theorem 2.3. *Assume that* $B = 1$, $C = 0$ *and* $L = 0$. *Then, the reduced Hamiltonian system* (5)-(7) *does not admit an additional first integral* $F : \mathbb{T}^2 \times \mathbb{R}^2 \to \mathbb{R}$ *which is a rational function in the variables* $\sin x, \cos x, \sin z, \cos z, p_x$ *and* p_z*.*

On the other hand, in Section 4.2 we consider a pertubation of a very simple case, where we prove the existence of splitting of separatrices of invariant tori. For $B = C = 0$, the ABC magnetic field has the simple expression

$$\mathbf{B}_{ABC} = (\sin z, \cos z, 0)\,,$$

which implies that the field is linear on each toroidal surface $z = z_0$, periodic or quasi-periodic depending on the value of $\tan z_0$. Concerning the equations of motion, the Hamiltonian function in Eq. (2) does not depend on x nor on y, so it follows that the equations are Liouville integrable with first integrals p_x, p_y and H. Moreover, it is not difficult to see that there is a family of invariant tori having homoclinic connections. If we consider a small perturbation $B = \mathcal{O}(\varepsilon)$ and $C = \mathcal{O}(\varepsilon)$, then we prove that most of these invariant tori persist (we denote them as $\mathcal{T}^{\varepsilon}_{p_x,p_y}$) and that their stable and unstable invariant manifolds intersect transversally. In particular, we establish the following result:

Theorem 2.4. *The Melnikov potential* $L : \mathbb{T}^2 \to \mathbb{R}$ *associated to the invariant torus* $\mathcal{T}^{\varepsilon}_{p_x,p_y}$ *of Eq.* (3) *for* $B = \mathcal{O}(\varepsilon)$ *and* $C = \mathcal{O}(\varepsilon)$ *is given by*

$$L(x, y) = L_1 \cos(x) + L_2 \sin(x) + L_3 \cos(y) + L_4 \sin(y),$$

where L_i *are constants that depend on* p_x *and* p_y*, and that do not vanish simultaneously for most values of these parameters.*

The non-degenerate critical points of the Melnikov potential $L(x, y)$ give rise to transverse homoclinic intersections between the perturbed whiskers of the torus $\mathcal{T}^{\varepsilon}_{p_x,p_y}$ provided that ε is small enough. From this result we conclude the existence of transverse intersections and hence chaos in the Hamiltonian system (2). To prove Theorem 2.4, we cannot directly apply the Melnikov potential in [13] since the unperturbed Hamiltonian H_0 is not of the form studied in this reference. Hence, we combine a hyperbolic KAM theorem proved in [16] with a variation of the construction of the Melnikov potential given in [13]. Notice that, for $C = 0$, the invariant tori obtained in Theorem 2.4 are far away from the equilibrium sets considered in Theorems 2.1 and 2.2, so they can be seen as the skeleton to construct more global solutions.

As far as we know, Theorems 2.3 and 2.4 are the first rigorous results on the complexity (non-integrability and chaos) of the motion of charges in magnetic fields, even though physicists have been aware of these phenomena for a long time [32, 34].

3 Local study of the reduced Hamiltonian

In this section we study the stability of the equilibrium points (both degenerate and non-degenerate) of the reduced Hamiltonian system (5)-(6) describing the motion of a charged particle in the presence of an ABC magnetic field with $C = 0$ (the so-called laminar ABC dynamo).

Section 3.1 is focused on the study of the stability of the set Γ_L of degenerate equilibria, concretely we show the existence of periodic and quasi-periodic trajectories in a neighborhood of Γ_L. In Section 3.2 we study in detail the local stability of the isolated equilibrium points P_i. In particular we analyze the bifurcation diagrams in terms of the parameters B and L and compute invariant manifolds and normal forms by means of the parametrization method combined with automatic differentiation.

We eventually present numerical simulations to illustrate the phenomena observed and to give a more global picture of the dynamics. A standard approach for monitoring the dynamics of a 2DOF Hamiltonian system is to compute a Poincaré section. Given a fixed value of $L \geq 0$ we consider a Poincaré section $\Sigma = \Sigma(L, H_0)$ defined by a hyperplane of the form $\{z = c\}$ restricted to a given energy level $H = H_0$, which we parametrize by means of (x, p_x). It is easy to check that, for Eq. (7), every Poincaré section of the form $\{z = c\}$, with $c \in [0, 2\pi]$, has a boundary of definition given by the implicit curve

$$\frac{1}{2}(p_x - \sin c)^2 + \frac{1}{2}(L - B\sin x - \cos c)^2 = H_0\,.$$

Unless otherwise indicated, we integrate the vector field using a Taylor method of order 20 (see Appendix A) asking for a local tolerance of 10^{-16} in the integration and 10^{-13} in the computation of the Poincaré section.

3.1 KAM tori near the degenerate set of minima

Our aim in this section is to study the local dynamics of the solutions to Eq. (7) in a neighborhood of the set of equilibrium points Γ_L. We shall assume the necessary and sufficient conditions $L < B+1$ and $L \neq 1-B$ for this set to be smooth (but possibly disconnected). Following ideas introduced by Braun [1, 5], combined with the use of twisted symplectic forms, we prove the existence of periodic and quasi-periodic solutions near Γ_L, provided that L is small. This assumption is key, as it allows us to reduce the problem to a perturbation of a 2DOF integrable Hamiltonian system with one small frequency, in such a way that Moser's twist theorem can be applied to a suitably defined Poincaré section.

Recall that the set Γ_L is a global minimum of the Hamiltonian H, cf. Eq. (5), and therefore the level sets of H near Γ_L are compact manifolds, which are diffeomorphic to two copies of $\mathbb{S}^1 \times \mathbb{S}^2$ provided that L is small enough. Accordingly, the set of equilibria Γ_L is Lyapunov stable (although each equilibrium point does not need to be stable) and the motion is confined within a neighborhood of Γ_L. In the following theorem we prove that, if L is small, there are quasi-periodic trajectories around some particular points of Γ_L. At the end of the section we shall give a heuristic description of other kinds of motions around Γ_L, which will be illustrated by some numerical computations.

Remark 3.1. *When $L < 1 - B$, the set Γ_L consists of two smooth closed curves which are graphs over the variable $x \in \mathbb{S}^1$. Each curve will be denoted by Γ_L^1 (with $z \in (0, \pi)$) and Γ_L^2 (with $z \in (\pi, 2\pi)$), respectively.*

Theorem 3.2. *Given a value of $0 < B < 1$, we assume that the parameter L satisfies $L = \mathcal{O}(\varepsilon)$, $L < 2B$ and $L < 1 - B$. For each $i \in \{1, 2\}$ and $\psi \in (0, \frac{\pi}{2})$, we define two regions of the form*

$$U_\varepsilon^i(\psi) := \{q = (x, z, p_x, p_z) \in \mathbb{T}^2 \times \mathbb{R}^2 : \mathrm{dist}\,(q, \Gamma_L^i) < \varepsilon,\, x \in (\frac{\pi}{2} - \psi, \frac{\pi}{2} + \psi)\}\,,$$
$$V_\varepsilon^i(\psi) := \{q = (x, z, p_x, p_z) \in \mathbb{T}^2 \times \mathbb{R}^2 : \mathrm{dist}\,(q, \Gamma_L^i) < \varepsilon,\, x \in (\frac{3\pi}{2} - \psi, \frac{3\pi}{2} + \psi)\}\,.$$

Then, for sufficiently small ε, the reduced Hamiltonian system (7) *has infinitely many periodic and quasi-periodic trajectories contained in $U_\varepsilon^i(\psi)$ and $V_\varepsilon^i(\psi)$ for each $\psi \in \Psi \subset (0, \frac{\pi}{2} - \arcsin(\frac{L}{2B}))$, at any energy level (the meaning of the subset Ψ will be clear from the proof, see the paragraph just after Lemma 3.3). In particular, they do not follow the curves Γ_L^i. Moreover, some of the quasi-periodic trajectories lying in $U_\varepsilon^i(\psi)$ (resp. in $V_\varepsilon^i(\psi)$) have a component $x(t)$ such that $\sup_{t\in\mathbb{R}} |x(t) - \frac{\pi}{2}| \approx \psi$ (resp. $\sup_{t\in\mathbb{R}} |x(t) - \frac{3\pi}{2}| \approx \psi$).*

The main difficulty to prove Theorem 3.2 is the presence of a reduced magnetic field (orthogonal to the $x - z$ plane) whose vector potential is $\mathbf{A} = (\sin z, B \cos x)$. The presence of this magnetic term prevents from using Braun's approach directly [5], and suggests introducing the change of variables

$$x \mapsto x\,, \qquad z \mapsto z\,, \qquad p_x - \sin z \mapsto p_x\,, \qquad p_z - B\cos x \mapsto p_z\,,$$

into Eq. (7). We obtain a new vector field which is no longer Hamiltonian with respect to the canonical symplectic form, but it is Hamiltonian with respect to the twisted symplectic form

$$\Omega := dx \wedge dp_x + dz \wedge dp_z + (B \sin x + \cos z) dx \wedge dz \,, \tag{9}$$

with associated Hamiltonian function

$$H = \frac{1}{2}(p_x^2 + p_z^2) + \frac{1}{2}(L - B \sin x - \cos z)^2 \,.$$

Accordingly, we have removed the magnetic term from the Hamiltonian by changing the symplectic form. Let us see that this approach is very convenient to prove the existence of quasi-periodic trajectories.

To this end, setting $I(x, z) := B \sin x + \cos z$, we consider an analytic function $F : U \to \mathbb{S}^1$ which is orthogonal to I, i.e. $\nabla F \cdot \nabla I = 0$, in a tubular neighborhood U of the set $\{I(x, z) = L\} \subset \mathbb{T}^2$. Assuming that $L < 1 - B$, this set consists of two smooth closed curves, which are the projections of Γ_L^i onto $\mathbb{T}^2$. We shall restrict ourselves to one connected component in what follows. The existence of F is obvious, and even though the explicit computation of F is not important in the construction, we can take

$$F(x, z) = \Big(\tan x + \frac{1}{\cos x}\Big)\Big(\tan\Big(\frac{z}{2}\Big)\Big)^B \,.$$

Now we introduce a coordinate system $(x, z, p_x, p_z) \mapsto (X, Y, p_X, p_Y)$ mapping $U \times \mathbb{R}^2$ onto $\mathbb{S}^1 \times (L - \delta, L + \delta) \times \mathbb{R}^2$, defined as

$$\begin{aligned}
X &= F(x, z) \,, \\
Y &= I(x, z) \,, \\
p_x &= \partial_x F(x, z) p_X + \partial_x I(x, z) p_Y \,, \\
p_z &= \partial_z F(x, z) p_X + \partial_z I(x, z) p_Y \,.
\end{aligned}$$

In these coordinates, the curve of equilibria Γ_L^i is given by $\mathbb{S}^1 \times \{L\} \times \{(0, 0)\}$ and the new Hamiltonian is

$$\tilde{H}(X, Y, p_X, p_Y) = \frac{1}{2}(h_F(X, Y) p_X^2 + h_I(X, Y) p_Y^2) + \frac{1}{2}(L - Y)^2 \,,$$

with $h_F(X, Y) := (\nabla F)^2(X, Y)$ and $h_I(X, Y) := (\nabla I)^2(X, Y)$. Observe that this diffeomorphism does not preserve the symplectic form (9), which in the new coordinates reads as

$$\tilde{\Omega} = dX \wedge dp_X + dY \wedge dp_Y + \frac{Y}{G} dX \wedge dY \,, \qquad G := \left| \frac{\partial(I, F)}{\partial(x, z)} \right| \,.$$

To study the dynamics of this system in a neighborhood of the curve of equilibria Γ_L^i we introduce the scaled variables (q_1, q_2, p_1, p_2) using a small parameter $\varepsilon > 0$ as

$$\begin{aligned} X &= \varepsilon q_1 \,, \\ L - Y &= \varepsilon q_2 \,, \\ p_X &= \varepsilon p_1 \,, \\ p_Y &= \varepsilon p_2 \,, \end{aligned}$$

which, after multiplying the energy by a factor ε^{-2}, gives rise to the new Hamiltonian

$$H_\varepsilon(q_1, q_2, p_1, p_2) = \frac{1}{2} a(\varepsilon q_1) p_1^2 + \frac{1}{2} b(\varepsilon q_1) p_2^2 + \frac{1}{2} q_2^2 + \varepsilon g(q_1, q_2, p_1, p_2; \varepsilon) \tag{10}$$

and the new symplectic form

$$\Omega_\varepsilon = dq_1 \wedge dp_1 + dq_2 \wedge dp_2 + \frac{\varepsilon q_2 - L}{G(\varepsilon q_1, \varepsilon q_2)} dq_1 \wedge dq_2 \,. \tag{11}$$

The functions $a(\varepsilon q_1)$ and $b(\varepsilon q_1)$ are obtained from the functions $h_F(X, Y)$ and $h_I(X, Y)$ by expanding around $Y = L$, i.e. $h_F(X, Y) = a(X) + \mathcal{O}(Y - L)$ and $h_I(X, Y) = b(X) + \mathcal{O}(Y - L)$. In the scaled variables the remaining terms are of the form $\mathcal{O}(Y - L) = \varepsilon h(q_1, q_2, p_1, p_2; \varepsilon)$, and putting all together we get the function $\varepsilon g(q_1, q_2, p_1, p_2)$.

Under the assumption that $L = \mathcal{O}(\varepsilon)$, the twisted symplectic form Ω_ε is a perturbation of the canonical symplectic form $\Omega_0 = dq_1 \wedge dp_1 + dq_2 \wedge dp_2$. Therefore, it is easy to check that the dynamics of the Hamiltonian system $(H_\varepsilon, \Omega_\varepsilon)$, cf. Eqs. (10) and (11), is equivalent to the dynamics of the Hamiltonian H_ε, with a modified εg term, with respect to the canonical symplectic form. We can now apply Braun's technique [1, 5] to the Hamiltonian system $(H_\varepsilon, \Omega_0)$ to prove the existence of quasi-periodic trajectories near the curve of equilibria.

Since the Hamiltonian H_ε is of harmonic oscillator type in the variables (q_2, p_2), up to a perturbative term εg, we can write this harmonic oscillator in a canonical form by introducing a symplectic change of variables defined by the generating function

$$S(q_1, q_2, \tilde{p}_1, \tilde{p}_2) = b(\varepsilon q_1)^{-1/4} q_2 \tilde{p}_2 + q_1 \tilde{p}_1 \,.$$

The transformed Hamiltonian is

$$\tilde{H}_\varepsilon(\tilde{q}_1, \tilde{q}_2, \tilde{p}_1, \tilde{p}_2) = \frac{1}{2} a(\varepsilon \tilde{q}_1) \tilde{p}_1^2 + \frac{1}{2} \sqrt{b(\varepsilon \tilde{q}_2)} \left(\tilde{p}_2^2 + \tilde{q}_2^2 \right) + \varepsilon \tilde{g}(\tilde{q}_1, \tilde{q}_2, \tilde{p}_1, \tilde{p}_2; \varepsilon) \,,$$

and introducing the action variable $R_2 = \frac{1}{2}(\tilde{p}_2^2 + \tilde{q}_2^2)$ associated to the harmonic oscillator, we get the Hamiltonian

$$\tilde{H}_\varepsilon(\tilde{q}_1, \theta_2, \tilde{p}_1, R_2) = \frac{1}{2} a(\varepsilon \tilde{q}_1) \tilde{p}_1^2 + \sqrt{b(\varepsilon \tilde{q}_1)} R_2 + \varepsilon \tilde{g}(\tilde{q}_1, \theta_2, \tilde{p}_1, R_2; \varepsilon) \,.$$

The Hamiltonian $\tilde{H}_\varepsilon$ without the perturbative term $\varepsilon\tilde{g}$ is clearly integrable, which suggests to apply a KAM type theorem to prove the existence of quasi-periodic trajectories near the curve of equilibria Γ_L^i (which in these variables is given by $\tilde{p}_1 = 0, R_2 = 0$). To express the coordinates $(\tilde{q}_1, \tilde{p}_1)$ in action-angle variables, it is particularly convenient to change the parametrization of time by defining a new Hamiltonian function

$$F_{\varepsilon,h}(\tilde{q}_1, \theta_2, \tilde{p}_1, R_2) := \frac{\tilde{H}_\varepsilon(\tilde{q}_1, \theta_2, \tilde{p}_1, R_2) - h}{\sqrt{b(\varepsilon\tilde{q}_1)}}\,.$$

It is obvious that the Hamiltonian vector field associated to the function $F_{\varepsilon,h}$ on the level $\{F_{\varepsilon,h} = 0\}$ is proportional to that of $\tilde{H}_\varepsilon$ on the level $\{\tilde{H}_\varepsilon = h\}$, the proportionality factor being $b(\varepsilon\tilde{q}_1)^{-1/2}$. Therefore, we can study the solutions of the Hamiltonian $\tilde{H}_\varepsilon$ by fixing an energy level $h > 0$ and studying the Hamiltonian

$$F_{\varepsilon,h} = R_2 + \frac{a(\varepsilon\tilde{q}_1)}{2\sqrt{b(\varepsilon\tilde{q}_1)}}\tilde{p}_1^2 - \frac{h}{\sqrt{b(\varepsilon\tilde{q}_1)}} + \varepsilon\tilde{g}_1(\tilde{q}_1, \theta_2, \tilde{p}_1, R_2; \varepsilon)\,,$$

where $\tilde{g}_1 := \tilde{g}/\sqrt{b}$. Neglecting the perturbative term $\tilde{g}_1$, the Hamiltonian $F_{\varepsilon,h}$ is integrable, and the study of its dynamics is reduced to analyze the 1DOF Hamiltonian system

$$F^1_{\varepsilon,h} := \frac{a(\varepsilon\tilde{q}_1)}{2\sqrt{b(\varepsilon\tilde{q}_1)}}\tilde{p}_1^2 - \frac{h}{\sqrt{b(\varepsilon\tilde{q}_1)}} \tag{12}$$

on the cylinder $(\tilde{q}_1, \tilde{p}_1) \in \mathbb{S}^1 \times \mathbb{R}$. Let us first prove the following auxiliary lemma:

Lemma 3.3. *The function $b(\varepsilon\tilde{q}_1) : \mathbb{S}^1 \to \mathbb{R}$ is not identically constant provided that $B > 0$. Moreover, if $L < 2B$, this function presents exactly two minima at the points $\frac{\pi}{2}, \frac{3\pi}{2} \in \mathbb{S}^1$ and two maxima at the points $\arcsin(\frac{L}{2B}), \arcsin(\frac{L}{2B}) + \pi \in \mathbb{S}^1$.*

Proof. By definition, we have that $b(\varepsilon\tilde{q}_1)$ is written in the original coordinates (x, z) as

$$\begin{aligned} b(\varepsilon\tilde{q}_1) &= h_I(x,z)\big|_{\{I(x,z)=L\}} = (\nabla I(x,z))^2\big|_{\{I(x,z)=L\}} \\ &= (B^2\cos^2 x + \sin^2 z)\big|_{\{I(x,z)=L\}} = 1 - L^2 + 2LB\sin x + B^2\cos 2x\,, \end{aligned} \tag{13}$$

for all $x \in \mathbb{S}^1$ (recall that Γ_L^i is a graph over x), and hence it is not identically constant, unless $B = 0$. Taking derivatives in Eq. (13) we immediately obtain that $b'(x) = 0$ if and only if $2B\cos x(L - 2B\sin x) = 0$. Assuming that $L < 2B$, we conclude that the critical points $x = \frac{\pi}{2}, \frac{3\pi}{2}$ are minima since $b''(\frac{\pi}{2}) = 4B^2 - 2LB > 0$ and $b''(\frac{3\pi}{2}) = 4B^2 + 2LB > 0$, and the other two critical points are maxima because $b''(\arcsin(\frac{L}{2B})) = b''(\arcsin(\frac{L}{2B}) + \pi) = -4B^2 + L^2 < 0$. □

A straightforward computation shows that the critical points of the Hamiltonian $F^1_{\varepsilon,h}$, cf. Eq. (12), are given by $(\tilde{q}_1^*, 0)$, with $\tilde{q}_1^*$ satisfying the equation $b'(\varepsilon\tilde{q}_1^*) = 0$. Lemma 3.3 then implies that there are four critical points: two corresponding to local minima of $b(\varepsilon\tilde{q}_1)$ on $\mathbb{S}^1$, which are of center type, and two associated to local maxima, which are of saddle type. Therefore, we conclude that the phase portrait of the Hamiltonian vector field defined by $F^1_{\varepsilon,h}$ has exactly two elliptic equilibria, which correspond to $x = \frac{\pi}{2}$ and $x = \frac{3\pi}{2}$ in the original variables. This is the reason why the regions $U^i_\varepsilon(\psi)$ and $V^i_\varepsilon(\psi)$ in the statement of Theorem 3.2 are centered at the points $x = \frac{\pi}{2}$ and $x = \frac{3\pi}{2}$ respectively. The periodic regions of each center point are bounded by a saddle loop associated to the maxima $\arcsin(\frac{L}{2B})$ and $\arcsin(\frac{L}{2B})+\pi$, and hence they cover an interval of x which is $x \in (\arcsin(\frac{L}{2B}), \pi+\arcsin(\frac{L}{2B}))$ and $x \in (\pi+\arcsin(\frac{L}{2B}), 2\pi+\arcsin(\frac{L}{2B}))$ respectively. This justifies the choice of the variable ψ in the range $\psi \in \Psi \subset (0, \frac{\pi}{2} - \arcsin(\frac{L}{2B})) \subset (0, \frac{\pi}{2})$ in the statement of Theorem 3.2. Note that we restrict to a subset Ψ since the perturbation $\varepsilon\tilde{g}_1$ typically causes a small splitting of the separatrices, and hence Ψ is of the form $(0, \frac{\pi}{2} - \arcsin(\frac{L}{2B}) + \mathcal{O}(\varepsilon))$.

It is easy to check that the period of the trajectories of $F^1_{\varepsilon,h}$ in a neighborhood of any of the two elliptic points is of order $1/\varepsilon$, which suggests to define an action variable εR_1 associated to the coordinates $(\tilde{q}_1, \tilde{p}_1)$ in the periodic region, thus yielding the following expression for the Hamiltonian $F_{\varepsilon,h}$:

$$F_{\varepsilon,h} = f(\varepsilon R_1) + R_2 + \varepsilon\tilde{g}_2(\theta_1, \theta_2, \varepsilon R_1, R_2; \varepsilon)\,.$$

The explicit expression of the function $f(\varepsilon R_1)$ is not necessary for our purposes. Observe that the frequency of the periodic solutions in the centre region of $F^1_{\varepsilon,h}$ is given by $\varepsilon f'(\varepsilon R_1)$. Moreover, this frequency is not a constant when R_1 varies because the period tends to infinity as the boundary of the centre domain (the saddle loop) is approached. This immediately implies that:

$$f''(\varepsilon R_1) \neq 0 \tag{14}$$

We are ready to prove the existence of quasi-periodic trajectories for the Hamiltonian system $F_{\varepsilon,h}$ on the level $\{F_{\varepsilon,h} = 0\}$ for any value of $h > 0$ and ε small enough. The corresponding equations of motion are

$$\begin{aligned}
\dot{\theta}_1 &= \varepsilon f'(\varepsilon R_1) + \varepsilon^2\partial_{\varepsilon R_1}\tilde{g}_2\,,\\
\dot{\theta}_2 &= 1 + \varepsilon\partial_{R_2}\tilde{g}_2\,,\\
\dot{R}_1 &= \varepsilon\partial_{\theta_1}\tilde{g}_2\,,\\
\dot{R}_2 &= \varepsilon\partial_{\theta_2}\tilde{g}_2\,.
\end{aligned}$$

Isolating the action R_2 from the equation $F_{\varepsilon,h}(\theta_1, \theta_2, \varepsilon R_1, R_2; \varepsilon) = 0$, and using θ_2 as the independent variable instead of t, the equations of motion can be written as

$$\begin{aligned}
\frac{d\theta_1}{d\theta_2} &= \varepsilon f'(\varepsilon R_1) + \varepsilon^2 A_1(\theta_1, \theta_2, \varepsilon R_1; \varepsilon)\,,\\
\frac{dR_1}{d\theta_2} &= \varepsilon A_2(\theta_1, \theta_2, \varepsilon R_1; \varepsilon)\,,
\end{aligned}$$

for some functions A_1 and A_2. Let us now consider the Poincaré section defined by $\{\theta_2 = 0\}$ on the submanifold $\{F_{\varepsilon,h} = 0\}$, whose return map is obtained by integrating this non-autonomous system of differential equations from $\theta_2 = 0$ to $\theta_2 = 2\pi$ in the variables θ_1 and R_1. Obviously, this is a symplectic map which in coordinates $\alpha := \theta_1$ and $J := \varepsilon R_1$ reads as

$$M_\varepsilon : \begin{pmatrix} \alpha \\ J \end{pmatrix} \longmapsto \begin{pmatrix} \alpha + \varepsilon f'(J) + \mathcal{O}(\varepsilon^2) \\ J + \mathcal{O}(\varepsilon^2) \end{pmatrix} .$$

This map is a perturbation of order ε^2 of a twist map with small rotation number of order ε. Since the non-degeneracy (or twist) condition $f''(J) \neq 0$ is fulfilled (see Eq. (14)), this is enough to apply Moser's twist theorem to M_ε because the perturbation is small compared to the twist $\varepsilon f'(J)$, cf. [5, 39]. We conclude that there exists a positive measure set of closed invariant curves with Diophantine rotation number for the map M_ε provided that ε is small enough, and therefore the existence of quasi-periodic trajectories for the Hamiltonian system $F_{\varepsilon,h}$ on the level $\{F_{\varepsilon,h} = 0\}$ is established. Additionally, the Poincaré-Birkhoff fixed point theorem implies the existence of infinitely many periodic trajectories. This works for any energy level $h > 0$, and proves the existence of periodic and quasi-periodic trajectories in any open subset of the period annulus corresponding to the local minima $x = \frac{\pi}{2}$ and $x = \frac{3\pi}{2}$, thus concluding the proof of the theorem.

Remark 3.4. *The function $b = h_I(x,z)|_{\{I(x,z)=L\}}$ computed in Eq. (12) coincides with the strength of the magnetic field on the set $\{I(x,z) = L\}$ up to a constant factor, i.e.*

$$h_I(x,z)|_{\{I(x,z)=L\}} = |\mathbf{B}_{ABC}|^2|_{\{I(x,z)=L\}} - L^2 .$$

Therefore, the local minima of b are given by the local minima of $|\mathbf{B}_{ABC}|$ on the aforementioned curve. In the configuration space $\mathbb{T}^3$ the set of equilibria Γ_L corresponds to two toroidal magnetic surfaces, given by the equation $B\sin x + \cos z = L$, with zero velocity, so Theorem 3.2 shows the existence of quasi-periodic trajectories with small velocity near these surfaces (in the regions $U^i_\varepsilon(\psi)$ and $V^i_\varepsilon(\psi)$). These confinement regions can be interpreted as magnetic bottles, since the motion takes place around the local minima of the magnetic field strength up to its local maxima.

To illustrate Theorem 3.2, in the left plot of Fig. 1 we show two quasi-periodic trajectories in the regions $U^1_\varepsilon(\psi)$ and $V^1_\varepsilon(\psi)$ respectively (for ψ small). We take $B = 0.3$, $L = 0.01$ and we fix the energy $H_0 = 0.01$. The two trajectories correspond to the initial conditions

$$\big(x, \arccos(L - B\sin x), p_x = \sin z, p_z = p_z(H_0, x)\big) \tag{15}$$

for $x = \frac{\pi}{2}$ and $x = \frac{3\pi}{2}$. As expected, these trajectories oscillate around the initial points.

Notice that the quasi-periodic and periodic motions that we have established in this section correspond to the librating regions associated to the pendulum (12). Although we do not present

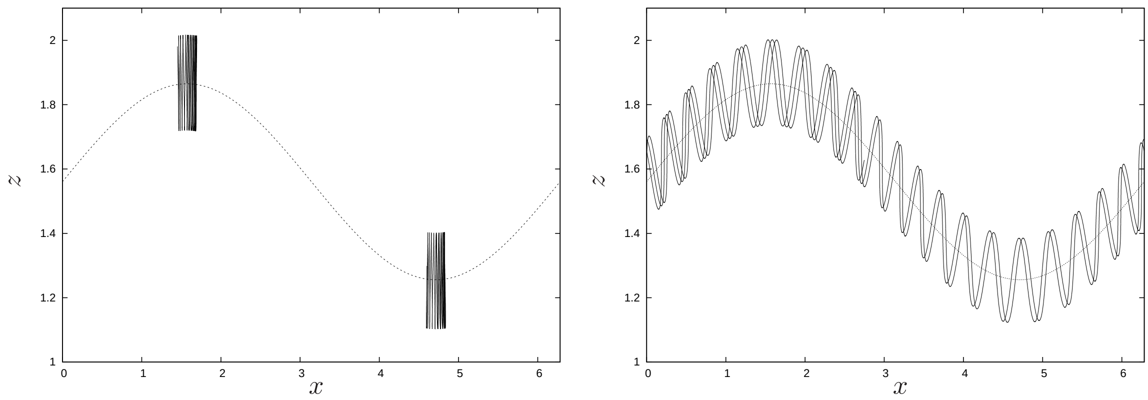

Figure 1: Projection on the $x-z$ plane of different motions close to the curve Γ^1_L for $B = 0.3$, $L = 0.01$ and energy $H_0 = 0.01$. Left: quasi-periodic solutions in the regions $U^1_\varepsilon(\psi)$ and $V^1_\varepsilon(\psi)$. Right: quasi-periodic trajectory that turns around Γ^1_L (see the text for details).

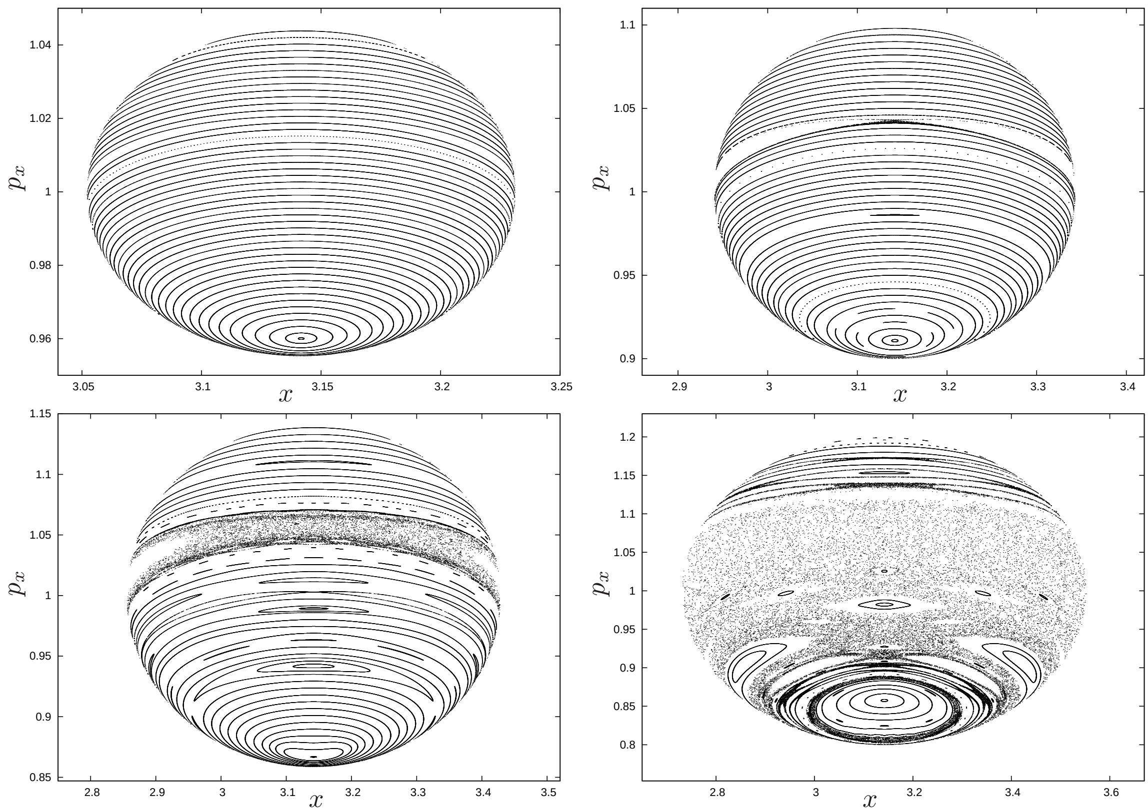

Figure 2: Behavior around the curve Γ^1_0. We show the Poincaré section $\{z = \pi/2\}$ corresponding to $L = 0$, $B = 1/2$ and $C = 0$. We take the energy values $H_0 = 0.001$, 0.005, 0.01 and 0.02, respectively.

a rigorous proof, let us provide some heuristic arguments and numerical evidences for the characterization of other kinds of motions on the level sets of H near the curve Γ_L^1. If we consider the rotating regions of the pendulum (12), we could obtain solutions where the variable x increases, turning around the curve Γ_L^1. We numerically illustrate the existence of such solutions in the right plot of Fig. 1, where we integrate the initial condition (15) with $x = 0$. Similar solutions could be constructed also using the saddle points of the Hamiltonian (12), by observing that they define (including the rotation given by the action R_2) two normally hyperbolic cylinders in phase space, which are foliated by periodic orbits. Then, one can study the effect of the perturbation on these normally hyperbolic cylinders and their heteroclinic connections. The study of these objects can provide significant information on the dynamics around the curve Γ_L^1 (resp. Γ_L^2).

Let us perform a more systematic numerical computation to observe quasi-periodic motions rotating around Γ_L^1. We fix the parameters $L = 0$ and $B = 1/2$, and we visualize the dynamics around the curve Γ_0^1 by considering the section $\Sigma = \{z = \pi/2\}$. We observe that Σ intersects Γ_0^1 at the points $(x, p_x) = (0, 1)$ and $(x, p_x) = (\pi, 1)$, so two connected components are expected (note that the values $x = 0$ and $x = \pi$ correspond to the local maxima of the function b studied in Lemma 3.3 for $L = 0$). In Fig. 2 we plot the dynamics for different small energies H_0. We have checked that the invariant tori that are observed in this figure rotate following the curve Γ_0^1, i.e. they behave similarly to the trajectory in the right plot of Fig. 1. Note that we have focused on the connected component around the point $(\pi, 1)$, the other one being totally equivalent.

Next, we fix $L = 0.75$ and $B = 0.53$ in order to illustrate that Theorem 3.2 may hold without the assumption $L = \mathcal{O}(\varepsilon)$. For these values, the set $\Gamma_{0.75}$ consists of a smooth closed curve which intersects the Poincaré section at the points $(x, p_x) \simeq (2.6504, 0)$ and $(x, p_x) \simeq (5.7920, 0)$ that correspond to $\sin(x) = -L/B$. In Fig. 3 we show several Poincaré sections $\{z = 0\}$ for different energies. Note that for energy $H_0 < H_1$ (top and center plots) we mainly observe the dynamics that "emanates" from the critical curve $\Gamma_{0.75}$. Actually, for small energies we observe two connected components around the previously mentioned points that are full of invariant tori. This shows (analogous results are obtained for other values of L) that there exist quasi-periodic motions in a neighborhood of the curve of equilibria Γ_L for larger values of L. Actually, the trajectories behave analogously to those in Fig. 1, that is, we observe trapped oscillations for initial conditions (15) in a neighborhood of $x = \frac{\pi}{2}$ and $x = \frac{3\pi}{2}$ and we observe global oscillations that rotate along the curve Γ_L for other values of x. When the energy H_0 of the section is increased, both components merge through a chaotic zone (see bottom plots in Fig. 3). For $H_0 > H_1 = 0.3042$ we also observe the dynamics around the point P_1, which is stable (see Section 3.2).

Remark 3.5. *In is interesting to note that in Figs. 2 and 3 (also later in Fig. 8) we observe invariant tori that are not diffeomorphic to invariant circles on the Poincaré section. In some cases we even obtain more that one connected component. The reason is that the section that we take is not globally transverse to the invariant tori. Moreover, the iterates on these connected components are not conjugate to a rotation and may present complex combinatorial dynamics.*

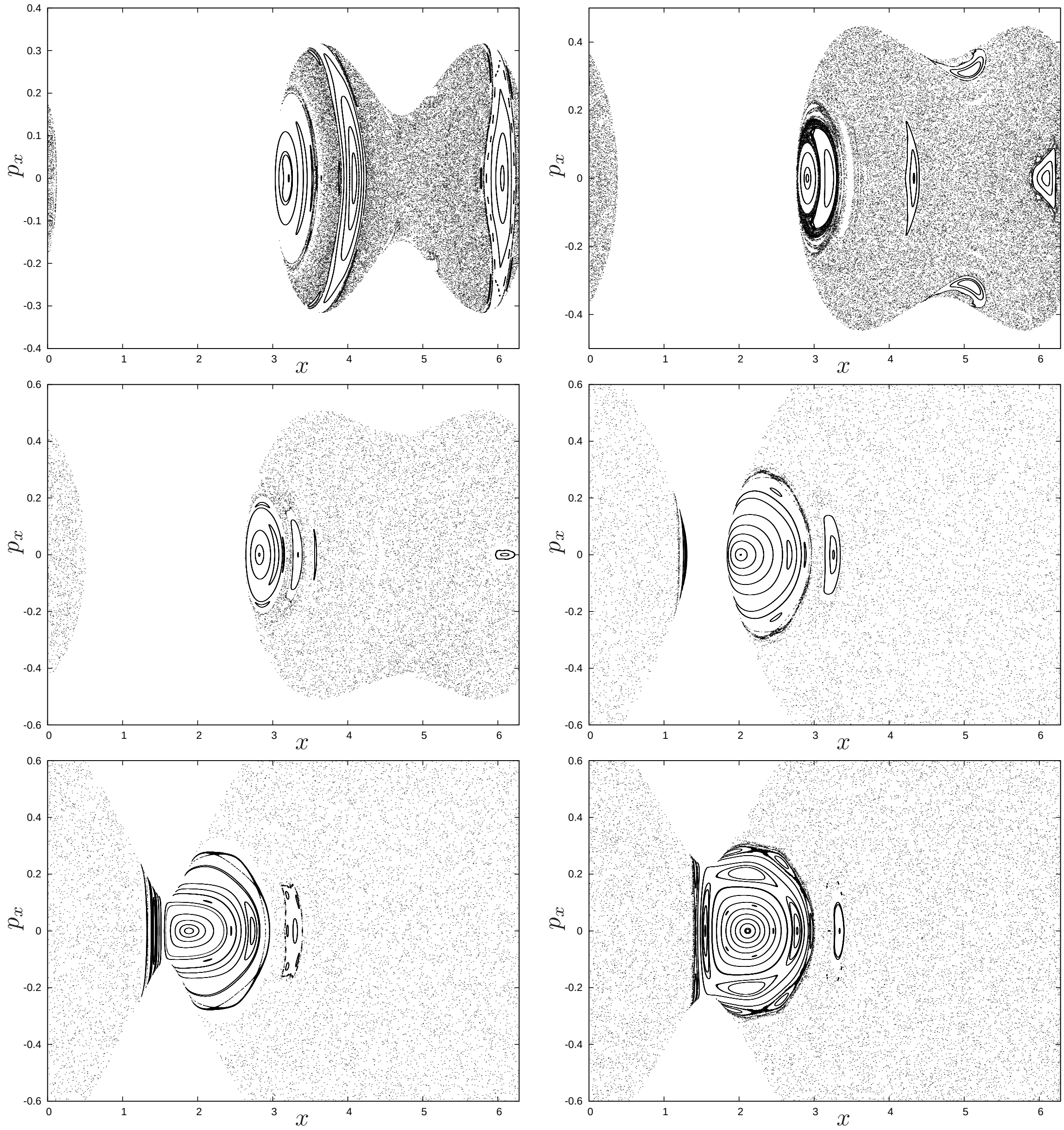

Figure 3: Poincaré section $\{z = 0\}$ corresponding to $L = 0.75$, $B = 0.53$ and $C = 0$ to illustrate the behavior around the elliptic fixed point P_1 (of energy $H_1 = 0.3042$) and the curve $\Gamma^1_{0.75}$. We show the energies $H_0 = 0.05$, 0.1, 0.13, 0.29, 0.31 and 0.33, respectively.

To highlight the numerical evidence of the existence of quasi-periodic motions close to Γ_L for $L = \mathcal{O}(1)$, we complement the qualitative picture given in Fig. 3 with a more quantitative indicator of the dynamics. In particular, we perform a frequency analysis to compute the rotation number θ of invariant curves in the Poincaré section that are close to the curve Γ_L of fixed points.

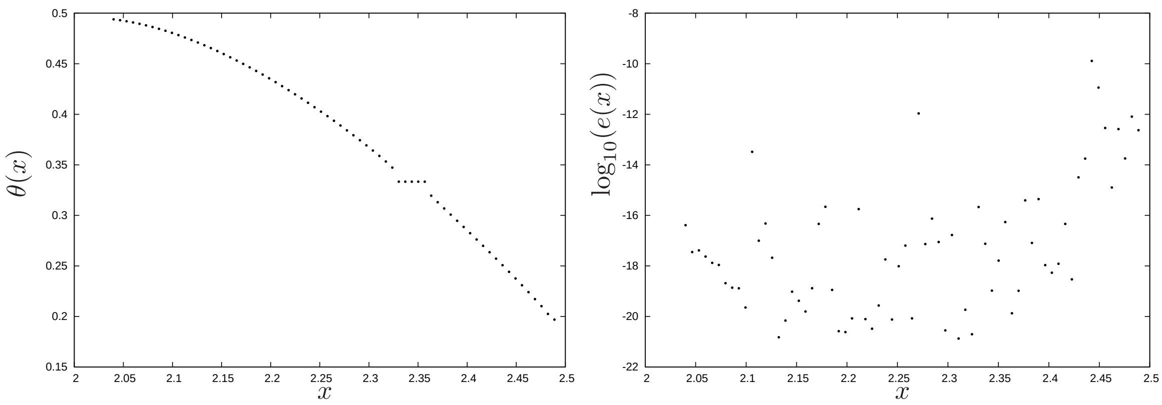

Figure 4: Left: We plot the rotation number (frequency analysis) $x \mapsto \theta(x)$ for a set of points in the fourth plot in Fig. 3 to detect quasi-periodic motions. We take a straight line of initial conditions of the form $(x, p_x) \in [2.04, 2.7] \times \{0\}$. Right: we plot $x \mapsto \log_{10}(e(x))$, the estimated error in the computation of $\theta(x)$ (see [30] for details on the estimation of this error).

To this end, we use the methodology presented in [30], which allows us to compute Diophantine rotation numbers with high precision. We compute the rotation number using [30, Algorithm 2.14] with $p = 6$ and $q = 16$. Trajectories have been computed using a Taylor method of order 34 (see Appendix A), asking for a local tolerance of 10^{-30} for integrating the vector field and 10^{-25} in the computation of the Poincaré section. This tolerance is larger than we need in this computation but we want to enhance that we can reach a very accurate precision. We fix $L = 0.75$, $B = 0.53$ and $H_0 = 0.29 < H_1$ (this corresponds to the fourth plot in Fig. 3) and we select 100 initial conditions on the section $\{z = 0\}$ of the form $(x, p_x) \in [2.04, 2.7] \times \{0\}$ that are contained in the big elliptic island observed in the plot (that corresponds to a Lyapunov orbit associated to $\Gamma_{0.75}$). We show $x \mapsto \theta(x)$ in the left plot of Fig. 4. As described in [30], the method also converges if θ is exactly resonant and at those points the rotation number is locally constant. Let us observe that the zone in Fig. 4 where $\theta(x)$ is constant corresponds to an island associated to an elliptic periodic orbit (see Fig. 3). Those points where $\theta(x)$ is non-constant (and hence, non-degenerate) and Diophantine correspond to invariant tori. In the right plot of Fig. 4 we show the estimated error $e(x)$ associated to every initial condition. This allows us to identify quasi-periodic motions. For example, the convergence of the rotation number associated to $x = 2.4492$ has an error 10^{-10}, so we can presume that the corresponding orbit is not quasi-periodic. On the contrary, the point $x = 2.139$ converges with an error 10^{-21}, so we can expect that this initial condition belongs to a true invariant torus. We refer to [30] for further details.

3.2 Stability of isolated equilibria

The goal of this section is to characterize the local dynamics of the solutions to Eq. (7) near the isolated critical points P_i. More precisely, in Section 3.2.1 we study the linear stability and the bifurcation diagrams of P_i in terms of the parameters B and L. In Section 3.2.2 we use the methodology introduced in [21] to compute the invariant manifolds (stable, unstable and center) associated to the critical points and normal forms. Finally, in Section 3.2.3, a direct computation of the Birkhoff normal form up to fourth order allows us to prove the existence of periodic and quasi-periodic trajectories in a neighborhood of the critical point P_1 for a large and open set of values of the parameters B and L.

3.2.1 Linear stability and bifurcation diagrams

The analysis of the linear stability of the equilibria P_i is tedious although elementary, and consists in the computation of the eigenvalues of the Jacobian matrix $DX_H(P_i)$ as functions of the parameters B and L. Let us summarize the results that we have obtained:

First equilibrium point: $P_1 = (\pi/2, 0, 0, 0)$**.** The Jacobian matrix at P_1 is

$$DX_H(P_1) = \begin{pmatrix} 0 & -1 & 1 & 0 \\ B & 0 & 0 & 1 \\ -B(L-1) & 0 & 0 & -B \\ 0 & -(L-B) & 1 & 0 \end{pmatrix}, \tag{16}$$

whose determinant is given by

$$\det(DX_H(P_1)) = B(B-L+1)^2 .$$

The eigenvalues of the matrix (16) are $\pm\lambda_+$ and $\pm\lambda_-$, where

$$\lambda_\pm^2 = \frac{\Delta_1 \pm \sqrt{\Delta_2}}{2}, \qquad \Delta_1 := -(1+B)L, \qquad \Delta_2 := \Delta_1^2 - 4\det(DX_H(P_1)). \tag{17}$$

The determinant is positive for all values of the parameters, except on the lines $L = B+1$ and $B = 0$. On these lines the equilibrium P_1 is parabolic (degenerate). Accordingly, to characterize the linear stability of P_1 it suffices to study the sign of the function Δ_2. A straightforward computation shows that the set $\Delta_2 = 0$ is given by the curve

$$L = \frac{2(1+B)(\sqrt[4]{B} - \sqrt[4]{B^3})^2}{(1-B)^2} . \tag{18}$$

Obviously, all the bifurcations of the linear stability of P_1 occur on the curves $L = B+1$ and $\Delta_2 = 0$, see Fig. 5 for a pictorial representation. Concretely, if $\Delta_2 < 0$ and $L \neq 0$ we have that the equilibrium is hyperbolic with eigenvalues $\lambda_+ = \bar{\lambda}_-$, and hence the point P_1 is unstable, of type stable focus - unstable focus. On the curve $\Delta_2 = 0$ the equilibrium is elliptic (so linearly stable) with resonant eigenvalues $\lambda_+ = \lambda_- = \mathrm{i}\sqrt{L(1+B)/2}$ provided that $L \neq 0$. In the region where $\Delta_2 > 0$ the equilibrium is elliptic with purely imaginary eigenvalues $\lambda_+ \neq \lambda_-$ if $L \neq B+1$, while on the line $L = B+1$ we have that $\lambda_+ = 0$ (parabolic) and $\lambda_- = \mathrm{i}\sqrt{L(1+B)}$ (elliptic). On the line $B = 0$ the equilibrium is also degenerate with $\lambda_+ = 0$ (parabolic) and $\lambda_- = \mathrm{i}\sqrt{L}$ (elliptic). Observe that there is a Hamiltonian-Hopf bifurcation on the curve $\Delta_2 = 0$. The most degenerate case is when $L = B = 0$, where the equilibrium has eigenvalues $\lambda_+ = \lambda_- = 0$.

Second equilibrium point: $P_2 = (\pi/2, \pi, 0, 0)$**.** The Jacobian matrix at P_2 is

$$DX_H(P_2) = \begin{pmatrix} 0 & 1 & 1 & 0 \\ B & 0 & 0 & 1 \\ -B(L+1) & 0 & 0 & -B \\ 0 & L-B & -1 & 0 \end{pmatrix}, \tag{19}$$

whose determinant is given by

$$\det(DX_H(P_2)) = -B(B-L-1)^2 .$$

The eigenvalues of the matrix (19) are $\pm\lambda_+$ and $\pm\lambda_-$, where

$$\lambda_\pm^2 = \frac{\Delta_1 \pm \sqrt{\Delta_2}}{2}, \qquad \Delta_1 := (1-B)L, \qquad \Delta_2 := \Delta_1^2 - 4\det(DX_H(P_2)) .$$

In the region of parameters $0 \leq B \leq 1$ and $L \geq 0$, the determinant $\det(DX_H(P_2))$ just vanishes on the line $B = 0$ and the point $(B, L) = (1, 0)$. Moreover, the function Δ_2 is positive everywhere except at the points $(B, L) = (0, 0)$ and $(B, L) = (1, 0)$. Therefore, if $B \neq 0$ and $(B, L) \neq (1, 0)$, we conclude that λ_+ is real and λ_- is purely imaginary, so the equilibrium point is of saddle-elliptic type, and hence unstable. When $B = 0$ the equilibrium is degenerate with eigenvalues $\lambda_+ = \sqrt{L}$ (saddle) and $\lambda_- = 0$ (parabolic), while for the point $(B, L) = (1, 0)$ the eigenvalues are $\lambda_+ = \lambda_- = 0$ (of parabolic-parabolic type).

Third equilibrium point: $P_3 = (3\pi/2, 0, 0, 0)$**.** The Jacobian matrix at P_3 is

$$DX_H(P_3) = \begin{pmatrix} 0 & -1 & 1 & 0 \\ -B & 0 & 0 & 1 \\ B(L-1) & 0 & 0 & B \\ 0 & -L-B & 1 & 0 \end{pmatrix}, \tag{20}$$

whose determinant is given by

$$\det(DX_H(P_3)) = -B(B+L-1)^2.$$

The eigenvalues of the matrix (20) are $\pm\lambda_+$ and $\pm\lambda_-$, where

$$\lambda_\pm^2 = \frac{\Delta_1 \pm \sqrt{\Delta_2}}{2}, \qquad \Delta_1 := (B-1)L, \qquad \Delta_2 := \Delta_1^2 - 4\det(DX_H(P_3))\,.$$

The determinant $\det(DX_H(P_3))$ vanishes on the lines $B=0$ and $L = 1-B$, where the eigenvalues are 0 (parabolic) and $\pm\mathrm{i}\sqrt{L}$ (elliptic). In the complement of these lines the function Δ_2 is positive, and we conclude that λ_+ is real and λ_- is purely imaginary, so the equilibrium point is of saddle-elliptic type (unstable).

Fourth equilibrium point: $P_4 = (3\pi/2, \pi, 0, 0)$**.** The Jacobian matrix at P_4 is

$$DX_H(P_4) = \begin{pmatrix} 0 & 1 & 1 & 0 \\ -B & 0 & 0 & 1 \\ B(L+1) & 0 & 0 & B \\ 0 & L+B & -1 & 0 \end{pmatrix}, \tag{21}$$

whose determinant is given by

$$\det(DX_H(P_4)) = B(B+L+1)^2\,.$$

The eigenvalues of the matrix (21) are

$$\lambda_\pm^2 = \frac{\Delta_1 \pm \sqrt{\Delta_2}}{2}, \qquad \Delta_1 := (B+1)L, \qquad \Delta_2 := \Delta_1^2 - 4\det(DX_H(P_4))\,.$$

In the region of parameters $0 \le B \le 1$ and $L \ge 0$, the determinant $\det(DX_H(P_4))$ just vanishes on the line $B = 0$. The bifurcation of the linear stability of P_4 occurs on the curve $\Delta_2 = 0$, which is given by

$$L = \frac{2(1+B)(\sqrt[4]{B} + \sqrt[4]{B^3})^2}{(1-B)^2}\,.$$

More precisely, if $\Delta_2 < 0$ and $L \neq 0$ we have that the equilibrium is hyperbolic with eigenvalues $\lambda_+ = \bar{\lambda}_-$, and hence the point P_4 is unstable (of type stable focus - unstable focus), while the equilibrium is elliptic provided that $L = 0$. For $\Delta_2 > 0$ we have that all eigenvalues are real satisfying $\lambda_+ > \lambda_-$, so the equilibrium is of stable-unstable type. On the bifurcation curve $\Delta_2 = 0$ the equilibrium is of saddle type as well, with eigenvalues $\lambda_+ = \lambda_- = \sqrt{L(B+1)/2}$. Finally, on the line $B = 0$ the equilibrium point is degenerate with eigenvalues $\lambda_+ = \sqrt{L}$ (unstable) and $\lambda_- = 0$ (parabolic).

Remark 3.6. *As observed in the beginning of Section 3, the equilibrium points P_i of the reduced system correspond to periodic trajectories following closed magnetic lines in the configuration space $\mathbb{T}^3$, so all the unstable equilibria previously discussed give rise to unstable periodic trajectories in $\mathbb{T}^3$. For example, the equilibrium P_3 if $B \neq 0$ and $B \neq 1$ corresponds to an unstable periodic trajectory following a hyperbolic closed magnetic line.*

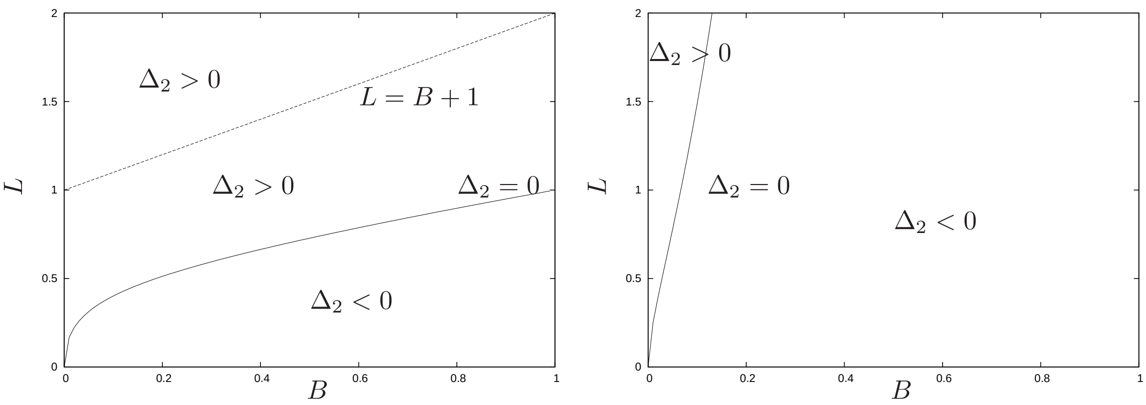

Figure 5: Bifurcation diagrams corresponding to the linear stability of the points P_1 (left plot) and P_4 (right plot). The point P_1 crosses a Hamiltonian-Hopf bifurcation on the curve $\Delta_2 = 0$ from hyperbolic to elliptic behavior, and for $L = B + 1$ and $B = 0$ the equilibrium is of parabolic-elliptic type. The point P_4 is hyperbolic (and hence unstable) if $B \neq 0$, bifurcating from focus-focus type (when $\Delta_2 < 0$) to saddle-saddle type (in the region $\Delta_2 \geq 0$). For $B = 0$ the equilibrium is degenerate of saddle-parabolic type.

3.2.2 Semi-analytic computations around the equilibrium points

Our aim in this section is to compute the invariant manifolds (stable, unstable or center) and the normal forms up to order k of the isolated equilibrium points P_i. It is well known that these objects are the main tools to study the dynamics near the equilibria (see e.g. [25, 40]). Nowadays these computations can be done in a very efficient and systematic way, not only due to the increase of the computer performance, but also due to the continuous development of algorithms. In our study we shall resort to a methodology described in [21] that consists in combining classical parametrization and normal form methods with the use of automatic differentiation techniques.

The use of *automatic differentiation* is suitable for manipulating Taylor expansions of the functions that appear in the functional equations involved in the computation of invariant manifolds and normal forms. Using this approach, we avoid to perform a sequence of changes of variables in the Hamiltonian vector field X_H, see Eq. (7), which is an expensive task. For the sake of completeness, we shall describe the fundamental ideas of the automatic differentiation methods in two appendices. In Appendix A we explain a Taylor method for the numerical integration of the vector field X_H, which is used to integrate the motion numerically. In Appendix B we present a brief discussion on the computation of the Taylor expansion of the composition of functions using automatic differentiation tools. For further discussions and details we refer to [4, 26] and [21, 25], respectively.

Let us remark that the problem of globalizing stable or unstable manifolds (growing them far away from the equilibrium point) is not considered here. This is a standard but very important step to characterize global properties of the dynamics. The interested reader is referred to [27, 40] for several numerical techniques of globalization.

We now describe the methodology of [21] to compute (local) invariant manifolds of isolated equilibrium points using the parametrization method and automatic differentiation. Let F be a vector field on a manifold $\mathcal{M}$ of dimension n. In general, the parametrization method consists in looking for a submanifold $\mathcal{N} = \Phi(N)$ of $\mathcal{M}$ of dimension $d \leq n$, given by the embedding $\Phi : N \to \mathcal{M}$, which is invariant under F. More precisely, there exists a vector field f in N such that

$$F(\Phi(s)) = D\Phi(s)f(s) \tag{22}$$

for all $s \in N$. Of course when $\mathcal{N} = \mathcal{M}$ then Φ is a diffeomorphism, so f simply corresponds to writing F in new coordinates. This allows us to compute invariant manifolds and normal forms in a unified way. Observe that if the pair (Φ, f) is a solution of Eq. (22) then for any diffeomorphism h of N we have another solution $(\Phi \circ h, (Dh)^{-1} f \circ h)$. This lack of uniqueness of solutions to Eq. (22) just corresponds to the ambiguity of choosing coordinates on N.

In order to describe an algorithm to compute the embedding Φ and the vector field f we introduce some notation regarding polynomials and power series of several variables (for more details see Appendix B). Let us consider a (formal) power series f in the variables $x = (x_1, \dots, x_d)$ with real or complex coefficients

$$f(x) = \sum_{k=0}^{\infty} f_k(x)\,,$$

where $f_k(x)$ is a homogeneous polynomial of degree k in the variables x. Then, we write

$$f_{\leq k}(x) = \sum_{j=0}^{k} f_j(x)\,, \qquad [f(x)]_k = f_k(x)$$

to denote the polynomials corresponding to the series truncated at degree k and the homogeneous part of degree k, respectively. We extend this notation in the obvious way for $f_{\geq k}(x)$, $f_{<k}(x)$ and $f_{>k}(x)$.

Consider the differential equation $\dot{z} = F(z)$, $z = (z_1, \dots, z_n)$, and assume that the origin is an equilibrium point, i.e. $F(0) = 0$. If $\Lambda \subset \mathbb{R}^n$ is an invariant subspace of dimension $d \leq n$ for the linearized system $\dot{z} = DF(0)z$, then we want to obtain an invariant manifold of F tangent to Λ. For the sake of simplicity let us assume that the Jacobian matrix $DF(0)$ is diagonal, possibly with complex eigenvalues, of the form

$$DF(0) = \begin{pmatrix} A_1 & 0 \\ 0 & A_2 \end{pmatrix}, \qquad \begin{aligned} A_1 &= \operatorname{diag}\{\lambda_1, \dots, \lambda_d\}\,, \\ A_2 &= \operatorname{diag}\{\mu_1, \dots, \mu_{n-d}\}\,, \end{aligned}$$

with respect to the splitting $z = (x, y)$, $x = (x_1, \dots, x_d)$, $y = (y_1, \dots, y_{n-d})$. The invariant subspace Λ can be identified with $\mathbb{R}^d$ through the coordinates x, and hence the invariant manifold is (locally) given by $\Phi(\mathbb{R}^d)$, where $\Phi : \mathbb{R}^d \to \mathbb{R}^n$ is a parametrization with $\Phi(0) = 0$ and coordinates $(s_1, \dots, s_d)$. The dynamics on this manifold is described by a vector field $f(s)$, with $f(0) = 0$. Our goal is to compute Φ and f by expanding Eq. (22) in Taylor series. To this end, we write $\Phi = (\phi, \psi)$ as

$$x = \phi(s) = s + \sum_{k\geq 2} \phi_k(s)\,, \qquad y = \psi(s) = \sum_{k\geq 2} \psi_k(s)\,,$$

and the inner dynamics as

$$f(s) = A_1 s + \sum_{k\geq 2} f_k(s)\,.$$

Now we solve Eq. (22) proceeding inductively and using these Taylor expansions. For $k \geq 2$ we want to compute $\phi_k(s)$, $\psi_k(s)$ and $f_k(s)$ assuming that the objects associated to the index $k-1$ have been computed. Moreover, we assume that we have computed the expansion of the left hand side of the equation (22) up to order $k-1$, i.e. the polynomial $[F(\Phi_{<k}(s))]_{<k}$. Since the automatic differentiation allows us to compute the polynomial $[F(\Phi_{<k}(s))]_k$ of order k , as we describe in Appendix B, we can write the equation involving only the terms of order k:

$$D\Phi_k(s)A_1 s - DF(0)\Phi_k(s) + D\Phi_1(s) f_k(s) = [F(\Phi_{<k}(s))]_k - \sum_{l=2}^{k-1} D\Phi_{k-l+1}(s) f_l(s). \tag{23}$$

If we write this equation using the splitting of variables (x, y) we get

$$D\phi_k(s)A_1 s - A_1\phi_k(s) = R_k^x(s) - f_k(s), \tag{24}$$
$$D\psi_k(s)A_1 s - A_2\psi_k(s) = R_k^y(s), \tag{25}$$

for $k \geq 2$, where $R_k^x(s)$ and $R_k^y(s)$ denote the splitting of the right hand side of Eq. (23) according to the variables (x, y). Eqs. (24) and (25) are cohomological equations whose resolution is immediate (see Remark 3.7 or details in [21]). Finally, we observe that, after solving these equations, the term $[F(\Phi_{\leq k}(s))]_k$ is obtained simply by adding $A\Phi_k(s)$ to $[F(\Phi_{<k}(s))]_k$.

Remark 3.7. *Let us write the components of $\psi_k(s)$ in terms of monomials as follows*

$$\psi_k^i = \sum_{|m|=k} \psi^i_{m_1,\ldots,m_d} s_1^{m_1} \cdots s_d^{m_d}\,, \qquad i = 1, \ldots, n-d\,,$$

and similarly for $\phi_k(s)$, $R_k^x(s)$ and $R_k^y(s)$. Then, Eq. (25) *can be solved as (the effect of resonances is discussed in Remark 3.8)*

$$\psi^i_{m_1,\ldots,m_d} = \frac{R^{y,i}_{m_1,\ldots,m_d}}{\langle m, \lambda\rangle - \mu_i}\,, \qquad i = 1, \ldots, n-d\,.$$

As explained just after Eq. (22)*, if we introduce this expression in Eq.* (24)*, then we have certain freedom to determine $\phi_k(s)$ and $f_k(s)$. A classical approach consists in taking $\phi_k(s) = 0$ and*

monomial	$\mathrm{Re}\,(\phi_k^{x_1})$	$\mathrm{Im}\,(\phi_k^{x_1})$	$\mathrm{Re}\,(\phi_k^{x_2})$	$\mathrm{Im}\,(\phi_k^{x_2})$
(1,0)	1	0	0	0
(0,1)	0	0	1	0
(3,0)	0.0113403	0.0168855	-0.0817181	0.0177975
(2,1)	-0.618905	-0.346844	0.0350485	0.0253622
(1,2)	0.0350485	-0.0253622	-0.618905	0.346844
(0,3)	-0.0817181	-0.0177975	0.0113403	-0.0168855
(5,0)	-0.00101004	-0.000140878	-0.00184279	0.000811331
(4,1)	0.00408142	-0.0246349	0.091185	0.0629073
(3,2)	0.310829	0.337956	-0.0219177	-0.0214635
(2,3)	-0.0219177	0.0214635	0.310829	-0.337956
(1,4)	0.091185	-0.0629073	0.00408142	0.0246349
(0,5)	-0.00184279	-0.000811331	-0.00101004	0.000140878
(7,0)	-6.06874e-05	-1.67125e-06	4.89254e-07	-0.000153928
(6,1)	0.00108264	0.00188071	0.00407172	0.00218829
(5,2)	-0.012883	0.0164263	-0.0355617	-0.0948781
(4,3)	-0.148707	-0.251264	0.0136528	0.0118445
(3,4)	0.0136528	-0.0118445	-0.148707	0.251264
(2,5)	-0.0355617	0.0948781	-0.012883	-0.0164263
(1,6)	0.00407172	-0.00218829	0.00108264	-0.00188071
(0,7)	4.89254e-07	0.000153928	-6.06874e-05	1.67125e-06
(9,0)	4.05839e-07	-2.6137e-06	2.07934e-06	-4.72245e-06
(8,1)	0.000116796	0.00015679	-0.000385053	0.000302365
(7,2)	0.000623713	-0.00266294	-0.00203353	-0.00600047
(6,3)	0.0129566	-0.00812757	-0.00906983	0.0789722
(5,4)	0.0690392	0.171715	-0.00957442	-0.00639341
(4,5)	-0.00957442	0.00639341	0.0690392	-0.171715
(3,6)	-0.00906983	-0.0789722	0.0129566	0.00812757
(2,7)	-0.00203353	0.00600047	0.000623713	0.00266294
(1,8)	-0.000385053	-0.000302365	0.000116796	-0.00015679
(0,9)	2.07934e-06	4.72245e-06	4.05839e-07	2.6137e-06

Table 1: Coefficients up to order 10 of the components ϕ^{x_1} and ϕ^{x_2} of the parametrization Φ (that reduces to normal form) of the unstable manifold corresponding to the equilibrium point P_1 for $B = 0.53$ and $L = 0.67$. We take the subspaces associated to $\lambda = (\lambda_+, \lambda_-)$ and $\mu = (-\lambda_+, -\lambda_-)$. Coefficients that are not included are exactly zero.

$f_k(s) = R_k^x(s)$ *for all* $k \geq 2$*, so* $\Phi = (\mathrm{Id}, \psi)$ *is a graph. This is called the* Graph Transform method*. On the contrary, under non-resonance conditions, we can take* $f_k(s) = 0$ *for all* $k \geq 2$ *and*

$$\phi^i_{m_1,\ldots,m_d} = \frac{R^{x,i}_{m_1,\ldots,m_d}}{\langle m, \lambda\rangle - \lambda_i}, \qquad i = 1, \ldots, d,$$

so the inner dynamics is written in normal form (see Remark 3.8). Of course there are intermediate cases (partial normal forms) that can be interesting depending on the context.

monomial	$\mathrm{Re}\,(\psi_k^{y_1})$	$\mathrm{Im}\,(\psi_k^{y_1})$	$\mathrm{Re}\,(\psi_k^{y_2})$	$\mathrm{Im}\,(\psi_k^{y_2})$
(3,0)	-0.011187	-0.0105581	0.0833003	-0.0223178
(2,1)	0.311185	-1.25878e-16	-0.0335609	-0.0316743
(1,2)	-0.0335609	0.0316743	0.311185	1.29693e-16
(0,3)	0.0833003	0.0223178	-0.011187	0.0105581
(5,0)	0.000768579	0.000223279	0.00194851	-0.000762485
(4,1)	0.0017664	0.018355	-0.0985917	-0.0599212
(3,2)	-0.249167	-0.108905	0.0252273	0.0297817
(2,3)	0.0252273	-0.0297817	-0.249167	0.108905
(1,4)	-0.0985917	0.0599212	0.0017664	-0.018355
(0,5)	0.00194851	0.000762485	0.000768579	-0.000223279
(7,0)	5.24792e-05	-8.18556e-06	-1.10868e-05	0.000155386
(6,1)	-0.000580396	-0.00153427	-0.00412356	-0.00237694
(5,2)	0.005208	-0.0149761	0.0436135	0.0973749
(4,3)	0.153651	0.126102	-0.016535	-0.0212821
(3,4)	-0.016535	0.0212821	0.153651	-0.126102
(2,5)	0.0436135	-0.0973749	0.005208	0.0149761
(1,6)	-0.00412356	0.00237694	-0.000580396	0.00153427
(0,7)	-1.10868e-05	-0.000155386	5.24792e-05	8.18556e-06
(9,0)	-3.73365e-07	2.29444e-06	-2.39553e-06	4.67049e-06
(8,1)	-0.000124267	-0.0001178	0.000407185	-0.000279282
(7,2)	-0.000768535	0.00182975	0.0019503	0.00618031
(6,3)	-0.00729995	0.0100739	0.00441953	-0.0844856
(5,4)	-0.086376	-0.105966	0.0106749	0.014461
(4,5)	0.0106749	-0.014461	-0.086376	0.105966
(3,6)	0.00441953	0.0844856	-0.00729995	-0.0100739
(2,7)	0.0019503	-0.00618031	-0.000768535	-0.00182975
(1,8)	0.000407185	0.000279282	-0.000124267	0.0001178
(0,9)	-2.39553e-06	-4.67049e-06	-3.73365e-07	-2.29444e-06

Table 2: Coefficients up to order 10 of the components ψ^{y_1} and ψ^{y_2} of the parametrization Φ (that reduces to normal form) of the unstable manifold corresponding to the equilibrium point P_1 for $B = 0.53$ and $L = 0.67$. We take the subspaces associated to $\lambda = (\lambda_+, \lambda_-)$ and $\mu = (-\lambda_+, -\lambda_-)$. Coefficients that are not included are exactly zero.

Remark 3.8. *Resonances play an important role in the study of cohomological equations. In this setting we find two types of resonances: on the one hand we have* primary resonances *associated to the eigenvalues of A_1 and A_2 that prevent the existence of the invariant manifold, and on the other hand we have* secondary resonances *associated to the eigenvalues of A_1, which prevent cancellations in the normal form. These resonances are given by*

$$\langle m, \lambda \rangle - \mu_i = 0 \qquad \textit{and} \qquad \langle m, \lambda \rangle - \lambda_i = 0\,,$$

respectively, where $\lambda = (\lambda_1, \ldots, \lambda_d)$ and $m \in \mathbb{N}^d$ is the multi-index of the monomial considered in the cohomological equation.

Remark 3.9. *Even if the matrix $DF(0)$ can be diagonalized, it is not usually diagonal in the* *original coordinates. Assume that C is the matrix of eigenvectors satisfying*

$$C^{-1}DF(0)C = \begin{pmatrix} A_1 & 0 \\ 0 & A_2 \end{pmatrix} .$$

In this case, it is not recommended to introduce this linear transformation into the vector field to diagonalize the linear part. The reason is that, in general, this transformation makes the nonlinear part more complicated, and therefore the automatic differentiation of $F(\Phi(s))$ turns out to be much more involved. A more convenient choice is to consider the formal vector field $C^{-1}F(C\Phi(s))$ in the automatic differentiation process.

Next we apply the described methodology to compute the invariant manifolds and normal forms of the equilibrium points P_i of the Hamiltonian vector field X_H. The results are not presented in the original variables (x, z, p_x, p_z) but in the coordinates (x_i, y_i), presented before (they depend on the particular subspace). In these new coordinates the Jacobian matrix of the field X_H is diagonal. All the computations have been performed with double precision (16 digits) using a C++ compiler, even though for space limitations we may show less digits. Eigenvalues and eigenvectors have been computed using the GSL routines [19].

First equilibrium point: $P_1 = (\pi/2, 0, 0, 0)$**.** Let us first consider the zone $\Delta_2 < 0$. For $B = 0.53$ and $L = 0.67$ we obtain the eigenvalues λ_+, λ_-, $-\lambda_+$ and $-\lambda_-$, where

$$\lambda_\pm = 0.2382639822530091 \pm \mathrm{i}\, 0.7545327860597331 . \tag{26}$$

In this case, we can compute 2-dimensional stable and unstable manifolds corresponding to the hyperbolic directions. Just to illustrate that the algorithm is very fast we mention that the computation of the 2-dimensional unstable manifold together with the inner normal form up to order 70 takes 0.38 seconds in a 3.20GHz Intel(R) Core(TM) i5 CPU. We refer to the discussion in [21] about the number of operations required and the asymptotic computational cost expected.

We check that the computations are correct by evaluating the error of invariance when we introduce the computed parametrization into Eq. (22). For example, we compute the unstable manifold up to order 15 and we evaluate Φ at a set of points $s = (s_1, s_2) = (j/100, j/100)$ for $1 \leq j \leq 100$. We take the subspaces associated to $\lambda = (\lambda_+, \lambda_-)$ and $\mu = (-\lambda_+, -\lambda_-)$. Then, we compute the invariance error as $e(s) := |F(\Phi(s)) - D\Phi(s)f(s)|$ and, since we are truncating our computations at order 15, we expect this error to behave as $e(s) = \mathcal{O}(s^{16})$. We check this by means of a linear fit of the function $\log(e(s))$ with respect to $\log(s)$. See the left plot of Fig. 6.

In Tables 1 and 2 we show some coefficients (up to order 10) of the parametrization $\Phi = (\phi^{x_1}, \phi^{x_2}, \psi^{y_1}, \psi^{y_2})$ (that reduces to normal form) of the unstable manifold associated to this equilibrium point. As before, we take the subspaces associated to $\lambda = (\lambda_+, \lambda_-)$ and $\mu = (-\lambda_+, -\lambda_-)$. The parametrization is complex because the eigenvalues are complex

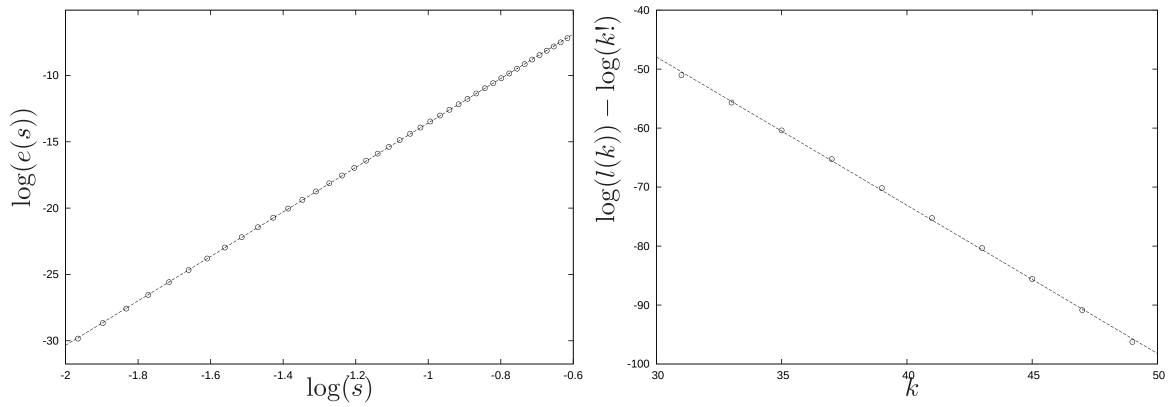

Figure 6: Left: We plot $\log(e(s))$ versus $\log(s)$, where $e(s)$ is the invariance error for the unstable manifold of the point P_1 (with $B = 0.53$ and $L = 0.67$). We take the subspaces associated to $\lambda = (\lambda_+, \lambda_-)$ and $\mu = (-\lambda_+, -\lambda_-)$. The slope of this plot is 16.76 ± 0.01. Right: Linear fit of the coefficients of the Birkhoff normal form of the equilibrium P_1 for $B = 0.53$ and $L = 0.75$, corresponding to the ordering $\lambda = (\lambda_+, -\lambda_+, \lambda_-, -\lambda_-)$. We check that the series of the normal form is of Gevrey-1 type by plotting $\log(l(k)) - \log(k!)$ versus k and observing a straight line.

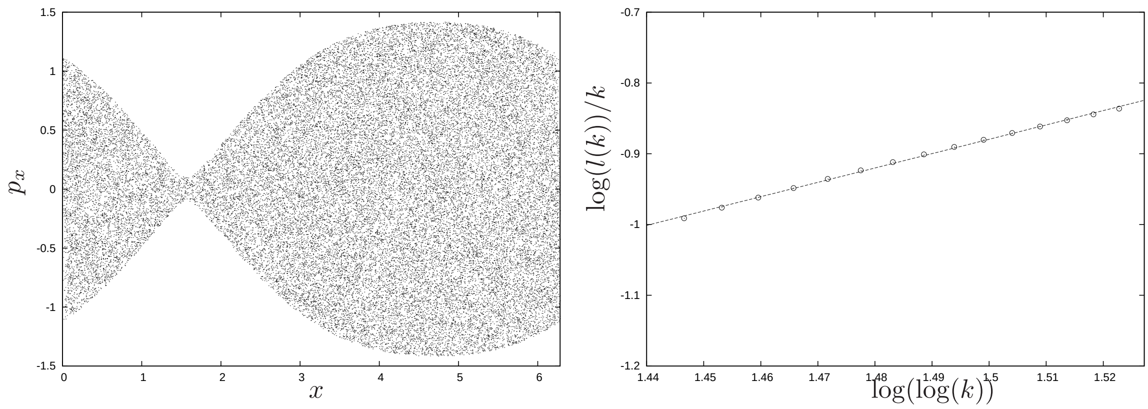

Figure 7: Left: A single orbit under the Poincaré map of the section $\{z = 0\}$ corresponding to $L = 0$, $B = 1/2$, $C = 0$ and $H_0 = 1.13$. This illustrates the global chaotic behavior (the point P_1 is of type stable focus - unstable focus) for these parameters. Right: We perform a linear fit of $\log(l(k))/k$ versus $\log\log(k)$ in order to check that the parametrization of the center manifold of P_2 is not analytic. Concretely, it turns out that the coefficients follow the law $l(k) \simeq CM^k(\log(k))^{\alpha k}$, where $\alpha = 2.02748 \pm 0.01981$.

numbers. It is straightforward to check that for the selected unstable eigenvalues we do not have primary and secondary resonances so the normal form of the 2-dimensional vector field f of the inner dynamics on the unstable manifold is

$$f(s_1, s_2) = \begin{pmatrix} \lambda_+ s_1 \\ \lambda_- s_2 \end{pmatrix}.$$

monomial	$\mathrm{Im}\,(f_k^{x_1})$	$\mathrm{Im}\,(f_k^{x_3})$	monomial	$\mathrm{Im}\,(f_k^{x_1})$	$\mathrm{Im}\,(f_k^{x_3})$
(1,0,0,0)	0.809833	0	(2,2,2,1)	0	-1.68445
(0,0,1,0)	0	0.701192	(2,1,2,2)	1.70915	0
(2,1,0,0)	0.0351767	0	(1,1,3,2)	0	-1.56222
(1,1,1,0)	0	-0.0980094	(1,0,3,3)	0.530282	0
(1,0,1,1)	0.0980356	0	(0,0,4,3)	0	-0.208442
(0,0,2,1)	0	-0.0628254	(5,4,0,0)	-0.271951	0
(3,2,0,0)	-0.0494464	0	(4,4,1,0)	0	1.01083
(2,2,1,0)	0	0.148326	(4,3,1,1)	-3.84344	0
(2,1,1,1)	-0.296731	0	(3,3,2,1)	0	7.26488
(1,1,2,1)	0	0.371816	(3,2,2,2)	-10.9868	0
(1,0,2,2)	-0.185958	0	(2,2,3,2)	0	13.2055
(0,0,3,2)	0	0.0870251	(2,1,3,3)	-9.0283	0
(4,3,0,0)	0.105806	0	(1,1,4,3)	0	6.78982
(3,3,1,0)	0	-0.356864	(1,0,4,4)	-1.76248	0
(3,2,1,1)	1.04483	0	(0,0,5,4)	0	0.609571

Table 3: Coefficients up to order 10 of the components f^{x_1} and f^{x_3} of the normal form $f = (f^{x_1}, f^{x_2}, f^{x_3}, f^{x_4})$ corresponding to the point P_1 for $B = 0.53$ and $L = 0.75$. We take the ordering $\lambda = (\lambda_+, -\lambda_+, \lambda_-, -\lambda_-)$. Notice that the vector field f is purely imaginary and its components f^{x_2} and f^{x_4} can be computed from f^{x_1} and f^{x_3}. For example, the monomial of index (m_1, m_2, m_3, m_4) of f^{x_2} is the conjugate of the monomial of index (m_2, m_1, m_3, m_4) of f^{x_1} and the same for f^{x_3} and f^{x_4}. Coefficients that are not included are exactly zero.

Next, we illustrate numerically the dynamics near the point P_1 when it is linearly unstable. This is the case for example if $L = 0$ and $B \neq 0$ (see Section 3.2). The point P_1 has energy $H_1 = 1.125$ and we consider the section $\{z = 0\}$. In the left plot of Fig. 7 we plot a single orbit of the Poincaré section corresponding to $B = 1/2$ and $H_0 = 1.13$ (slighly larger than H_1). As expected, the dynamics is strongly chaotic.

On the other hand, we consider the region where P_1 is elliptic. For $B = 0.53$ and $L = 0.75$ the equilibrium point has eigenvalues λ_+, $-\lambda_+$, λ_-, and $-\lambda_-$, where

$$\lambda_+ = \mathrm{i}\,0.8098330758524813\,, \quad \lambda_- = \mathrm{i}\,0.7011921200750256\,.$$

In this case we take the full linear space $\Lambda = \mathbb{R}^4$ rather than an invariant subspace, which is equivalent to compute the normal form of the system (see the discussion following Eq. (22)). Notice that we are not using the Hamiltonian structure of the problem, but essentially what we are computing is the Birkhoff normal form of the equilibrium point P_1. It is easy to check that there are no primary resonances and that the secondary resonances are given by

$$\{m \in \mathbb{N}^4 \,:\, \{m_1 - m_2 = \pm 1, m_3 = m_4\} \cup \{m_1 = m_2, m_3 - m_4 = \pm 1\}\}\,.$$

In Table 3 we show the coefficients, up to order 10, of the normal form $f = (f^{x_1}, f^{x_2}, f^{x_3}, f^{x_4})$ corresponding to the ordering $(\lambda_+, -\lambda_+, \lambda_-, -\lambda_-)$ of the eigenvalues. Let us remark that,

monomial	$\mathrm{Re}\,(\psi_k^{y_1})$	$\mathrm{Im}\,(\psi_k^{y_1})$	$\mathrm{Re}\,(\psi_k^{y_2})$	$\mathrm{Im}\,(\psi_k^{y_2})$
(3,0)	-0.00595678	-0.00423827	-0.00595678	0.00423827
(2,1)	-0.0423915	-0.0121093	-0.0423915	0.0121093
(1,2)	-0.0423915	0.0121093	-0.0423915	-0.0121093
(0,3)	-0.00595678	0.00423827	-0.00595678	-0.00423827
(5,0)	-0.000198242	-1.23151e-06	-0.000198242	1.23151e-06
(4,1)	-0.00151237	0.000296865	-0.00151237	-0.000296865
(3,2)	-0.0035099	0.00186054	-0.0035099	-0.00186054
(2,3)	-0.0035099	-0.00186054	-0.0035099	0.00186054
(1,4)	-0.00151237	-0.000296865	-0.00151237	0.000296865
(0,5)	-0.000198242	1.23151e-06	-0.000198242	-1.23151e-06
(7,0)	9.07057e-06	-3.85226e-07	9.07057e-06	3.85226e-07
(6,1)	7.77543e-05	-2.80586e-05	7.77543e-05	2.80586e-05
(5,2)	0.000175073	-0.00044502	0.000175073	0.00044502
(4,3)	-0.000993973	-0.00165169	-0.000993973	0.00165169
(3,4)	-0.000993973	0.00165169	-0.000993973	-0.00165169
(2,5)	0.000175073	0.00044502	0.000175073	-0.00044502
(1,6)	7.77543e-05	2.80586e-05	7.77543e-05	-2.80586e-05
(0,7)	9.07057e-06	3.85226e-07	9.07057e-06	-3.85226e-07
(9,0)	2.95261e-07	-1.40807e-07	2.95261e-07	1.40807e-07
(8,1)	8.44548e-07	-5.17037e-06	8.44548e-07	5.17037e-06
(7,2)	-4.19034e-05	-2.61652e-05	-4.19034e-05	2.61652e-05
(6,3)	-0.000187548	0.000154405	-0.000187548	-0.000154405
(5,4)	0.000229417	0.000870602	0.000229417	-0.000870602
(4,5)	0.000229417	-0.000870602	0.000229417	0.000870602
(3,6)	-0.000187548	-0.000154405	-0.000187548	0.000154405
(2,7)	-4.19034e-05	2.61652e-05	-4.19034e-05	-2.61652e-05
(1,8)	8.44548e-07	5.17037e-06	8.44548e-07	-5.17037e-06
(0,9)	2.95261e-07	1.40807e-07	2.95261e-07	-1.40807e-07

Table 4: Coefficients up to order 10 of the components ψ^{y_1} and ψ^{y_2} of the graph parametrization $\Phi = (\mathrm{Id}_{2\times 2}, \psi)$ of the center manifold corresponding to the equilibrium point P_2 for $B = 0.53$ and $L = 0.75$. We consider the ordering $\lambda = (\lambda_-, -\lambda_-)$ and $\mu = (\lambda_+, -\lambda_+)$. Coefficients that are not included are exactly zero.

in order to improve the numerical stability of the procedure (controlling the growth of the coefficients in the expansions) we have scaled the lengths of the eigenvectors by a factor 5.

According to normal form estimates (see e.g. [12]) this expansion of f is expected to be of Gevrey-1 type, this meaning that the coefficients should grow as $cM^k k!$, where k is the degree of the coefficient and c, M are positive real numbers. To check this, we define $l(k)$ as the maximum L_1 norm of the (vector) coefficients of the monomials of order k in the vector field f. Then, we compute the normal form up to order 50 and we perform a linear fit of the expression $\log(l(k)) - \log(k!)$ obtaining the values (see the right plot in Fig. 6)

$$\log c = 27.479 \pm 0.84 \qquad \log M = -2.5139 \pm 0.02\,.$$

In Section 3.2.3 we shall present a low order computation of the Birkhoff normal form of

monomial	$\mathrm{Re}\,(f_k^{x_1})$	$\mathrm{Im}\,(f_k^{x_1})$	$\mathrm{Re}\,(f_k^{x_2})$	$\mathrm{Im}\,(f_k^{x_2})$
(1,0)	6.93889e-17	0.853957	0	0
(0,1)	0	0	6.93889e-17	-0.853957
(3,0)	9.30845e-18	0.0316676	-6.54358e-18	-0.0365082
(2,1)	8.59748e-18	0.0806328	-1.10278e-17	-0.0950027
(1,2)	-1.23286e-17	0.0950027	7.29663e-18	-0.0806328
(0,3)	-7.22868e-18	0.0365082	8.62335e-18	-0.0316676
(5,0)	-2.18646e-19	-0.00246689	1.53721e-19	0.00262129
(4,1)	-2.735e-18	-0.0153811	3.44386e-18	0.0148381
(3,2)	8.22506e-19	-0.035697	5.73466e-18	0.0336934
(2,3)	5.47795e-18	-0.0336934	-2.25519e-19	0.035697
(1,4)	3.00289e-18	-0.0148381	-2.53673e-18	0.0153811
(0,5)	1.57732e-19	-0.00262129	-2.14635e-19	0.00246689
(7,0)	-1.98776e-20	1.33784e-05	1.0823e-20	-4.21331e-06
(6,1)	1.90181e-19	4.88131e-05	-3.2318e-19	2.28043e-05
(5,2)	1.97204e-18	7.3586e-05	-2.82151e-18	0.00013836
(4,3)	2.91442e-19	0.000426225	-4.12666e-18	-4.0195e-05
(3,4)	-3.74206e-18	4.0195e-05	5.63031e-20	-0.000426225
(2,5)	-2.59858e-18	-0.00013836	1.851e-18	-7.3586e-05
(1,6)	-2.77009e-19	-2.28043e-05	1.76146e-19	-4.88131e-05
(0,7)	1.3609e-20	4.21331e-06	-2.17699e-20	-1.33784e-05
(9,0)	3.2045e-21	1.21261e-06	-3.90214e-21	-1.14871e-06
(8,1)	3.47435e-20	1.51676e-05	-4.20048e-20	-1.63263e-05
(7,2)	-6.25014e-20	7.67223e-05	6.29703e-20	-9.94602e-05
(6,3)	-1.03478e-18	1.70359e-05	1.37665e-18	-0.000162984
(5,4)	-4.75846e-20	-0.000525435	2.01814e-18	0.00020516
(4,5)	2.12105e-18	-0.00020516	-2.98515e-19	0.000525435
(3,6)	1.40492e-18	0.000162984	-1.13213e-18	-1.70359e-05
(2,7)	8.80349e-20	9.94602e-05	-9.09863e-20	-7.67223e-05
(1,8)	-3.74735e-20	1.63263e-05	3.11842e-20	-1.51676e-05
(0,9)	-3.69109e-21	1.14871e-06	3.06035e-21	-1.21261e-06

Table 5: Coefficients up to order 10 of the components f^{x_1} and f^{x_2} of the dynamics reduced to the center manifold, using the Graph transform method, corresponding to the equilibrium point P_2 for $B = 0.53$ and $L = 0.75$. We consider the ordering $\lambda = (\lambda_-, -\lambda_-)$ and $\mu = (\lambda_+, -\lambda_+)$. Coefficients that are not included are exactly zero.

the elliptic point P_1, obtaining explicit expressions for the Birkhoff coefficients of order 4 as functions of B and L.

Second (and third) equilibrium point: $P_2 = (\pi/2, \pi, 0, 0)$**.** For all values of B and L, except for some degenerate cases, this equilibrium point is of saddle-elliptic type, as we described in Section 3.2.1. For example, when $B = 0.53$ and $L = 0.75$, the eigenvalues of the Jacobian matrix are λ_+, $-\lambda_+$, λ_- and $-\lambda_-$, where

$$\lambda_+ = 1.040068346742913\,, \qquad \lambda_- = \mathrm{i}\,0.8539567705080487\,. \tag{27}$$

Let us compute the center manifold associated to the elliptic eigenvalues, taking $\lambda =$

monomial	$\mathrm{Re}\,(\phi_k^{x_1})$	$\mathrm{Im}\,(\phi_k^{x_1})$	$\mathrm{Re}\,(\phi_k^{x_2})$	$\mathrm{Im}\,(\phi_k^{x_2})$
(1,0)	1	0	0	0
(0,1)	0	0	1	0
(3,0)	0.0185417	-3.94357e-18	-0.010688	1.48143e-18
(2,1)	0	0	-0.055625	1.93702e-18
(1,2)	-0.055625	-2.69868e-18	0	0
(0,3)	-0.010688	-1.682e-18	0.0185417	3.54244e-18
(5,0)	-0.000458799	-1.78236e-19	0.000313424	9.60176e-20
(4,1)	-0.0136963	3.09019e-20	0.0061211	-6.10422e-19
(3,2)	0	0	0.0308924	7.46343e-19
(2,3)	0.0308924	-6.63068e-19	0	0
(1,4)	0.0061211	5.60148e-19	-0.0136963	3.15244e-20
(0,5)	0.000313424	-8.48694e-20	-0.000458799	1.52258e-19
(7,0)	-1.12594e-05	4.52245e-21	1.33899e-05	-2.66398e-22
(6,1)	-4.7191e-05	1.02515e-19	9.66223e-05	2.00689e-20
(5,2)	0.00675534	1.4728e-19	-0.00237708	7.54189e-19
(4,3)	0	0	-0.0131499	1.96645e-19
(3,4)	-0.0131499	-4.01767e-19	0	0
(2,5)	-0.00237708	-7.67028e-19	0.00675534	-6.19302e-20
(1,6)	9.66223e-05	-1.68143e-20	-4.7191e-05	-7.70449e-20
(0,7)	1.33899e-05	2.12157e-22	-1.12594e-05	-3.51252e-21
(9,0)	3.5812e-07	3.2186e-22	-2.21341e-07	-2.93059e-22
(8,1)	2.13392e-05	5.63667e-21	-1.85669e-05	-6.55377e-21
(7,2)	0.000132207	-2.77792e-20	-0.000128352	-5.14491e-20
(6,3)	-0.00428297	-5.71999e-19	0.00128406	-5.5083e-19
(5,4)	0	0	0.00775412	2.9801e-19
(4,5)	0.00775412	-1.20723e-19	0	0
(3,6)	0.00128406	5.76128e-19	-0.00428297	4.46016e-19
(2,7)	-0.000128352	4.77185e-20	0.000132207	1.07716e-20
(1,8)	-1.85669e-05	5.56645e-21	2.13392e-05	-5.02538e-21
(0,9)	-2.21341e-07	2.34157e-22	3.5812e-07	-2.65541e-22

Table 6: Coefficients up to order 10 of the components ϕ^{x_1} and ϕ^{x_2} of the parametrization Φ of the center manifold corresponding to the equilibrium point P_2 for $B = 0.53$ and $L = 0.75$. We consider the ordering $\lambda = (\lambda_-, -\lambda_-)$ and $\mu = (\lambda_+, -\lambda_+)$. Coefficients that are not included are exactly zero.

$(\lambda_-, -\lambda_-)$ and $\mu = (\lambda_+, -\lambda_+)$. It is easy to check that in this case there are no primary resonances. For this point, we compute the graph representation of the center manifold (see Remark 3.7) up to order 100 (it takes 1.5 seconds). In Table 4 we show some coefficients (up to order 10) of the parametrization $\Phi = (\mathrm{Id}_{2\times 2}, \psi^{y_1}, \psi^{y_2})$ of this center manifold and in Table 5 we show some coefficients of $f(s)$, the dynamics reduced to the center manifold.

We recall that in the unpublished manuscript [29] it was shown that, even if the center manifold is not analytic, its coefficients grow in a very mild way (see also computations in [21]). Concretely, in the right plot of Fig. 7 we check that the quantity $l(k)$ introduced before follows the law $l(k) = cM^k(\log k)^{\alpha k}$, where $\alpha = 2.02748 \pm 0.01981$, for large k.

monomial	$\mathrm{Re}\,(\psi_k^{y_1})$	$\mathrm{Im}\,(\psi_k^{y_1})$	$\mathrm{Re}\,(\psi_k^{y_2})$	$\mathrm{Im}\,(\psi_k^{y_2})$
(3,0)	-0.00595678	-0.00423827	-0.00595678	0.00423827
(2,1)	-0.0423915	-0.0121093	-0.0423915	0.0121093
(1,2)	-0.0423915	0.0121093	-0.0423915	-0.0121093
(0,3)	-0.00595678	0.00423827	-0.00595678	-0.00423827
(5,0)	-7.65097e-05	-0.000107562	-7.65097e-05	0.000107562
(4,1)	0.000179792	0.000262544	0.000179792	-0.000262544
(3,2)	0.00160518	0.00130928	0.00160518	-0.00130928
(2,3)	0.00160518	-0.00130928	0.00160518	0.00130928
(1,4)	0.000179792	-0.000262544	0.000179792	0.000262544
(0,5)	-7.65097e-05	0.000107562	-7.65097e-05	-0.000107562
(7,0)	7.58392e-06	1.77381e-07	7.58392e-06	-1.77381e-07
(6,1)	0.000159565	8.82675e-05	0.000159565	-8.82675e-05
(5,2)	-0.000194005	-0.000344785	-0.000194005	0.000344785
(4,3)	-0.00315023	-0.00119772	-0.00315023	0.00119772
(3,4)	-0.00315023	0.00119772	-0.00315023	-0.00119772
(2,5)	-0.000194005	0.000344785	-0.000194005	-0.000344785
(1,6)	0.000159565	-8.82675e-05	0.000159565	8.82675e-05
(0,7)	7.58392e-06	-1.77381e-07	7.58392e-06	1.77381e-07
(9,0)	8.70891e-08	7.2597e-08	8.70891e-08	-7.2597e-08
(8,1)	-3.36914e-06	2.41887e-06	-3.36914e-06	-2.41887e-06
(7,2)	-0.000105269	-5.24195e-05	-0.000105269	5.24195e-05
(6,3)	-2.8743e-05	0.000140305	-2.8743e-05	-0.000140305
(5,4)	0.00125041	0.000502969	0.00125041	-0.000502969
(4,5)	0.00125041	-0.000502969	0.00125041	0.000502969
(3,6)	-2.8743e-05	-0.000140305	-2.8743e-05	0.000140305
(2,7)	-0.000105269	5.24195e-05	-0.000105269	-5.24195e-05
(1,8)	-3.36914e-06	-2.41887e-06	-3.36914e-06	2.41887e-06
(0,9)	8.70891e-08	-7.2597e-08	8.70891e-08	7.2597e-08

Table 7: Coefficients up to order 10 of the components ψ^{y_1} and ψ^{y_2} of the parametrization Φ of the center manifold corresponding to the equilibrium point P_2 for $B = 0.53$ and $L = 0.75$. We consider the ordering $\lambda = (\lambda_-, -\lambda_-)$ and $\mu = (\lambda_+, -\lambda_+)$. Coefficients that are not included are exactly zero.

Observe that if the expansion were analytic this constant α would be 0.

Another possibility is to compute the inner dynamics using the normal form parametrization (see Remark 3.7). In this case, the secondary resonances are given by all the natural numbers $(m_1, m_2) \in \mathbb{N}^2$ satisfying $\{m_1 - m_2 = \pm 1\}$. In Tables 6 and 7 we show some coefficients (up to order 10) of the parametrization $\Phi = (\phi^{x_1}, \phi^{x_2}, \psi^{y_1}, \psi^{y_2})$ of this center manifold and in Table 8 we show some coefficients of $f(s)$, the corresponding normal form.

Computations regarding 1-dimensional stable (or unstable) manifolds of this point can be easily performed (we considered a 2-dimensional example for the point P_1). We also obserse that the study of the point P_3 is analogous to P_2. Indeed, an interesting case that we want to illustrate is when the point P_3 has the same energy as P_1. This occurs for

monomial	$\mathrm{Re}\,(f_k^{x_1})$	$\mathrm{Im}\,(f_k^{x_1})$	$\mathrm{Re}\,(f_k^{x_2})$	$\mathrm{Im}\,(f_k^{x_2})$
(1,0)	6.93889e-17	0.853957	0	0
(0,1)	0	0	6.93889e-17	-0.853957
(2,1)	8.59748e-18	0.0806328	0	0
(1,2)	0	0	7.29663e-18	-0.0806328
(3,2)	8.91419e-19	-0.0509597	0	0
(2,3)	0	0	-6.22969e-19	0.0509597
(4,3)	-3.18624e-19	0.0176595	0	0
(3,4)	0	0	1.34295e-19	-0.0176595
(5,4)	3.14502e-19	-0.00996741	0	0
(4,5)	0	0	1.29737e-19	0.00996741

Table 8: Coefficients up to order 10 of the components f^{x_1} and f^{x_2} of the normal form dynamics reduced to the center manifold, corresponding to the equilibrium point P_2 for $B = 0.53$ and $L = 0.75$. We consider the ordering $\lambda = (\lambda_-, -\lambda_-)$ and $\mu = (\lambda_+, -\lambda_+)$. The corresponding parametrization is given in Tables 6 and 7. Coefficients that are not included are exactly zero.

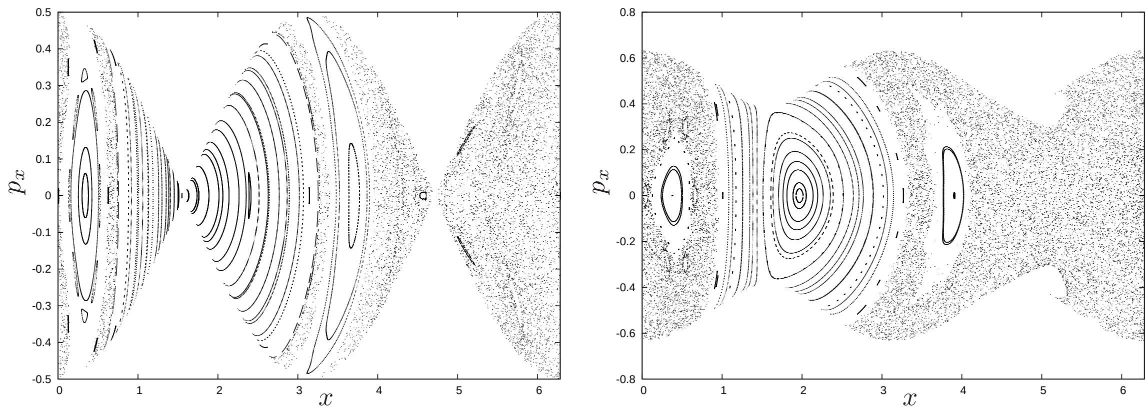

Figure 8: For $L = 1$, $B = 1/2$ and $C = 0$ we consider the neighborhood of the fixed point P_1, which is elliptic. The left plot corresponds to $H_0 = 0.125$ and the right one to $H_0 = 0.2$.

example for $L = 1$ and $B = 1/2$, where we have $H_1 = H_3 = 0.125$. In the left plot of Fig. 8 we consider the Poincaré section $\{z = 0\}$ corresponding to $H_0 = 0.125$, thus observing both equilibrium points. For higher energies (right plot of the same figure) we observe invariant tori close to the elliptic point P_1 and a large chaotic zone close to the saddle-elliptic point P_3.

Fourth equilibrium point: $P_4 = (3\pi/2, \pi, 0, 0)$. We showed in Section 3.2.1 that for $\Delta_2 < 0$ (and $L \neq 0$) we have the same situation that for P_1 in the hyperbolic case (stable focus - unstable focus). Hence, we shall concentrate on the case $\Delta_2 > 0$, where all the eigenvalues λ_+, λ_-, $-\lambda_+$ and $-\lambda_-$ of the Jacobian matrix are real, with $\lambda_+ > \lambda_-$.

It is straightforward to see that there are no primary resonances. Moreover, the secondary resonances of the normal form of the inner dynamics on the 2-dimensional unstable

monomial	$\psi_k^{y_1}$	$\psi_k^{y_2}$	$f_k^{x_1}$	$f_k^{x_2}$
(1,0)	0	0	-0.944991	0
(0,1)	0	0	0	-0.870053
(3,0)	-0.0994835	0.106097	-0.34439	-0.381632
(2,1)	0.310254	-0.332017	1.07602	1.18615
(1,2)	-0.323633	0.347306	-1.11662	-1.22554
(0,3)	0.112845	-0.121375	0.385213	0.421226
(5,0)	-0.00205931	0.00223559	0.00574643	0.00629344
(4,1)	0.0108957	-0.0118361	-0.0278447	-0.0305628
(3,2)	-0.0230744	0.0250792	0.0537762	0.0591733
(2,3)	0.0244459	-0.026582	-0.0517174	-0.0570702
(1,4)	-0.0129554	0.014093	0.0247531	0.0274045
(0,5)	0.00274742	-0.00298976	-0.00471357	-0.00523825
(7,0)	-3.87259e-05	4.1966e-05	0.000111378	0.000120531
(6,1)	0.000286344	-0.000310823	-0.0008163	-0.000884995
(5,2)	-0.000908924	0.000988251	0.00255803	0.00277822
(4,3)	0.00160549	-0.00174843	-0.00444285	-0.00483368
(3,4)	-0.00170428	0.00185893	0.00461883	0.00503372
(2,5)	0.0010872	-0.00118767	-0.0028741	-0.00313755
(1,6)	-0.000385892	0.000422179	0.000991129	0.00108379
(0,7)	5.87883e-05	-6.44083e-05	-0.000146113	-0.000160039
(9,0)	2.87867e-07	-3.01601e-07	4.97583e-06	5.34087e-06
(8,1)	-2.64586e-06	2.73831e-06	-4.73011e-05	-5.08024e-05
(7,2)	1.06767e-05	-1.08994e-05	0.00019954	0.000214431
(6,3)	-2.47897e-05	2.49083e-05	-0.000490299	-0.000527166
(5,4)	3.6419e-05	-3.5899e-05	0.000773361	0.000831917
(4,5)	-3.49925e-05	3.36682e-05	-0.000812087	-0.000873969
(3,6)	2.18787e-05	-2.03814e-05	0.000567719	0.000611238
(2,7)	-8.51431e-06	7.57236e-06	-0.000254796	-0.000274435
(1,8)	1.84529e-06	-1.52457e-06	6.66171e-05	7.17784e-05
(0,9)	-1.65119e-07	1.18771e-07	-7.73072e-06	-8.33258e-06

Table 9: Coefficients up to order 10 of the graph parametrization $\Phi = (\mathrm{Id}_{2\times 2}, \psi)$ of the 2-dimensional stable manifold and the components f^{x_1} and f^{x_2} of the inner dynamics, corresponding to the equilibrium point P_4 for $B = 0.1$ and $L = 1.5$. We take $\lambda = (-\lambda_+, -\lambda_-)$ and $\mu = (\lambda_+, \lambda_-)$.

manifold are given by the natural numbers m_1, m_2 such that

$$m_1\lambda_+ + m_2\lambda_- = \lambda_+ \qquad \text{or} \qquad m_1\lambda_+ + m_2\lambda_- = \lambda_- \,.$$

The first equation has solutions $m_1 = 1$, $m_2 = 0$ and $m_1 = 0$, $m_2 = \lambda_+/\lambda_-$ provided that $\lambda_+/\lambda_- \in \mathbb{N}$. The second equation has the unique solution $m_1 = 0$ and $m_2 = 1$. Therefore, we have to study the natural values of the quotient λ_+/λ_- as a function of the parameters B and L, that is (see Section 3.2.1)

$$\frac{\lambda_+}{\lambda_-} = \sqrt{\frac{\Delta_1 + \sqrt{\Delta_2}}{\Delta_1 - \sqrt{\Delta_2}}} = \sqrt{\frac{\Delta_1^2 + 2\Delta_1\sqrt{\Delta_2} + \Delta_2}{\Delta_1^2 - \Delta_2}} = n,$$

for $n \in \mathbb{N}$. Introducing the expressions of Δ_1 and Δ_2 in terms of the parameters B and L we obtain

$$\frac{(B+1)^2L^2 + (B+1)L\sqrt{(B+1)^2L^2 - 4B(B+L+1)^2}}{2B(B+L+1)^2} = n^2 + 1\,. \tag{28}$$

Obviously, this equation has infinitely many solutions since the left hand side tends to infinity when $B \to 0^+$. These solutions form a set of curves in the space of parameters (B, L). Accordingly, the normal form of the inner dynamics on the 2-dimensional unstable manifold at the point P_4 is the following:

$$f(s_1, s_2) = \begin{pmatrix} \lambda_+ s_1 + \alpha s_2^{\lambda_+/\lambda_-} \\ \lambda_- s_2 \end{pmatrix} \tag{29}$$

where the constant α vanishes provided that $\lambda_+/\lambda_- \notin \mathbb{N}$, i.e. if the pair (B, L) is not a solution of Eq. (28).

To illustrate this case, we take $B = 0.1$ and $L = 1.5$ (the case $\Delta_2 > 0$). For these parameters we have

$$\lambda_+ = 0.9449906626753889\,, \quad \lambda_- = 0.8700532440352883\,.$$

We compute, for example, the 2-dimensional stable manifold using the graph parametrization. We take $\lambda = (-\lambda_+, -\lambda_-)$ and $\mu = (\lambda_+, \lambda_-)$. Both the parametrization $\Phi = (\mathrm{Id}_{2\times 2}, \psi)$ and the corresponding inner dynamics are given (up to order 10) in Table 9. Note that $\lambda_+/\lambda_- \simeq 1.086$ so we can correct the parametrization in order to express the reduced dynamics as Eq. (29) with $\alpha = 0$.

3.2.3 Birkhoff normal form and quasi-periodic trajectories around the elliptic equilibrium P_1

We saw in Section 3.2.1 that the equilibrium point $P_1 = (\pi/2, 0, 0, 0)$ of the Hamiltonian vector field X_H is elliptic provided that $\Delta_2 > 0$ and $L \neq B + 1$. In this section we shall study this case in more detail by computing the Birkhoff normal form up to 4th order as a function of the parameters B and L. This computation will allow us to apply a KAM theorem to prove perpetual stability of the equilibrium P_1 and existence of infinitely many periodic and quasi-periodic motions in a neighborhood of P_1 for an open and dense set of values (B, L).

To this end, assume that B and L satisfy that $\Delta_2 > 0$ and $L \neq B + 1$. We first compute the normal (diagonal) form of the quadratic part of the Hamiltonian, see Eq. (5). The eigenvalues of the Jacobian matrix of X_H at P_1 computed in Section 3.2.1 are $\mathrm{i}\omega_1$, $\mathrm{i}\omega_2$, $-\mathrm{i}\omega_1$ and $-\mathrm{i}\omega_2$, cf. Eq. (17), with

$$\omega_1 := \sqrt{\frac{(1+B)L - \sqrt{(1+B)^2L^2 - 4B(B-L+1)^2}}{2}} \tag{30}$$

and

$$\omega_2 := \sqrt{\frac{(1+B)L + \sqrt{(1+B)^2L^2 - 4B(B-L+1)^2}}{2}}\,. \tag{31}$$

After a tedious but straightforward computation we compute a basis of eigenvectors for the matrix (16), associated to the eigenvalues $\mathrm{i}\omega_1$, $\mathrm{i}\omega_2$, $-\mathrm{i}\omega_1$, $-\mathrm{i}\omega_2$, which is given by the columns of the matrix

$$P := \begin{pmatrix} \omega_1(1+B) & \omega_2(1+B) & \omega_1(1+B) & \omega_2(1+B) \\ C_1\mathrm{i} & C_2\mathrm{i} & -C_1\mathrm{i} & -C_2\mathrm{i} \\ C_3\mathrm{i} & C_4\mathrm{i} & -C_3\mathrm{i} & -C_4\mathrm{i} \\ \omega_1^3 - BL\omega_1 & \omega_2^3 - BL\omega_2 & \omega_1^3 - BL\omega_1 & \omega_2^3 - BL\omega_2 \end{pmatrix}, \tag{32}$$

with

$$\begin{aligned} C_1 &:= (BL - B - B^2 - \omega_1^2)\,, \\ C_2 &:= (BL - B - B^2 - \omega_2^2)\,, \\ C_3 &:= (BL - B - B^2 + B\omega_1^2)\,, \\ C_4 &:= (BL - B - B^2 + B\omega_2^2)\,. \end{aligned}$$

This matrix provides the change of variables transforming the Jacobian matrix of X_H at P_1 into a diagonal matrix. However, the matrix P is not symplectic, so let us modify its columns in order to obtain a symplectic matrix $\tilde{P}$, that is $\tilde{P}^\top J \tilde{P} = J$, where J is the matrix representation of the canonical symplectic 2-form in $\mathbb{R}^4$. A direct computation shows that

$$P^\top JP = \begin{pmatrix} 0 & 0 & 2\omega_1(M+N\omega_1^2) & 0 \\ 0 & 0 & 0 & 2\omega_2(M+N\omega_2^2) \\ -2\omega_1(M+N\omega_1^2) & 0 & 0 & 0 \\ 0 & -2\omega_2(M+N\omega_2^2) & 0 & 0 \end{pmatrix}$$

where

$$\begin{aligned} M &:= B(L-1-B)(2+2B-L) + B^2L(L-1-B)\,, \\ N &:= 2B + 2B^2 - BL + L\,. \end{aligned}$$

It is easy to check that the function $M + N\omega_2^2$ is positive for any values of B and L while the function $M + N\omega_1^2$ changes sign on the line $L = B + 1$, more precisely $M + N\omega_1^2 < 0$ if and only if $L < 1 + B$. Since the computation of the symplectic matrix $\tilde{P}$ depends on the sign of $M + N\omega_1^2$, we need to consider two zones in the space of parameters:

Zone I: $M + N\omega_1^2 < 0 \Leftrightarrow L < 1 + B$. Defining

$$\lambda_1 := \sqrt{-2(M+N\omega_1^2)\omega_1}, \qquad \lambda_2 := \sqrt{2(M+N\omega_2^2)\omega_1},$$

we divide the four columns of the matrix P, cf. Eq. (32), by the factors λ_1, λ_2, λ_1 and λ_2, respectively. Then, the matrix $\tilde{P}$ is obtained by permutation of the first and third columns of this new P (it is straightforward to check that $\tilde{P}^\top J\tilde{P} = J$). It follows that, using the variables $(x - \pi/2, z, p_x, p_z)^\top = \tilde{P} \cdot (\tilde{x}, \tilde{z}, \tilde{p}_x, \tilde{p}_z)^\top$, the quadratic part of the new Hamiltonian is

$$H_2(\tilde{x}, \tilde{y}, \tilde{p}_x, \tilde{p}_y) = -\mathrm{i}\omega_1 \tilde{x}\tilde{p}_x + \mathrm{i}\omega_2 \tilde{y}\tilde{p}_y \,.$$

We can write H_2 in real coordinates by means of the transformation

$$q_1 = \frac{\tilde{x} + \mathrm{i}\tilde{p}_x}{\sqrt{2}}\,, \quad p_1 = \frac{\mathrm{i}\tilde{x} + \tilde{p}_x}{\sqrt{2}}\,, \quad q_2 = \frac{\tilde{z} + \mathrm{i}\tilde{p}_z}{\sqrt{2}}\,, \quad p_2 = \frac{\mathrm{i}\tilde{z} + \tilde{p}_z}{\sqrt{2}}\,, \tag{33}$$

thus obtaining

$$H_2(q_1, q_2, p_1, p_2) = -\frac{\omega_1}{2}(q_1^2 + p_1^2) + \frac{\omega_2}{2}(q_2^2 + p_2^2)\,.$$

The critical point of this Hamiltonian is obviously of saddle type, so the stability of the equilibrium point P_1 in this zone cannot be decided just from the second order term of the Hamiltonian, but we need to check some non-degeneracy conditions involving the Birkhoff normal form up to fourth order.

Zone II: $M + N\omega_1^2 > 0 \Leftrightarrow L > 1 + B$**.** Defining

$$\lambda_1 := \sqrt{2(M + N\omega_1^2)\omega_1}, \qquad \lambda_2 := \sqrt{2(M + N\omega_2^2)\omega_1},$$

we obtain the symplectic matrix $\tilde{P}$ simply by dividing the four columns of the matrix P, cf. Eq. (32), by the factors λ_1, λ_2, λ_1 and λ_2, respectively. Accordingly, using the variables $(x - \pi/2, z, p_x, p_z)^\top = \tilde{P} \cdot (\tilde{x}, \tilde{z}, \tilde{p}_x, \tilde{p}_z)^\top$ and the transformation (33), we obtain that the quadratic part of the new Hamiltonian is

$$H_2(q_1, q_2, p_1, p_2) = \frac{\omega_1}{2}(q_1^2 + p_1^2) + \frac{\omega_2}{2}(q_2^2 + p_2^2)\,.$$

The critical point of this Hamiltonian is an isolated minimum, and hence we infer that the equilibrium point P_1 is Lyapunov stable (Dirichlet theorem) in this zone. To prove the existence of quasi-periodic trajectories it is necessary to compute higher order terms.

Using the previous computations involving the quadratic part of the Hamiltonian, we are now ready to compute the Birkhoff normal form up to 4th order. Changing the variables by the translation

$$(x, z, p_x, p_z) \to (x - \pi/2, z, p_x, p_z)\,,$$

and still denoting by (x, z, p_x, p_z) the new variables, the expansion of the Hamiltonian around the equilibrium point P_1, see Eq. (5), is given by

$$H = H(P_1) + H_2 + \underbrace{h_1 x^4 + h_2 x^3 p_z + h_3 x^2 z^2 + h_4 z^4 + h_5 z^3 p_x}_{H_4} + \dots\,,$$

where $H(P_1) = \frac{1}{2}(L - B - 1)^2$ and

$$h_1 := \frac{B(1-L)}{24}\,, \quad h_2 := -\frac{B}{6}\,, \quad h_3 := \frac{B}{4}\,, \quad h_4 := \frac{B-L}{24}\,, \quad h_5 := \frac{1}{6}\,.$$

Note that the third order terms of the Hamiltonian vanish, which simplifies the computation of the Birkhoff normal form. Introducing the symplectic linear transformation given by the matrix $\tilde{P}$ computed above, which depends on the zone of the space of parameters, and assuming that there are no resonances up to order 4, that is

$$\omega_1 k_1 + \omega_2 k_2 \neq 0\,, \qquad k_i \in \mathbb{Z}\,,\ |k_1| + |k_2| \leq 4\,, \tag{34}$$

we get the Birkhoff normal form up to 4th order:

$$H = H(P_1) + H_2 + B_a \tilde{x}^2 \tilde{p}_x^2 + B_b \tilde{z}^2 \tilde{p}_z^2 + B_c \tilde{x}\tilde{z}\tilde{p}_x\tilde{p}_z + \ldots .$$

Since the terms of order 3 vanish, we do not need to compute the change of variables that removes the non-resonant terms of order 4. The coefficients B_a, B_b and B_c have the following expression in terms of the functions h_i and the elements $\tilde{P}_{i,j}$ of the matrix $\tilde{P}$ $(1 \leq i, j \leq 4)$:

$$\begin{aligned}
B_a :=\ & 6h_1\tilde{P}_{1,3}^2\tilde{P}_{1,1}^2 + 3h_2\tilde{P}_{1,3}\tilde{P}_{4,3}\tilde{P}_{1,1}^2 + 3h_2\tilde{P}_{1,3}^2\tilde{P}_{4,1}\tilde{P}_{1,1} + h_3\tilde{P}_{1,1}^2\tilde{P}_{2,3}^2 + 4h_3\tilde{P}_{1,3}\tilde{P}_{2,3}\tilde{P}_{1,1}\tilde{P}_{2,1}\\
&+ h_3\tilde{P}_{1,3}^2\tilde{P}_{2,1}^2 + 6h_4\tilde{P}_{2,3}^2\tilde{P}_{2,1}^2 + 3h_5\tilde{P}_{2,3}\tilde{P}_{3,3}\tilde{P}_{2,1}^2 + 3h_5\tilde{P}_{2,3}^2\tilde{P}_{3,1}\tilde{P}_{2,1}\\
B_b :=\ & 6h_1\tilde{P}_{1,4}^2\tilde{P}_{1,2}^2 + 3h_2\tilde{P}_{1,4}\tilde{P}_{4,4}\tilde{P}_{1,2}^2 + 3h_2\tilde{P}_{1,4}^2\tilde{P}_{4,2}\tilde{P}_{1,2} + h_3\tilde{P}_{1,2}^2\tilde{P}_{2,4}^2 + 4h_3\tilde{P}_{1,4}\tilde{P}_{2,4}\tilde{P}_{1,2}\tilde{P}_{2,2}\\
&+ h_3\tilde{P}_{1,4}^2\tilde{P}_{2,2}^2 + 6h_4\tilde{P}_{2,4}^2\tilde{P}_{2,2}^2 + 3h_5\tilde{P}_{2,4}\tilde{P}_{3,4}\tilde{P}_{2,2}^2 + 3h_5\tilde{P}_{2,4}^2\tilde{P}_{3,2}\tilde{P}_{2,2}\\
B_c :=\ & 24h_1\tilde{P}_{1,4}\tilde{P}_{1,1}\tilde{P}_{1,2}\tilde{P}_{1,3} + 6h_2\tilde{P}_{1,3}\tilde{P}_{4,4}\tilde{P}_{1,1}\tilde{P}_{1,2} + 6h_2\tilde{P}_{1,4}\tilde{P}_{4,3}\tilde{P}_{1,1}\tilde{P}_{1,2} + 6h_2\tilde{P}_{1,4}\tilde{P}_{4,2}\tilde{P}_{1,1}\tilde{P}_{1,3}\\
&+ 6h_2\tilde{P}_{1,4}\tilde{P}_{4,1}\tilde{P}_{1,2}\tilde{P}_{1,3} + 4h_3\tilde{P}_{1,2}\tilde{P}_{2,4}\tilde{P}_{1,1}\tilde{P}_{2,3} + 4h_3\tilde{P}_{1,3}\tilde{P}_{2,4}\tilde{P}_{1,1}\tilde{P}_{2,2} + 4h_3\tilde{P}_{1,4}\tilde{P}_{2,3}\tilde{P}_{1,1}\tilde{P}_{2,2}\\
&+ 4h_3\tilde{P}_{1,3}\tilde{P}_{2,4}\tilde{P}_{2,1}\tilde{P}_{1,2} + 4h_3\tilde{P}_{1,4}\tilde{P}_{2,3}\tilde{P}_{2,1}\tilde{P}_{1,2} + 4h_3\tilde{P}_{1,4}\tilde{P}_{2,2}\tilde{P}_{2,1}\tilde{P}_{1,3} + 24h_4\tilde{P}_{2,4}\tilde{P}_{2,1}\tilde{P}_{2,2}\tilde{P}_{2,3}\\
&+ 6h_5\tilde{P}_{2,3}\tilde{P}_{3,4}\tilde{P}_{2,1}\tilde{P}_{2,2} + 6h_5\tilde{P}_{2,4}\tilde{P}_{3,3}\tilde{P}_{2,1}\tilde{P}_{2,2} + 6h_5\tilde{P}_{2,4}\tilde{P}_{3,2}\tilde{P}_{2,1}\tilde{P}_{2,3} + 6h_5\tilde{P}_{2,4}\tilde{P}_{3,1}\tilde{P}_{2,2}\tilde{P}_{2,3}.
\end{aligned}$$

The coefficients B_a, B_b and B_c are explicit functions of the parameters B and L and depend through the matrix elements $\tilde{P}_{i,j}$ on whether we consider the zone I or II. Now, if we introduce the transformation (33) and define the action variables $I_1 = (q_1^2 + p_1^2)/2$ and $I_2 = (q_2^2 + p_2^2)/2$, we get that the Hamiltonian H is a perturbation of the integrable Hamiltonian

$$H_{\mathrm{int}} := H(P_1) \pm \omega_1 I_1 + \omega_2 I_2 - B_a I_1^2 - B_b I_2^2 - B_c I_1 I_2 \tag{35}$$

that defines the frequency map $\omega(I) = \nabla_I H_{\mathrm{int}}$. This concludes the computation of the Birkhoff normal form up to 4th order. To check the values of the parameters for which the non-resonance condition (34) holds, it is enough to consider the resonances $[2:1]$ and $[3:1]$, i.e. $\omega_2 = 2\omega_1$ and $\omega_2 = 3\omega_1$. (The resonance $[1:1]$ coincides with the curve $\Delta_2 = 0$, where the Hamiltonian-Hopf bifurcation takes place, and hence it is excluded from this study.) A short computation

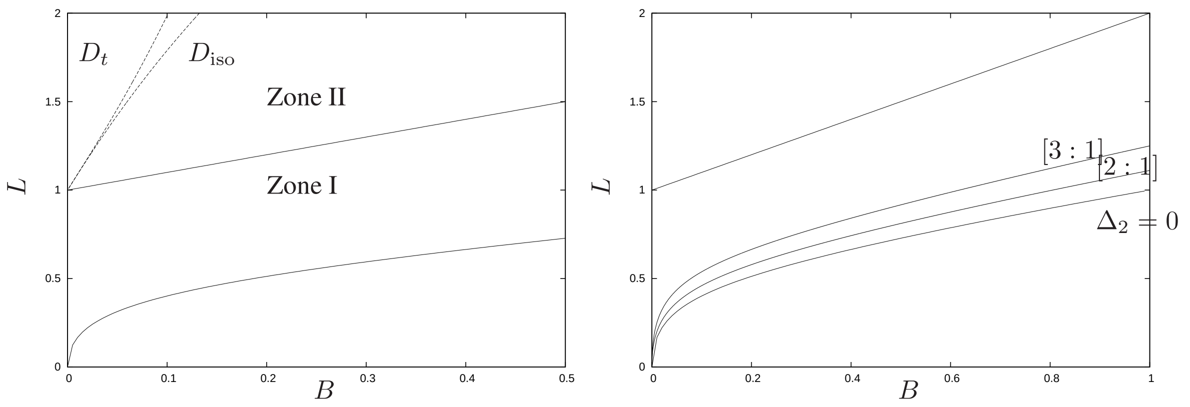

Figure 9: Left: Curves representing the violation of non-degeneracy conditions in the space of parameters. Curve D_t corresponds to (37), and curve $D_{\rm iso}$ corresponds to (38). Right: Curves representing the Hopf and parabolic bifurcations and also the resonant lines $[2:1]$ and $[3:1]$.

shows that these resonances define the following curves on the space of parameters (see the right plot of Fig. 9):

$$L = \frac{2\sqrt{B}(B+1)}{c(1+B)+2\sqrt{B}}\,, \tag{36}$$

where $c = \sqrt{8/9}$ for the resonance $[2:1]$ and $c = \sqrt{3/4}$ for the resonance $[3:1]$.

The computation of the Birkhoff normal form up to 4th order allows us to study the stability of the equilibrium point and the existence of periodic and quasi-periodic trajectories using KAM theory. For this we must check a non-degeneracy condition for the unperturbed Hamiltonian $H_{\rm int}$, cf. Eq. (35). Concretely, $H_{\rm int}$ satisfies the twist condition (in the sense of Kolmogorov) if

$$\det\left(\frac{\partial \omega}{\partial I}(I)\right) \neq 0 \iff 4B_aB_b - B_c^2 \neq 0\,. \tag{37}$$

On the other hand, $H_{\rm int}$ satisfies the isoenergetic non-degeneracy condition provided that

$$\det\begin{pmatrix} \frac{\partial\omega}{\partial I}(I) & \omega(I) \\ \omega(I)^\top & 0 \end{pmatrix}_{(I_1=0,I_2=0)} \neq 0 \iff \omega_1^2 B_b + \omega_2^2 B_a \pm \omega_1\omega_2 B_c \neq 0\,, \tag{38}$$

where the $\pm$ sign depends on the whether we consider the zone I or II, respectively.

The twist condition (37) is violated on a curve in the space of parameters that we denote by D_t, see the left plot of Fig. 9. The isoenergetic condition (38) is not satisfied on a curve that we denote by $D_{\rm iso}$ in the left plot of Fig. 9. Both conditions fail also at the line $L = B+1$. Let us recall that the point P_1 is parabolic at the line $L = B+1$ that separates Zone I and Zone II, and that the curve $\Delta_2 = 0$, which limits the bottom of Zone I, is given by Eq. (18). Note that the curves D_t and $D_{\rm iso}$ approach each other tangentially at the point $(B,L) = (0,1)$ and are contained in Zone II. Applying the classical KAM theorem [38] we conclude that for any (B, L) in Zones I and II which is not contained in D_t, in the curve $L = B + 1$, nor in the $[3 : 1]$ and $[2 : 1]$ resonance curves, there exist a large Cantor set of quasi-periodic trajectories near the elliptic equilibrium P_1. On the other hand, for any (B, L) in Zones I and II which is not contained in the curve D_{iso} nor in the aforementioned resonant lines, the isoenergetic KAM theorem [12] implies that on each energy level there exist infinitely many quasi-periodic trajectories in any small neighborhood of the equilibrium point P_1. Since these invariant tori separate the energy levels, we also get that P_1 is Lyapunov stable and that there are infinitely many periodic trajectories on account of the Poincaré-Birkhoff theorem. This proves Theorem 2.2 stated in Section 2. We refer to [12, 38] for estimates on the measure of these invariant tori as one approaches the equilibrium point (e.g. if ω_1 and ω_2 are Diophantine, then the complement of the set filled by invariant tori has measure exponentially small with respect to the distance to the point).

We finish this section with a few comments on the motion of the charge in the configuration space. The elliptic equilibrium P_1 corresponds to an elliptic periodic trajectory of the charge which follows a magnetic line in $\mathbb{T}^3$. It is easy to see that this magnetic line is elliptic, with characteristic exponents $\pm i\sqrt{B}$, provided that $B \neq 0$, and it is surrounded by toroidal magnetic surfaces. As far as the motion of charges is concerned, if the parameters B and $L = p_y$ (a constant of the motion) belong to the open and dense set described above (where isoenergetic KAM theorem can be applied) then we conclude that a charge lying in a small enough neighborhood of this magnetic line will remain in a neighborhood of the line for all time provided that its velocity in the transversal directions is small. This shows the existence of confinement regions of the motion.

4 Chaos and non-integrability of the motion

In this section we shall highlight the complexity of the dynamics of charges under ABC magnetic fields, which is described by the 3DOF Hamiltonian system (2)-(3). More precisely, we shall focus on the non-integrability and the existence of chaos in the sense of splitting of separatrices. In Section 4.1 we show that for $B = 1$, $C = 0$ and $L = 0$, there does not exist an additional analytic first integral (of certain type) using Morales-Ramis theory. In Section 4.2 we prove the existence of a transverse intersection of the stable and unstable manifolds associated to invariant tori when B and C are small enough using a Melnikov potential approach. This implies that there is a chaotic invariant set, which illustrates by means of a toy model, the complex behavior of the motion of plasma charged particles in a tokamak. Moreover, the normally hyperbolic invariant manifold obtained in this range of parameters can be seen as an skeleton to study global behavior of the motion.

4.1 Analytic non-integrability via Morales-Ramis theory

In this section we assume that $C = 0$, which allows us to consider the reduced 2DOF Hamiltonian system (5)-(7) in the coordinates $(x, z, p_x, p_z) \in \mathbb{T}^2 \times \mathbb{R}^2$. Our goal is to prove that this system does not admit an additional first integral of certain type when the parameter $L = 0$. The tool that we shall use is Morales-Ramis theory [33], for which we need a particular solution of Eqs. (7) in order to compute the Galois group of its associated normal variational equation. In the case that $B = 1$ and $L = 0$ there is a periodic trajectory $\gamma(t)$ that can be used for this purpose, which corresponds to the motion along the closed curve given by $\{(x, y, z) \in \mathbb{T}^3 : y = y_0, z = x + \pi/2\}$ for any $y_0 \in \mathbb{S}^1$, which is the union of two heteroclinic magnetic lines connecting two singular points of the ABC magnetic field. A straightforward computation yields the following expression of the trajectory $\gamma(t)$ in the reduced coordinates:

$$
\begin{aligned}
x(t) &= t\,, \\
z(t) &= t + \pi/2\,, \\
p_x(t) &= \cos t + 1\,, \\
p_z(t) &= \cos t + 1\,.
\end{aligned}
$$

This trajectory corresponds to motion along the curve $\{(x, y, z) \in \mathbb{T}^3 : y = y_0, z = x + \pi/2\}$ with momentum $p_y = 0$ and velocity $\dot{y} = 0$. Notice that it is no longer a solution of Eqs. (7) for $L \neq 0$.

The main result of this section is Theorem 2.3 stated in Section 2. To prove it, we consider the normal variational equation (NVE) of the Hamiltonian ODEs (7) with $L = 0$ at the trajectory $\gamma(t)$. A straightforward computation shows that Eqs. (7) are equivalent to the following system of second order differential equations, which is very convenient to compute the NVE:

$$
\begin{aligned}
\ddot{x} &= -(\cos x + \dot{z})(\sin x + \cos z)\,, \\
\ddot{z} &= (\sin z + \dot{x})(\sin x + \cos z)\,.
\end{aligned}
$$

The variational equation can be computed substituting $x(t) = t + \xi_1(t)$ and $z(t) = t + \pi/2 + \xi_2(t)$ into these equations, thus yielding

$$
\begin{aligned}
\ddot{\xi}_1 &= \cos t(\cos t + 1)(-\xi_1 + \xi_2)\,, \\
\ddot{\xi}_2 &= -\cos t(\cos t + 1)(-\xi_1 + \xi_2)\,.
\end{aligned}
$$

Therefore, the NVE is the second order ODE for the variable $\xi := -\xi_1 + \xi_2$, which reads as:

$$
\ddot{\xi} = -2\cos t(1 + \cos t)\xi\,. \tag{39}
$$

Notice that the equation for $\eta := \xi_1 + \xi_2$ is $\ddot{\eta} = 0$, which simply means that two of the four eigenvalues of the variational equation at $\gamma(t)$ are 1 (those corresponding to the direction of the trajectory and its Hamiltonian conjugate). The computation of the Galois group of Eq. (39) can be done using Kovacic's algorithm [28]. To this end we first algebrize the equation changing the time variable as $s = \exp(it)$, thus obtaining

$$\xi'' + \frac{1}{s}\,\xi' - \frac{(1+s)^2(1+s^2)}{2s^4}\,\xi = 0\,.$$

Here the derivative with respect to s is denoted by ξ'. It is convenient to change the unknown ξ by $\psi := s^{1/2}\xi$ to write the ODE in the way Kovacic's algorithm is usually stated:

$$\psi'' = \frac{2 + 4s + 3s^2 + 4s^3 + 2s^4}{4s^4}\,\psi\,. \tag{40}$$

Since this ODE is of the form $\psi'' = r(s)\psi$, where $r(s)$ is a rational function, Kovacic's algorithm can be directly applied to conclude that this equation does not have any non trivial Liouvillian solution, and hence its Galois group is $SL(2,\mathbb{C})$. Computations are straightforward, so details are omitted.

To apply Morales-Ramis theory in order to study the analytic integrability of the Hamiltonian system (5)-(7), we have to complexify the phase space $\mathbb{T}^2 \times \mathbb{R}^2$. This is easy after realizing that the phase space is the cotangent bundle $T^*(\mathbb{S}^1 \times \mathbb{S}^1)$, and that the complexification of $\mathbb{S}^1$ is $\mathbb{C}^* = \mathbb{C}\backslash\{0\}$, so the complex phase space is $T^*(\mathbb{C}^* \times \mathbb{C}^*)$. A convenient symplectic coordinate system to perform this complexification is given by

$$\begin{aligned}
\tilde{x} &= \exp(ix)\,,\\
\tilde{z} &= \exp iz\,,\\
\tilde{p}_x &= -ip_x \exp(-ix)\\
\tilde{p}_z &= -ip_z \exp(-iz)\,.
\end{aligned}$$

The complexification of the trajectory $\gamma(t)$ in these coordinates $(\tilde{x}, \tilde{z}, \tilde{p}_x, \tilde{p}_z) \in T^*(\mathbb{C}^* \times \mathbb{C}^*)$ is the Riemann surface $\gamma_{\mathbb{C}}(t)$:

$$\begin{aligned}
\tilde{x} &= \exp(it)\,,\\
\tilde{z} &= i\exp(it)\,,\\
\tilde{p}_x &= -i\Big(\frac{1}{2} + \exp(-it) + \frac{1}{2}\exp(-2it)\Big)\,,\\
\tilde{p}_z &= -\Big(\frac{1}{2} + \exp(-it) + \frac{1}{2}\exp(-2it)\Big)\,,
\end{aligned}$$

for $t \in \mathbb{C}$. It is ready to see that the singularities (of irregular type) $s = 0$ and $s = \infty$ of the NVE (40) do not belong to the phase space $T^*(\mathbb{C}^* \times \mathbb{C}^*)$. The reason is that, after the change $s = \exp(it)$, we have that $\lim_{s\to 0}\gamma_{\mathbb{C}}(t)$ is the point $(0,0) \notin \mathbb{C}^* \times \mathbb{C}^*$ in the $(\tilde{x}, \tilde{z})$ variables and it tends to infinity in the $(\tilde{p}_x, \tilde{p}_z)$ variables, while $\lim_{s\to\infty}\gamma_{\mathbb{C}}(t)$ goes to infinity in the (x, z) variables. Accordingly, to apply Morales-Ramis theory, we have to compactify the phase space

$T^*(\mathbb{C}^* \times \mathbb{C}^*)$, which forces to consider a class of meromorphic functions that remains meromorphic after compactification, and hence a natural class is that of rational functions in the variables $(\tilde{x}, \tilde{z}, \tilde{p}_x, \tilde{p}_z)$. In the original variables this obviously implies that the functions are rational in $\sin x, \cos x, \sin z, \cos z, p_x$ and p_z. Since the Galois group of the NVE (39) is not Abelian (it is $SL(2, \mathbb{C})$), we conclude that Theorem 2.3 then follows from a direct application of a result by Morales and Ramis [33, Theorem 4.3].

4.2 Splitting of separatrices and Melnikov potential

In this section we consider the 3DOF Hamiltonian system (2)-(3) and we prove that, for small generic values of B and C, there exist invariant tori whose associated stable and unstable manifolds (also called whiskers) intersect transversally. It is well known that this implies the existence of a chaotic invariant set, i.e. a hyperbolic invariant set supporting a horseshoe type dynamics. Our method of proof is a modification of the construction presented in [13] combined with a hyperbolic KAM theorem proved in [16]. The additional aspects that we have to consider, which prevent from a direct application of [13], are related to the fact that our unperturbed Hamiltonian H_0 is not of the form studied in the aforementioned reference.

We assume that the parameters B and C are small enough and we write them, for the sake of convenience, as $B = \varepsilon\tilde{B}$ and $C = \varepsilon\tilde{C}$, so that ε is a 1-dimensional perturbation parameter. Accordingly, the Hamiltonian H, cf. Eq. (2), is quadratic in ε and has the form $H = H_0 + \varepsilon H_1 + \mathcal{O}(\varepsilon^2)$, where the unperturbed Hamiltonian H_0 (i.e. for $B = C = 0$) is given by

$$H_0 := \frac{1}{2}(p_x - \sin z)^2 + \frac{1}{2}(p_y - \cos z)^2 + \frac{p_z^2}{2}, \tag{41}$$

and the first order term of the perturbation is

$$H_1 := -[\tilde{C}\cos y(p_x - \sin z) + \tilde{B}\sin x(p_y - \cos z) + p_z(\tilde{B}\cos x + \tilde{C}\sin y)]. \tag{42}$$

This is the only term of the ε-expansion of H that is needed in this section. The Hamiltonian H_0 is Liouville integrable (with additional first integrals p_x and p_y), so we can integrate its dynamics to deduce that it has a 4-dimensional normally hyperbolic invariant manifold foliated by 2-dimensional non-degenerate invariant tori. Details will be given below. This setting of invariant tori with homoclinic connections (the associated stable and unstable manifolds coincide) suggests using a Melnikov function to study the splitting of separatrices for $\varepsilon \neq 0$ small enough. Let us divide the construction of the Melnikov potential in four steps, as in Ref. [13].

Step 1: Study of the integrable Hamiltonian H_0. The system of ODEs associated to the unperturbed Hamiltonian H_0, cf. Eq. (41), is:

$$\begin{aligned} \dot{x} &= p_x - \sin z, & \dot{p}_x &= 0, \\ \dot{y} &= p_y - \cos z, & \dot{p}_y &= 0, \\ \dot{z} &= p_z, & \dot{p}_z &= p_x\cos z - p_y\sin z, \end{aligned} \tag{43}$$

so p_x and p_y are constants of the motion. There is no loss of generality in taking positive values of p_x and p_y, so we shall assume it in what follows. The integration of this system of ODEs is elementary. Indeed, the equations in the variables (z, p_z) correspond to a pendulum-like system, depending on the parameters p_x, p_y, which has a hyperbolic equilibrium at the point

$$z^* = \arctan \frac{p_x}{p_y} + \pi, \qquad p_z^* = 0\,.$$

Since $p_x > 0$ and $p_y > 0$, a straightforward computation yields the identities

$$\sin z^* = \frac{-p_x}{\sqrt{p_x^2 + p_y^2}}\,, \qquad \cos z^* = \frac{-p_y}{\sqrt{p_x^2 + p_y^2}}\,, \tag{44}$$

thus implying that the energy $H_0^* := H_0(x, y, z^*, p_x, p_y, p_z^*)$ of the equilibrium point is given by

$$H_0^* = \frac{1}{2}(p_x - \sin z^*)^2 + \frac{1}{2}(p_y - \cos z^*)^2 = \frac{1}{2}\left(1 + \sqrt{p_x^2 + p_y^2}\right)^2 \geq \frac{1}{2}\,.$$

This expression implies that $p_x^2 + p_y^2 = (\sqrt{2H_0^*} - 1)^2$, so a very convenient way of writing the constants of the motion p_x and p_y is the following

$$p_x = (\sqrt{2H_0^*} - 1)\sin\alpha\,, \qquad p_y = (\sqrt{2H_0^*} - 1)\cos\alpha\,,$$

with $\alpha = \arctan \frac{p_x}{p_y} \in (0, \pi/2)$ and $H_0^* > 1/2$. With this notation, the pendulum-like equation in the variables (z, p_z) reads as

$$\ddot{z} = p_x \cos z - p_y \sin z = (\sqrt{2H_0^*} - 1)\sin(\alpha - z)\,,$$

thus obtaining that there is a homoclinic orbit connecting the equilibrium point given by

$$z^0(t) = 4 \arctan \mathrm{e}^{\lambda t} + \alpha + \pi\,, \quad p_z^0(t) = \frac{2\lambda}{\cosh(\lambda t)}\,, \tag{45}$$

where

$$\lambda := \sqrt{\sqrt{2H_0^*} - 1} = (p_x^2 + p_y^2)^{1/4} \tag{46}$$

is the positive eigenvalue of the hyperbolic equilibrium. It is straightforward to check that $z^0(t) \to z^*$ and $p_z^0(t) \to p_z^* = 0$, exponentially with exponent λ, as $t \to \pm\infty$. There is a second homoclinic trajectory connecting the equilibrium point given by $\bar{z}^0(t) = -z^0(t) + 2\alpha$ and $\bar{p}_z^0(t) = -p_z^0(t)$, but it will not be used in what follows.

The previous computations imply that the Hamiltonian system H_0 has a 4-dimensional normally hyperbolic invariant manifold

$$\Lambda := \{(q, p) \in \mathbb{T}^3 \times \mathbb{R}^3 \,:\, z = z^*, p_z = p_z^*, p_x > 0, p_y > 0\}\,,$$

which is foliated by 2-dimensional invariant tori $\mathcal{T}_{p_x,p_y}$ obtained by fixing the values of $p_x > 0$ and $p_y > 0$ in Λ, i.e. $\Lambda = \bigcup_{p_x,p_y} \mathcal{T}_{p_x,p_y}$. An easy computation shows that the dynamics on each invariant torus $\mathcal{T}_{p_x,p_y}$ is linear with frequency vector $\omega = (\omega_1, \omega_2)$ given by

$$\begin{aligned} \omega_1 &:= p_x - \sin(\arctan(p_x/p_y) + \pi) \\ &= p_x(1 + (p_x^2 + p_y^2)^{-1/2}) = \sqrt{2H_0^*}\sin\alpha = -\sqrt{2H_0^*}\sin z^* \,, \end{aligned} \tag{47}$$

$$\begin{aligned} \omega_2 &:= p_y - \cos(\arctan(p_x/p_y) + \pi) \\ &= p_y(1 + (p_x^2 + p_y^2)^{-1/2}) = \sqrt{2H_0^*}\cos\alpha = -\sqrt{2H_0^*}\cos z^* \,. \end{aligned} \tag{48}$$

The stable and unstable manifolds of Λ, which coincide, are 5-dimensional invariant sets defined by

$$W^s(\Lambda) = W^u(\Lambda) = \{(q,p) \in \mathbb{T}^3 \times \mathbb{R}^3 \,:\, z = z^0(\tau), p_z = p_z^0(\tau), \tau \in \mathbb{R}\} \,,$$

so obviously the set Λ is the union of the stable (unstable) manifolds of the invariant tori $\mathcal{T}_{p_x,p_y}$, i.e.

$$W^s(\Lambda) = \bigcup_{p_x,p_y} W^s(\mathcal{T}_{p_x,p_y}) = W^u(\Lambda) = \bigcup_{p_x,p_y} W^u(\mathcal{T}_{p_x,p_y}) \,.$$

In order to work with the invariant tori $\mathcal{T}_{p_x,p_y}$ and their whiskers $W^s(\mathcal{T}_{p_x,p_y}) = W^u(\mathcal{T}_{p_x,p_y})$, we introduce appropriate parametrizations. First, the torus $\mathcal{T}_{p_x,p_y} \subset \Lambda$ can be defined as the image of an embedding $u^* : \mathbb{T}^2 \to \mathbb{T}^3 \times \mathbb{R}^3$ of the form

$$u^*(x,y) = (x, y, z^*, p_x, p_y, p_z^*) \,, \tag{49}$$

where p_x and p_y are fixed and $(x,y) \in \mathbb{T}^2$, so that $u^*(\mathbb{T}^2) = \mathcal{T}_{p_x,p_y}$. Moreover, for the stable manifold $W^s(\mathcal{T}_{p_x,p_y})$ we introduce the embedding $u^0 : \mathbb{R} \times \mathbb{T}^2 \to \mathbb{T}^3 \times \mathbb{R}^3$ of the form

$$u^0(\tau, x, y) = (x + F_1(\tau), y + F_2(\tau), z^0(\tau), p_x, p_y, p_z^0(\tau)) \,, \tag{50}$$

where $\tau \in \mathbb{R}$, $(x,y) \in \mathbb{T}^2$, the functions z^0 and p_z^0 are defined in Eq. (45), and

$$\begin{aligned} F_1(\tau) &:= \sin(z^*)\tau - \int_0^\tau \sin(z^0(\sigma))d\sigma \,, \\ F_2(\tau) &:= \cos(z^*)\tau - \int_0^\tau \cos(z^0(\sigma))d\sigma \,. \end{aligned}$$

It is easy to check that $u^0(\mathbb{R} \times \mathbb{T}^2) = W^s(\mathcal{T}_{p_x,p_y})$. The parametrizations (49) and (50) have been chosen in such a way that

$$\begin{aligned} &t \mapsto u^*(x + \omega_1 t, y + \omega_2 t) \,, \\ &t \mapsto u^0(\tau + t, x + \omega_1 t, y + \omega_2 t) \end{aligned}$$

are solutions of the unperturbed Hamiltonian system (43) with initial conditions $u^*(x,y)$ and $u^0(\tau, x, y)$, respectively.

We observe that the functions F_1 and F_2 depend on the constants p_x and p_y through z^* and z^0, but we omit this dependence in order to avoid cumbersome notation. After straightforward but tedious computations we can obtain the following explicit formulas:

$$F_1(\tau) = \left(\frac{2(\tanh(\lambda\tau)-1)}{\lambda} + \frac{2}{\lambda}\right)\sin z^* - \left(\frac{2\mathrm{sech}(\lambda\tau)}{\lambda} - \frac{2}{\lambda}\right)\cos z^*\,,$$
$$F_2(\tau) = \left(\frac{2(\tanh(\lambda\tau)-1)}{\lambda} + \frac{2}{\lambda}\right)\cos z^* + \left(\frac{2\mathrm{sech}(\lambda\tau)}{\lambda} - \frac{2}{\lambda}\right)\sin z^*\,,$$

where the constant λ is defined in Eq. (46). These functions allow us to compute the *phase shift* of any trajectory when traveling along $W^s(\mathcal{T}_{p_x,p_y})$, which is associated to the coupling between the variables z, p_x and p_y in the unperturbed Hamiltonian H_0, Indeed, the phase-shift is defined by the limits (that do not depend on τ)

$$\begin{array}{ll} x_+ := \lim_{t\to\infty} F_1(\tau+t)\,, & x_- := \lim_{t\to-\infty} F_1(\tau+t)\,, \\ y_+ := \lim_{t\to\infty} F_2(\tau+t)\,, & y_- := \lim_{t\to-\infty} F_2(\tau+t)\,, \end{array}$$

which can be explicitly computed, taking into account the expressions of F_1 and F_2, to yield

$$x_\pm = 2\frac{(\mp p_x - p_y)}{(p_x^2+p_y^2)^{3/4}}\,, \qquad y_\pm = 2\frac{(p_x \mp p_y)}{(p_x^2+p_y^2)^{3/4}}\,.$$

The main property related to the phase shift is the following estimate that shows that the trajectories on the invariant torus $\mathcal{T}_{p_x,p_y}$ corrected by the phase shift, and the trajectories on the whiskers $W^{s,u}(\mathcal{T}_{p_x,p_y})$, are exponentially close with rate λ as $t \to \pm\infty$. More precisely

$$\begin{array}{ll} |u^0(\tau+t, x+\omega_1 t, y+\omega_2 t) - u^*(x+x_+ +\omega_1 t, y+y_+ +\omega_2 t)| \leq C\mathrm{e}^{-\lambda t}\,, & t \geq 0\,, \\ |u^0(\tau+t, x+\omega_1 t, y+\omega_2 t) - u^*(x+x_- +\omega_1 t, y+y_- +\omega_2 t)| \leq C\mathrm{e}^{-\lambda |t|}\,, & t \leq 0\,, \end{array} \tag{51}$$

for any $\tau \in \mathbb{R}$ and $(x,y) \in \mathbb{T}^2$, for some constant $C > 0$. These estimates, which can be easily proved using the explicit expressions obtained before and that reflect the normal hiperbolicity of the invariant torus $\mathcal{T}_{p_x,p_y}$, will be used later on to justify the construction of the Melnikov potential.

Remark 4.1. *It is interesting to note that the invariant tori* $\mathcal{T}_{p_x,p_y}$ *correspond to the toroidal magnetic surfaces* $z = z^*$ *in the configuration space* $\mathbb{T}^3$*. Moreover, the magnetic field on each surface is linear, i.e.* $\mathbf{B}_{ABC}|_{z=z^*} = (\sin z^*, \cos z^*, 0)$*, and the trajectories follow the magnetic lines. Let us observe that the slope of the magnetic lines* $\tan z^*$ *coincides with the ratio of the frequencies* ω_1/ω_2*, cf. Eqs.* (47) *and* (48)*.*

Step 2: A hyperbolic KAM theorem. In order to study the splitting of separatrices in the perturbed Hamiltonian system H, we need to establish the existence of a whiskered torus that is a deformation of the invariant torus $\mathcal{T}_{p_x,p_y}$ provided that ε is small enough, as well as its local stable and unstable manifolds. This result is often referred as a *hyperbolic KAM theorem* since it follows from a convergent KAM-like iteration scheme. The hyperbolic KAM theorem used in [13, Section 2.1] was proved by Eliasson in [14, Theorem B], but we cannot apply it here because our unperturbed Hamiltonian H_0 has not the same form as in Eliasson's construction, concretely it contains a coupling term between the variables z, p_x and p_y. Instead, we resort to a parametrization method recently developed in [16]. The following theorem, which is a slight rewording of [16, Theorem 9.3], deals with the persistence of whiskered invariant tori for Hamiltonian systems, and is enough for our purposes. As usual, we denote by

$$J = \begin{pmatrix} 0 & \mathrm{Id}_n \\ -\mathrm{Id}_n & 0 \end{pmatrix}$$

the standard symplectic matrix.

Theorem 4.2. *Let H be an analytic Hamiltonian function on a $2n$-dimensional manifold $\mathcal{M}$ endowed with the canonical symplectic structure J. Assume that*

1. *The frequency vector $\omega \in \mathbb{R}^r$, $r < n$, satisfies a Diophantine condition, i.e., there exist constants $\gamma > 0$ and $\nu > r - 1$ such that*

$$|\langle \omega, k \rangle| \geq \frac{\gamma}{|k|_1^\nu}, \qquad \forall k \in \mathbb{Z}^r \backslash \{0\}.$$

2. *There exists an embedding $u : \mathbb{T}^r \to \mathcal{M}$ which corresponds to an approximate invariant torus with frequency ω of the Hamiltonian vector field X_H, that is*

$$\frac{d}{dt} u(\theta + \omega t) = X_H(u(\theta + \omega t)) + e(\theta + \omega t),$$

   where e is the error function, satisfying $\|e\| \leq \varepsilon$ for a suitable norm of C^ω functions.

3. *Twist condition: the average of the $(r \times r)$-matrix*

$$A(\theta) := N(\theta) Du(\theta)^\top [D^2 H(u(\theta)) + J D^2 H(u(\theta)) J] Du(\theta) N(\theta),$$

   where $N(\theta) := (Du(\theta)^\top Du(\theta))^{-1}$, is non-singular, i.e. $\det[A]_{\mathbb{T}^r} \neq 0$.

4. *Spectral condition: there is an analytic splitting*

$$T_{u(\theta)} \mathcal{M} = \mathcal{E}^s_{u(\theta)} \oplus \mathcal{E}^u_{u(\theta)} \oplus \mathcal{E}^c_{u(\theta)}$$

   invariant under the linearized equation

$$\frac{d}{dt} U_\theta(t) = J D^2 H(u(\theta + \omega t)) U_\theta(t), \qquad U_\theta(0) = \mathrm{Id},$$

in the sense that $U_\theta(t)\mathcal{E}^\sigma_{u(\theta)} = \mathcal{E}^\sigma_{u(\theta+\omega t)}$, for $\sigma = s, u, c$. Moreover, the center subspace $\mathcal{E}^c_{u(\theta)}$ has dimension $2r$. We denote by $U^\sigma_\theta(t)$, for $\sigma = s, c, u$, the projection of $U_\theta(t)$ according to the above splitting. Then, we assume that there exist $\beta_1, \beta_2, \beta_3 > 0$ and $C > 0$, all of them independent of θ and satisfying $\beta_3 < \beta_1$ and $\beta_3 < \beta_2$, such that the splitting is characterized by the following rate conditions:

$$
\begin{aligned}
&|U^s_\theta(t)U^s_\theta(\tau)^{-1}| \le C\mathrm{e}^{-\beta_1(t-\tau)}, && t \ge \tau \ge 0\,.\\
&|U^u_\theta(t)U^u_\theta(\tau)^{-1}| \le C\mathrm{e}^{\beta_2(t-\tau)}, && t \le \tau \le 0\,.\\
&|U^c_\theta(t)U^c_\theta(\tau)^{-1}| \le C\mathrm{e}^{\beta_3|t-\tau|}, && t, \tau \in \mathbb{R}\,.
\end{aligned}
$$

Then, if ε is small enough, there exists an embedding $u_\varepsilon : \mathbb{T}^r \to \mathcal{M}$ that corresponds to a true invariant torus of X_H of frequency vector ω, and $\|u_\varepsilon - u\|$ is controlled by an amount of order ε.

Now we apply this theorem in order to study the persistence of the invariant torus $\mathcal{T}_{p_x,p_y}$ of the Hamiltonian (41) under perturbations. To this end, we notice that the parametrization u^* of an invariant torus for the unperturbed system H_0, see Eq. (49), gives us a parametrization of an approximately invariant torus for the perturbed Hamiltonian H, the error function being

$$e(x, y) = -\varepsilon J\nabla H_1(u^*(x, y)) + \mathcal{O}(\varepsilon^2),$$

where H_1 is given in (42). It is obvious that $||e(x, y)|| \le C_k\varepsilon$ for any C^k norm. Item 2 of Theorem 4.2 then holds for the parametrization $u^*(x, y)$, so $\mathcal{T}_{p_x,p_y}$ is a good candidate to persist (up to a small deformation) after perturbations. To fulfill item 1 of the theorem we have to choose the values p_x and p_y such that the frequency vector (ω_1, ω_2), cf. Eqs. (47) and (48), is Diophantine. Indeed, this is possible because

$$k_1\omega_1 + k_2\omega_2 = \sqrt{2H_0^*}\cos\alpha(k_1\tan\alpha + k_2)\,,$$

and we simply have to select α such that $(\tan\alpha, 1) = (p_x/p_y, 1)$ is a Diophantine vector, which holds for a dense set of values of p_x and p_y.

Next, we have to check that the twist and spectral conditions of Theorem 4.2 hold for the approximately invariant torus $u^*(x, y)$ of the Hamiltonian system H. Indeed, an easy computation shows that

$$A(x, y) = -\begin{pmatrix}1 & 0\\ 0 & 1\end{pmatrix} + \mathcal{O}(\varepsilon)\,,$$

so its average is clearly non-singular for ε small enough.

Finally, we check the spectral condition. To this end, notice that H_0 gives rise to an splitting formed by a 4-dimensional center subspace (the tangent space of Λ, given by the tangent directions of the torus and the symplectic conjugate ones), a 1-dimensional stable subspace of rate $-\lambda$ and a 1-dimensional unstable subspace of rate λ (associated to the hyperbolic equilibrium (z^*, p_z^*) of the pendulum-like subsystem of H_0). With the notation of item 4 of Theorem 4.2 we have that $\beta_1^0 = \beta_2^0 = \lambda$ and $\beta_3^0 = 0$, recall that λ is a positive number defined in Eq. (46).

Now we use a perturbative result in [16, Proposition 8.19], which says that an invariant splitting with the properties described in item 4 of Theorem 4.2 is persistent under perturbations, and we conclude that the Hamiltonian $H = H_0 + \mathcal{O}(\varepsilon)$ also defines a perturbed invariant splitting with the same properties as the invariant splitting of H_0. Moreover, the constants $\beta_1, \beta_2, \beta_3$ can be estimated as

$$\beta_1 = \lambda + \mathcal{O}(\varepsilon)\,, \quad \beta_2 = \lambda + \mathcal{O}(\varepsilon)\,, \quad \beta_3 = \mathcal{O}(\varepsilon)\,,$$

and hence the rate conditions $\beta_3 < \beta_1$ and $\beta_3 < \beta_2$ hold provided that ε is small enough (remember that we are assuming that $p_x > 0$ and $p_y > 0$).

Since all the hypotheses of Theorem 4.2 are satisfied by the embedding u^* of $\mathcal{T}_{p_x,p_y}$, for an appropriate choice of p_x and p_y, the theorem implies that there exists a parametrization u^*_ε of an invariant torus of the Hamiltonian H, so that

$$\mathcal{T}^\varepsilon_{p_x,p_y} := u^*_\varepsilon(\mathbb{T}^2)$$

is ε-close to $\mathcal{T}_{p_x,p_y}$, and its local stable and unstable manifolds are ε-close to $W^{s,u}(\mathcal{T}_{p_x,p_y})$.

Remark 4.3. *Recall from Eqs.* (47) *and* (48) *that the frequency vector of an invariant torus* $\mathcal{T}_{p_x,p_y}$ *of* H_0 *is given by* $(\omega_1, \omega_2) = -\sqrt{2H_0^*}(\sin z^*, \cos z^*)$. *Let us also observe that such invariant torus corresponds to a toroidal magnetic surface* $z = z^*$ *of the ABC magnetic field* $\mathbf{B}_{ABC} = (\sin z, \cos z, 0)$ *with* $B = C = 0$. *Then, it turns out that* (ω_1, ω_2) *is Diophantine if and only if the slope of the unperturbed magnetic field on the toroidal magnetic surface* $z = z^*$ *is Diophantine. We conclude that invariant tori* $\mathcal{T}^\varepsilon_{p_x,p_y}$ *of* H *are associated to deformed toroidal magnetic surfaces of the perturbed magnetic field* $\mathbf{B}_{ABC}$ *with* $B = \varepsilon\tilde{B}$ *and* $C = \varepsilon\tilde{C}$. *The existence of these toroidal magnetic surfaces is an easy application of Moser's theorem, since the return map of the unperturbed magnetic field on the section* $\{y = 0\}$ *is given by* $(x, z) \to (x + 2\pi \tan z, z)$, *which is a twist map with non-degenerate rotation number* $\tan z$.

Step 3: The Melnikov potential. Once we have established the existence of the whiskered invariant torus $\mathcal{T}^\varepsilon_{p_x,p_y}$, the next step is to study the intersection of its stable and unstable manifolds. It turns out that our system admits a Melnikov potential of the same form that [13, Equation (31)], even though our Hamiltonian H_0 has a different coupling term involving the variables z, p_x and p_y. Concretely, the splitting is measured by means of the following result:

Theorem 4.4. *The Melnikov potential* $L : \mathbb{T}^2 \to \mathbb{R}$ *associated to the invariant torus* $\mathcal{T}^\varepsilon_{p_x,p_y}$ *of the Hamiltonian system* H *is defined by*

$$L(x, y) = -\int_{-\infty}^{\infty} (H_1 - [H_1]_{\mathbb{T}^2} - \{\chi, H_0\})(u^0(t, x + \omega_1 t, y + \omega_2 t))dt \tag{52}$$

where u^0 *is the parametrization of the unperturbed whisker introduced in Eq.* (50) *and* $\chi(x, y)$ *is a function associated to the first order correction of* $\mathcal{T}^\varepsilon_{p_x,p_y}$ *with respect to* $\mathcal{T}_{p_x,p_y}$ *that will be defined below. Recall that* H_0 *and* H_1 *are defined in Eqs.* (41) *and* (42), *respectively, and that* $[\cdot]_{\mathbb{T}^2}$ *denotes the average on the torus, as usual.*

The proof of this theorem is essentially the same as the proof of [13, Proposition 5], so we will not give all the details. We will focus just on the aspects that are not straightforward from [13] because of the presence of a different coupling term in H_0. In particular, we need to prove results analogous to Lemmas 2 and 3 of [13, Section 2.2]. Note that the hyperbolic KAM theorem established in [13, Section 2.1] is substituted by Theorem 4.2 in our context. To this end, we have to compute the first order expansion in ε of the parametrization

$$u_\varepsilon^*(x,y) = u^*(x,y) + \varepsilon u_1^*(x,y) + \mathcal{O}(\varepsilon^2)$$

of the perturbed invariant torus $\mathcal{T}^\varepsilon_{p_x,p_y} = u_\varepsilon^*(\mathbb{T}^2)$. The following lemma plays the role of [13, Lemma 2]:

Lemma 4.5. *Let us consider a perturbed torus $\mathcal{T}^\varepsilon_{p_x,p_y}$ with Diophantine frequency vector ω, and denote by*

$$u_\varepsilon^*(x,y) =: (x_\varepsilon^*, y_\varepsilon^*, z_\varepsilon^*, p_{x,\varepsilon}^*, p_{y,\varepsilon}^*, p_{z,\varepsilon}^*) \tag{53}$$

the coordinates of its parametrization, where their dependence with $(x,y) \in \mathbb{T}^2$ is not explicitly written for the sake of brevity. Then

$$p_{x,\varepsilon}^* = p_x + \varepsilon(\zeta_1 - \partial_x\chi) + \mathcal{O}(\varepsilon^2)\,, \tag{54}$$

$$p_{y,\varepsilon}^* = p_y + \varepsilon(\zeta_2 - \partial_y\chi) + \mathcal{O}(\varepsilon^2)\,, \tag{55}$$

where ζ_1, ζ_2 are constants, and $\chi(x,y)$ is the solution of the small divisors equation

$$L_\omega\chi = H_1(u^*(x,y)) - [H_1(u^*(x,y))]_{\mathbb{T}^2}\,, \qquad L_\omega = \omega_1\partial_x + \omega_2\partial_y\,. \tag{56}$$

Proof. Since u_ε^* is an invariant torus of the Hamiltonian system $H = H_0 + \varepsilon H_1 + \mathcal{O}(\varepsilon^2)$, it satisfies the equation

$$L_\omega u_\varepsilon^*(x,y) = J\nabla H(u_\varepsilon^*(x,y))\,,$$

which in the coordinates introduced in (53) reads as

$$\begin{aligned}
L_\omega x_\varepsilon^*(x,y) &= p_{x,\varepsilon}^* - \sin(z_\varepsilon^*) + \partial_{p_x}H_1(u_\varepsilon^*(x,y)) + \mathcal{O}(\varepsilon^2)\,,\\
L_\omega y_\varepsilon^*(x,y) &= p_{y,\varepsilon}^* - \cos(z_\varepsilon^*) + \partial_{p_y}H_1(u_\varepsilon^*(x,y)) + \mathcal{O}(\varepsilon^2)\,,\\
L_\omega z_\varepsilon^*(x,y) &= p_{z,\varepsilon}^* + \partial_{p_z}H_1(u_\varepsilon^*(x,y)) + \mathcal{O}(\varepsilon^2)\,,\\
L_\omega p_{x,\varepsilon}^*(x,y) &= -\partial_x H_1(u_\varepsilon^*(x,y)) + \mathcal{O}(\varepsilon^2)\,,\\
L_\omega p_{y,\varepsilon}^*(x,y) &= -\partial_y H_1(u_\varepsilon^*(x,y)) + \mathcal{O}(\varepsilon^2)\,,\\
L_\omega p_{z,\varepsilon}^*(x,y) &= p_{x,\varepsilon}^*\cos(z_\varepsilon^*) - p_{y,\varepsilon}^*\sin(z_\varepsilon^*) - \partial_z H_1(u_\varepsilon^*(x,y)) + \mathcal{O}(\varepsilon^2)\,.
\end{aligned}$$

Expanding these equations with respect to ε and taking the first order terms we get

$$L_\omega x_1^*(x,y) = p_{x,1}^* - \cos(z^*)z_1^* + \partial_{p_x}H_1(u^*(x,y))\,, \tag{57}$$

$$L_\omega y_1^*(x,y) = p_{y,1}^* + \sin(z^*) z_1^* + \partial_{p_y} H_1(u^*(x,y))\,, \tag{58}$$
$$L_\omega z_1^*(x,y) = p_{z,1}^* + \partial_{p_z} H_1(u^*(x,y))\,, \tag{59}$$
$$L_\omega p_{x,1}^*(x,y) = -\partial_x H_1(u^*(x,y))\,, \tag{60}$$
$$L_\omega p_{y,1}^*(x,y) = -\partial_y H_1(u^*(x,y))\,, \tag{61}$$
$$L_\omega p_{z,1}^*(x,y) = \sin(z^*)(p_{y,1}^* - p_x z_1^*) + \cos(z^*)(p_{x,1}^* - p_y z_1^*) - \partial_z H_1(u^*(x,y))\,. \tag{62}$$

To prove the lemma we have to solve Eqs. (60) and (61) to obtain $p_{x,1}^*$ and $p_{y,1}^*$. Using the definition of the function $\chi(x,y)$, cf. Eq. (56), we obtain that

$$L_\omega(p_{x,1}^* + \partial_x \chi) = -\partial_x H_1(u^*(x,y)) + \partial_x H_1(u^*(x,y)) = 0\,,$$

and since ω is a non-resonant (in fact Diophantine) vector, we conclude that

$$p_{x,1}^* + \partial_x \chi = \zeta_1\,,$$

for some constant ζ_1, thus proving Eq. (54). The proof of Eq. (55) is completely analogous. □

Remark 4.6. *The constants $\zeta_1 = [p_{x,1}^*]_{\mathbb{T}^2}$ and $\zeta_2 = [p_{y,1}^*]_{\mathbb{T}^2}$ can be computed taking averages in equations* (57)*,* (58) *and* (62)*. This provides a set of equations to determine these constants, but we omit this computation because the precise values of ζ_1 and ζ_2 will not be used in what follows.*

The proof of [13, Lemma 3] on certain asymptotic properties of the perturbed whiskers of $\mathcal{T}_{p_x,p_y}^\varepsilon$ in our context follows proceeding as in [13], mutatis mutandis, using the hyperbolic KAM theorem 4.2 and the asymptotic estimate for the phase shift established in Eq. (51). Details are omitted to avoid unnecessary repetitions.

Finally, the last property that we need to check to prove Theorem 4.4 is to show that the Melnikov potential $L(x,y)$ of Eq. (52) is a well defined analytic function. If the function $H_1 - [H_1]_{\mathbb{T}^2} - \{\chi, H_0\}$ is identically 0 when evaluated at the parametrization $u^*(x,y)$ of the unperturbed invariant torus $\mathcal{T}_{p_x,p_y}$, it is standard that the convergence of the integral defining $L(x,y)$ follows from the normal hiperbolicity and the asymptotic estimate (51) for the phase shift (see Eq. (33) and the discussion that follows in Ref. [13]). Indeed, this property can be easily checked using Eq. (41) for the expression of H_0, Eqs. (47) and (48) for ω_1 and ω_2, and Eq. (56) defining χ, i.e.

$$\{\chi, H_0\}(u^*(x,y)) = (p_x - \sin z^*)\partial_x \chi + (p_y - \cos z^*)\partial_y \chi = (\omega_1 \partial_x + \omega_2 \partial_y)\chi = L_\omega \chi\,,$$

to yield that

$$[H_1 - [H_1]_{\mathbb{T}^2} - \{\chi, H_0\}](u^*(x,y)) = H_1(u^*(x,y)) - [H_1(u^*(x,y))]_{\mathbb{T}^2} - L_\omega \chi = 0\,.$$

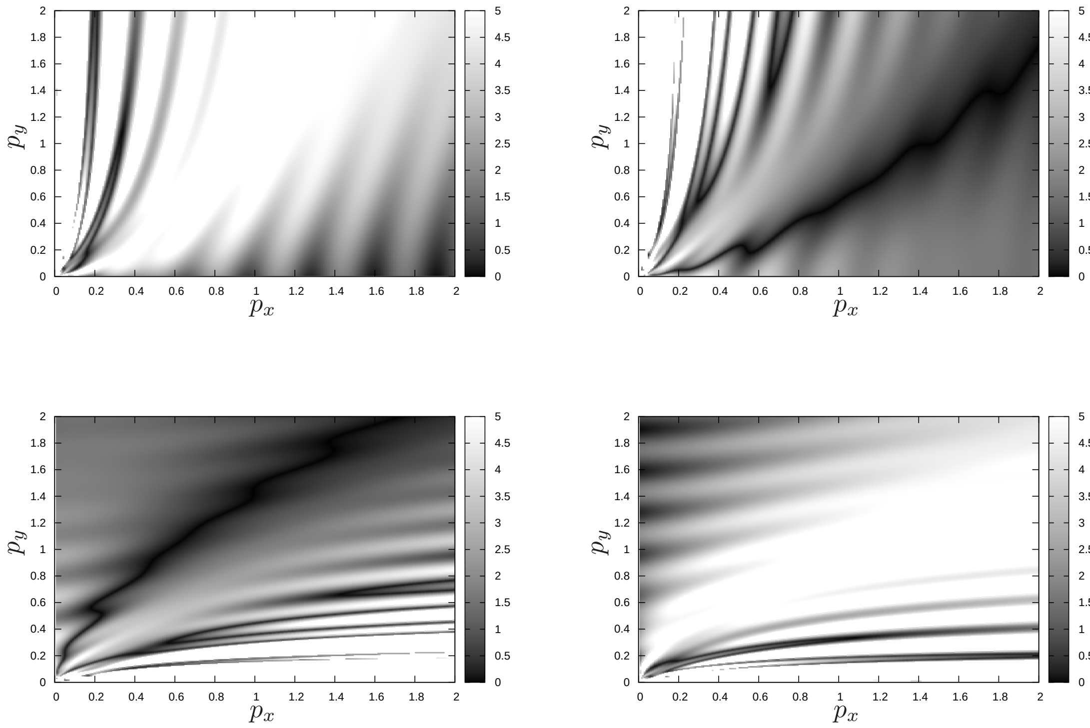

Figure 10: Coefficients of the Melnikov potential (63) in the space of parameters p_x and p_y. We plot $L_1/\tilde{B}$ (top-left), $L_2/\tilde{B}$ (top-right), $L_3/\tilde{C}$ (bottom-left) and $L_4/\tilde{C}$ (bottom-right). We use a grey color palette that shows in black those points where these coefficients vanish.

Finally, proceeding as in the proof of [13, Proposition 5], it is not difficult to state the connection between the Melnikov potential and the splitting of the invariant whiskers of the torus.

Step 4: Transverse intersection of the perturbed whiskers. Let us now compute the explicit expression of the Melnikov potential $L(x,y)$ for the perturbation H_1 considered in this paper, cf. Eq. (42). First, we note that Eq. (56) for $\chi(x,y)$ can be easily solved to give

$$\chi = \tilde{B}\frac{\omega_2}{\omega_1}\cos x - \tilde{C}\frac{\omega_1}{\omega_2}\sin y\,,$$

where we have used that $[H_1(u^*(x,y))]_{\mathbb{T}^2} = 0$. Then, after a straightforward but long computation, we obtain the Melnikov potential, which is the following trigonometric polynomial:

$$L(x,y) = L_1\cos(x) + L_2\sin(x) + L_3\cos(y) + L_4\sin(y), \tag{63}$$

where the constants L_i are defined by these convergent integrals:

$$L_1 = \tilde{B} \int_{-\infty}^{\infty} \Big((p_y - \cos z^0 - \frac{\omega_2}{\omega_1}(p_x - \sin z^0)) \sin(\omega_1 t + F_1) + p_z^0 \cos(\omega_1 t + F_1) \Big) dt \,,$$
$$L_2 = \tilde{B} \int_{-\infty}^{\infty} \Big((p_y - \cos z^0 - \frac{\omega_2}{\omega_1}(p_x - \sin z^0)) \cos(\omega_1 t + F_1) - p_z^0 \sin(\omega_1 t + F_1) \Big) dt \,,$$
$$L_3 = \tilde{C} \int_{-\infty}^{\infty} \Big((p_x - \sin z^0 - \frac{\omega_1}{\omega_2}(p_y - \cos z^0)) \cos(\omega_2 t + F_2) + p_z^0 \sin(\omega_2 t + F_2) \Big) dt \,,$$
$$L_4 = \tilde{C} \int_{-\infty}^{\infty} \Big(- (p_x - \sin z^0 - \frac{\omega_1}{\omega_2}(p_y - \cos z^0)) \sin(\omega_2 t + F_2) + p_z^0 \cos(\omega_2 t + F_2) \Big) dt \,.$$

Observe that the coefficients L_i only depend on p_x and p_y, and they do not vanish simultaneously for most values of these parameters (see Fig. 10). This proves Theorem 2.4 stated in Section 2. The non-degenerate critical points of the Melnikov potential $L(x, y)$ give rise to transverse homoclinic intersections between the perturbed whiskers of the torus $\mathcal{T}^{\varepsilon}_{p_x,p_y}$ provided that ε is small enough. Since the critical points (x_c, y_c) of the Melnikov potential (63) are

$$x_c = \arctan \frac{L_2}{L_1} \,, \qquad y_c = \arctan \frac{L_4}{L_3} \,,$$

which are non-degenerate for generic values of (p_x, p_y) provided that $\tilde{B} \neq 0$ and $\tilde{C} \neq 0$, we conclude the existence of transverse intersections and hence chaos in the Hamiltonian system H for small enough values of B and C, as we desired to prove.

Remark 4.7. *The results presented in this section imply that the motion of a charge near the perturbed magnetic surfaces shown in Remark 4.3 is chaotic provided that $B \neq 0$ and $C \neq 0$ are small enough. Additionally, since these magnetic surfaces correspond to normally hyperbolic invariant tori, there are some trajectories which are asymptotic to them, but generically all the motions are unstable.*

5 Conclusions and final remarks

In this paper we have studied the motion of a charged particle in the presence of ABC magnetic fields. In the case $C = 0$, which is the so-called laminar ABC dynamo, we have analyzed the local dynamics near the different equilibria of the reduced system in terms of the parameter B (see Section 3). For the particular case $C = 0$, $B = 1$ and $L = 0$ we have proved that there does not exist an additional first integral of the motion of certain regularity (cf. Section 4.1). In Section 4.2 we have established the existence of a normally hyperbolic invariant manifold and a chaotic invariant set for small generic values of the parameters B and C, which is obtained by means of the intersection of stable and unstable whiskers of the perturbed invariant tori inside the normally hyperbolic invariant manifold.

This work has established some interesting connections between the dynamics of a charge and the structure of the ABC magnetic fields, so let us summarize them:

1. For $C = 0$, $B > 0$ and $L \ll 1$ (the conserved momentum p_y is small), there is a toroidal magnetic surface in $\mathbb{T}^3$ such that the motion with small velocity is confined in a neighborhood of it and exhibits periodic and quasi-periodic trajectories (see Theorem 2.1 and Section 3.1).

2. For $C = 0$ and a large set of values of (B, L) there is a closed magnetic line in $\mathbb{T}^3$, which is the core of a family of toroidal magnetic surfaces, such that the motion is confined for all time in a neighborhood of this magnetic line. Such region is associated to the elliptic equilibrium point P_1 (see Theorem 2.2 and Section 3.2.3).

3. For $C = 0$ and generic values of (B, L), there are three unstable periodic trajectories in the configuration space $\mathbb{T}^3$ (those associated to the unstable equilibria P_2, P_3 and P_4 of the reduced system), which follow closed magnetic lines (see Remark 3.6).

4. For small generic values of B and C, there is a family of toroidal magnetic surfaces supporting quasi-periodic and chaotic motions in a neighborhood of them (see Theorem 2.4 and Section 4.2). As far as we know this is the first rigorous verification of chaos for the motion of a charge in a magnetic field, see e.g. [1, Problem 7.1].

All these results can be interpreted in the context of plasma physics since the motion of charges in ABC magnetic fields is a toy model for the motion of plasma charged particles in a tokamak. In this respect, the existence of confinement regions around closed magnetic lines that we have proved is particularly relevant, the only downside being that this confinement is in the symmetric case $C = 0$ (laminar dynamo). To finish, we would like to call the reader's attention to the following open problems and future lines of research:

Problem 5.1. *For generic values of B and C, we have seen that the set of equilibrium points of the motion in the full ABC system is given by a 3-dimensional submanifold $\mathcal{N}$ that is diffeomorphic to $\mathbb{T}^3$. In this work we have studied the local behavior of this submanifold for the particular case $C = 0$ and arbitrary values of B. The most interesting case $C > 0$ is more demanding and a very rich dynamics is expected. Facing this case may require to use singular perturbation theory and computational methods.*

Problem 5.2. *Apart from equilibrium points and periodic orbits, it would be interesting to detect and characterize regions in phase space carrying quasi-periodic motions for arbitrary values of C (beyond the equilibrium submanifold $\mathcal{N}$), starting of course with $C \ll 1$. Studying the stability of these objects and the possible connections between them is key in order to understand the global dynamics of the ABC system. This study can provide a wide set of fruitful results that can be remarkable in the context of plasma physics (stability, transport phenomena, design of devices, etc).*

Problem 5.3. *When B and C are small but not zero, we have seen that the motion associated to the ABC magnetic field is non integrable, which is the most interesting (and typical) situation in regard to plasma physics. In this case we have proved that the motion is chaotic and that there is a normally hyperbolic invariant manifold, so being a 3DOF Hamiltonian system one would expect the existence of Arnold diffusion. This is a very important phenomenon in the context of confinement of hot plasmas for fusion power generation because of the harmful plasma-wall interaction. The study of Arnold diffusion in ABC magnetic fields will be the goal of a future contribution.*

Acknowledgements

The authors are very grateful to David Blázquez-Sanz for his explanations and suggestions concerning Morales-Ramis theory and its application in this context. A.L. is supported by the Spanish MICINN-FEDER grant MTM2009-06973, the CUR-DIUE grant 2009SGR859 and the Juan de la Cierva program JCI-2010-06517. D.P.-S. is supported by the Spanish MINECO under grant no. MTM2010-21186-C02-01, the ICMAT Severo Ochoa project SEV-2011-0087 and the Ramón y Cajal program.

References

[1] J. Aguirre, A. Luque and D. Peralta-Salas, Motion of charged particles in magnetic fields created by symmetric configuration of wires. Phys. D 239 (2010) 654–674.

[2] E.M. Alessi, A. Farrés, À. Jorba, C. Simó and A. Vieiro, Efficient Usage of Self Validated Integrators for Space Applications. European Space Agency, the Advanced Concepts Team, Ariadna Final Report 07-5202 (2008). Available electronically at `http://www.maia.ub.es/dsg/2008/index.shtml`

[3] V.I. Arnold, Sur la topologie des écoulements stationnaires des fluides parfaits. C. R. Acad. Sci. Paris 261 (1965) 17–20.

[4] R. Barrio, Performance of the Taylor series method for ODEs/DAEs. Appl. Math. Comput. 163 (2005) 525–545.

[5] M. Braun, Particle motions in a magnetic field. J. Differential Equations 8 (1970) 294–332.

[6] P. Caldirolli and M. Guida, Helicoidal trajectories of a charge in a nonconstant magnetic field. Adv. Differential Equations 12 (2007) 601–622.

[7] C. Castilho, The motion of a charged particle on a Riemannian surface under a non-zero magnetic field. J. Differential Equations 171 (2001) 110–131.

[8] S. Chandrasekhar and L. Woltjer, On force-free magnetic fields. Proc. Natl. Acad. Sci. 44 (1958) 285–289.

[9] C. Chicone, A geometric approach to regular perturbation theory with an application to hydrodynamics. Trans. Amer. Math. Soc. 347 (1995) 4559–4598.

[10] C. Chicone, *Ordinary Differential Equations with Applications*. Springer, New York, 1999.

[11] S. Childress, New solutions of the kinematic dynamo problem. J. Math. Phys. 11 (1970) 3063–3076.

[12] A. Delshams and P. Gutierrez, Estimates on Invariant Tori near an Elliptic Equilibrium Point of a Hamiltonian System. J. Differential Equations 131 (1996) 277–303.

[13] A. Delshams and P. Gutierrez, Splitting Potential and the Poincaré-Melnikov Method for Whiskered Tori in Hamiltonian Systems. J. Nonlinear Sci. 10 (2000) 433–476.

[14] L.H. Eliasson, Biasymptotic solutions of perturbed integrable Hamiltonian systems. Bol. Soc. Bras. Mat 25 (1994) 343–411.

[15] N. Flyer, B. Fornberg, S. Thomas and B.C. Low, Magnetic field confinement in the solar corona I: force-free magnetic fields. Astrophys. J. 606 (2004) 1210–1222.

[16] E. Fontich, R. de la Llave and Y. Sire, Construction of invariant whiskered tori by a parameterization method. Part I: Maps and flows in finite dimensions. J. Differential Equations 246 (2009) 3136–3213.

[17] J. Fortágh and C. Zimmermann, Magnetic microtraps for ultracold atoms. Rev. Mod. Phys. 79 (2007) 235–289.

[18] A.D. Gilbert, Magnetic field evolution in steady chaotic flows. Phil. Trans. R. Soc. Lond. A 339 (1992) 627–656.

[19] GSL-GNU Scientific library. `http://www.gnu.org/software/gsl/gsl.html`. Last update in 2008.

[20] E.M. Haacke, R.W. Brown, R. Venkatesan and M.R. Thompson, *Magnetic Resonance Imaging*. Wiley, New York (1999).

[21] A. Haro, Automatic differentiation tools in computational dynamical systems. Preprint available electronically at `http://www.maia.ub.es/dsg/preprints.html` (2008).

[22] D.-B. Huang, X.-H. Zhao and H.-H. Dai, Invariant tori and chaotic streamlines in the ABC flow. Phys. Lett. A 237 (1998) 136–140.

[23] M. Iñarrea, V. Lanchares, J.F. Palacián, A.I. Pascual, J.P. Salas and P. Yanguas, Symplectic coordinates on $\mathbb{S}^2 \times \mathbb{S}^2$ for perturbed Keplerian problems: Application to the dynamics of a generalised Störmer problem. J. Differential Equations 250 (2011) 1386–1407.

[24] J.D. Jackson, *Classical Electrodynamics*. Wiley, New York (1999)

[25] À. Jorba, A methodology for the numerical computation of normal forms, centre manifolds and first integrals of Hamiltonian systems. Exp. Math. 8 (1999) 155–195.

[26] À. Jorba and M. Zou, A software package for the numerical integration of ODEs by means of high-order Taylor methods. Exp. Math. 14 (2005) 99–117.

[27] B. Krauskopf, H. M. Osinga, E. J. Doedel, M. E. Henderson, J. Guckenheimer, A. Vladimirsky, M. Dellnitz and O. Junge, A survey of methods for computing (un)stable manifolds of vector fields. Internat. J. Bifur. Chaos Appl. Sci. Engrg. 15 (2005) 763–791.

[28] J.J. Kovacic, An algorithm for solving second order linear homogeneous differential equations. J. Symbolic Computation 2 (1986) 3–43.

[29] R. de la Llave and À. Jorba, Regularity properties of center manifolds and applications. Preprint.

[30] A. Luque and J. Villanueva, Numerical computation of rotation numbers of quasi-periodic planar curves. Phys. D 238 (2009) 2025–2044.

[31] A.J. Maciejewski and M. Przybylska, Non integrability of ABC flow. Phys. Lett. A 303 (2002) 265–272.

[32] L. Michelotti, *Intermediate Classical Dynamics with Applications to Beam Physics*. Wiley, New York (1995).

[33] J.J. Morales-Ruiz, *Differential Galois Theory and Non-integrability of Hamiltonian Systems*. Birkhauser, Basel (1999).

[34] T.G. Northrop, *The Adiabatic Motion of Charged Particles*. Interscience, New York (1963).

[35] D. Pinheiro and R.S. Mackay, Interaction of two charges in a uniform magnetic field I: planar problem. Nonlinearity 19 (2006) 1713–1745.

[36] D. Pinheiro and R.S. Mackay, Interaction of two charges in a uniform magnetic field II: spatial problem. J. Nonlinear Sci. 18 (2008) 615–666.

[37] C.J.A. Pires, et al., Magnetic field structure in the TCABR tokamak due to ergodic limiters with a non-uniform current distribution. Plasma Phys. Control. Fusion 47 (2005) 1609–1632.

[38] J. Poschel, Integrability of Hamiltonian systems on Cantor sets. Comm. Pure Appl. Math. 35 (1982) 653–695.

[39] C.L. Siegel and J.K. Moser, *Lectures on Celestial Mechanics*. Springer-Verlag, New York, 1971.

[40] C. Simó, On the Analytical and Numerical Approximation of Invariant Manifolds. In Méthodes Modernes de la Mécanique Céleste, pp. 285–329, Editions Frontières, Paris, 1990.

[41] C. Simó, Global dynamics and fast indicators. Global analysis of dynamical systems, 373–389, IOP, Bristol, 2001.

[42] A.M. Soward, Fast dynamo action in a steady flow. J. Fluid Mech. 180 (1987) 267–295.

[43] J.B. Taylor, Relaxation of toroidal plasma and generation of reverse magnetic fields. Phys. Rev. Lett. 33 (1974) 1139–1141.

[44] J.B. Taylor, Relaxation and magnetic reconnection in plasmas. Rev. Mod. Phys. 58 (1986) 741–763.

[45] F. Truc, Trajectoires borneés d'une particule soumise á un champ magnétique symétrique linéaire. Ann. Inst. Henri Poincaré A 64 (1996) 127–154.

[46] R.K. Varma, Classical and macroquantum dynamics of charged particles in a magnetic field. Phys. Rep. 378 (2003) 301–434.

[47] G.E. Vekstein, N.A. Bobrova and S.V. Bulanov, On the motion of charged particles in a sheared force-free magnetic field. J. Plasma Phys. 67 (2002) 215–221.

[48] D.G. Wentzel, Motion of charged particles in a force-free magnetic field. Astrophys. J. 126 (1957) 559–564.

[49] D.M. Willis, The motion of an isolated charged particle in a simple force-free magnetic field. Planet. Space Sci. 14 (1966) 483–501.

[50] S.L. Ziglin, Splitting of the separatrices and the nonexistence of first integrals in systems of differential equations of Hamiltonian type with two degrees of freedom. Math. USSR Izv. 31 (1988) 407–421.

[51] S.L. Ziglin, The ABC flow is not integrable for A=B. Funct. Anal. Appl. 30 (1996) 137–138.

A Taylor method for the integration of vector fields

Although Runge-Kutta methods are still popular in some scientific and technical communities, it is well known that Taylor methods are much more efficient to perform both long term and high accurate computations (to the extent that the use of explicit methods is a suitable choice). Actually, very efficient packages have been developed to this purpose and are available to the public (see [4, 26]). Moreover, it turns out that developing a Taylor integrator for the ABC system is specially simple. The aim of this appendix is to briefly describe the implementation of Taylor methods. The reason is not only presenting this method to readers from more applied fields, but it turns out that the underlying idea of automatic differentiation is very close to the one used to evaluate normal forms (to be described in Appendix B).

Consider the initial value problem

$$x'(t) = f(t, x(t)) \,, \qquad x(a) = x_0 \,,$$

where f is assumed to be analytic in its domain of definition, and $x(t)$ is assumed to be defined for $t \in [a, b]$. We are interested in approximating the function $x(t)$ on $[a, b]$ by a polynomial. The idea of the Taylor method is very simple: given the initial condition $x(t_0) = x_0$, where $t_0 = a$, the value $x(t_0 + h_0)$ is approximated from the Taylor series of the solution $x(t)$ at $t = t_0$. We obtain the sequence

$$x(t_0) = x_0, \qquad x(t_{m+1}) = x(t_m) + \sum_{j=1}^{N} \frac{x^{(j)}(t_m)}{j!} h_m^j,$$

where $m = 0, \ldots, M-1$, $t_{m+1} = t_m + h_m$, $h_m > 0$ and $t_0 = a, t_M = b$. The number N is called the *order of the Taylor method*.

It is clear that obtaining formulas for the derivatives $x^{(j)}(t)$ is a very difficult task. Moreover, this involves cumbersome expressions so it will take a significant amount of time to evaluate them. This shortcoming is overcome by means of the so-called *automatic differentiation* methods. They allow us to evaluate the derivatives of a given function without obtaining a closed formula for them. In general, the number of arithmetic operations required to compute the derivatives up to order k using automatic differentiation is of order $\mathcal{O}(k^2)$.

For the ABC system, we rewrite the differential equation (7) as follows

$$\dot{x} = V_1 \,, \quad \dot{z} = V_2 \,, \quad \dot{p}_x = V_3 \,, \quad \dot{p}_z = V_4 \,, \tag{64}$$

where $V_1 := p_x - \sin z$, $V_2 := p_z - B\cos x$, $V_3 := B(P_1 - P_2)$, $V_4 := -P_3 + P_4$, $P_1 := P_0 \cos x$, $P_2 := V_2 \sin x$, $P_3 := P_0 \sin z$, $P_4 := V_1 \cos z$ and $P_0 := (L - B\sin x - \cos z)$. Notice that we have decomposed the vector field in a combination of elementary operations, i.e., sums, products and trigonometric functions. Then, we use the following elementary fact (see for example [26]).

Lemma A.1. *Given $a(t) = \sum_{j\geq 0} a_j t^j$ and $b(t) = \sum_{j\geq 0} b_j t^j$, we have*

- *If* $c(t) = a(t) \pm b(t)$*, then* $c_k = a_k \pm b_k$*.*
- *If* $c(t) = a(t)b(t)$*, then* $c_k = \sum_{j=0}^{k} a_{k-j} b_j$*.*
- *If* $c(t) = \cos(a(t))$ *and* $s(t) = \sin(a(t))$*, then*

$$c_k = \frac{-1}{k} \sum_{j=1}^{k} j s_{k-j} a_j \, , \qquad s_k = \frac{1}{k} \sum_{j=1}^{k} j c_{k-j} a_j \, .$$

Remark A.2. *It is possible to derive similar formulas for other functions, like quotients, inverse trigonometric functions, the exponential, the logarithm, powers of series, etc. In general, this works for any function that is known to be defined as the solution of a differential equation (e.g. Bessel functions).*

There are several possibilities to select the order N and the step size h of the Taylor method (see for example [26, 41]). In practice, it is common to choose N minimizing the global number of operations and h (which is bounded by the radius of convergence of the power series) that provides a prescribed accuracy.

Although Taylor methods are not difficult to implement, we observe that a Taylor integrator has to be specifically coded for a given vector field. As we mentioned, there are computer programs that are able to write such a specific integrator, although in our case we have written our own *ad-hoc* Taylor integrator using a C++ compiler.

Let us compare the use of Taylor methods with other classical explicit integrators of Runge-Kutta-Felhberg type. Concretely, we integrate the trajectory corresponding to $H_0 = 0.16$, $B = 0.5$, $L = 1$, $x = 1$, $z = 0$ and $p_x = 0$. The final integration time is $t = 20000$. Computations have been performed in a 3.20GHz Intel(R) Core(TM) i5 CPU. We remark that, contrary to the RK4 and RK8 codes, our Taylor programm has not been optimized so the computational cost of the Taylor integrator can still be improved.

For example, if we select a local tolerance of $\varepsilon = 10^{-12}$, it takes 4.39 seconds to integrate the previous trajectory using RK4 and the final deviation in the energy is $5 \cdot 10^{-8}$. Using RK8 we improve to 1.18 seconds and a deviation of 10^{-10}. A Taylor method of order $N = 20$ takes 0.37 seconds and the final deviation is $8 \cdot 10^{-12}$. Similarly, if we select a local tolerance of 10^{-15}, it takes 17.27 seconds with RK4 (the final deviation is $2 \cdot 10^{-11}$); 2.64 seconds with RK8 (the final deviation is $2 \cdot 10^{-14}$) and 0.53 seconds with Taylor of order $N = 20$ (the final deviation is $8 \cdot 10^{-15}$).

Finally, we remark that the Taylor method is specially suitable for high accuracy computations. Since the cost is of order $\mathcal{O}(N^2)$, it is clear that if we increase the accuracy from ε to ε^2, we can simply increase the order of the method to $2N$ so that the number of operations is increased by a factor 4. On the contrary, if we keep the order N then, in order to achieve the new accuracy, we have to take a step size close to $\varepsilon^{1/N} h$. Notice that this increases the number of operations by a factor $\varepsilon^{-1/N}$ which is dramatic. When using a numerical integrator of fixed order (e.g. Runge-Kutta) the only possibility to increase accuracy is to reduce the step size. From this point of view, fixed order methods are strongly penalized for high accuracies. In the previous trajectory, if we select a local tolerance of 10^{-31}, it takes 3765.84 seconds with RK8; 14.08 seconds with Taylor of order $N = 20$ and 7.37 seconds with Taylor of order $N = 40$.

B Symbolic manipulation of multivariate power series and automatic differentiation

For the sake of completeness, in this appendix we provide a brief introduction to the symbolic manipulation of multivariate power series in the context of this work. The main interest is to evaluate the composition of power series by means of automatic differentiation, which is used in the computation of invariant manifolds and normal forms in Section 3.2.2.

Nowadays there are several commercial computer packages that, in principle, are able to deal with the computations mentioned here, such us the well-known Maple and Mathematica. They have the advantage of being very general, but paying the prize of not being very efficient (both in time and memory) in each concrete case. Hence, in order to tackle particular problems it is convenient (sometimes it is mandatory) to build an efficient algebraic manipulator in order to handle power series in a very fast way, and using as little memory as possible. Precise ideas regarding the implementation of such manipulators are given in [21, 25].

Let us consider a (formal) power series f in the variables $x = (x_1, \ldots, x_d)$ with coefficients in certain commutative ring

$$f(x) = \sum_{k=0}^{\infty} f_k(x) = \sum_{k=0}^{\infty} \sum_{\substack{l \in \mathbb{N}_*^d \\ |l|=k}} f_{l_1,\ldots,l_d} x_1^{l_1} \cdots x_d^{l_d} \,, \tag{65}$$

where $f_k(x)$ is a homogeneous polynomial of degree k in the variables $(x_1, \ldots, x_d)$. A simple way to manipulate multivariate power series is to sort the different multi-indices of the series in reverse lexicographic order. Concretely, given a multi-index $l = (l_1, \ldots, l_d)$ of degree k, we introduce the integer number $\bar{l} = l_d l_{d-1} \cdots l_1$ and we say that $l < l'$ (the multi-indices l and l' are in reverse lexicographic order) if and only if $\bar{l} < \bar{l}'$. Then, we simply encode the coefficients of the series (65) in an array following this order. For example, if $d = 2$ we have

$$[f_{0,0}, f_{1,0}, f_{0,1}, f_{2,0}, f_{1,1}, f_{0,2}, f_{3,0}, f_{2,1}, f_{1,2}, f_{0,3}, \ldots] \,.$$

Then, all the symbolic manipulations to be performed with such power series (multiplication, differentiation, evaluation of Poisson brackets, solution of cohomological equations, etc) depend on two simple tasks:

1. Given a coefficient in the n-th position of the array of coefficients, what is the multi-index $l = (l_1, \ldots, l_d)$ that corresponds to this coefficient? This can be obtained directly from a precomputed combinatorial table `table[n][j]` that stores the index l_j.

2. Given a multi-index $l = (l_1, \ldots, l_d)$, coded by an array `*ind`, what is the position of the corresponding coefficient in the previous array?

There are several ways of implementing the previous tasks depending on whether we are interested in speed or in memory cost [21, 25]. Using the tasks described above it is straightforward to implement routines to manipulate homogeneous polynomials and extend them to manipulate power series. For example, the product of the series $f(x)$ and $g(x)$ is given by

$$p(x) = f(x)g(x) = \sum_{k=0}^{\infty} p_k(x) \,, \qquad p_k(x) = \sum_{j=0}^{k} f_j(x) g_{k-j}(x) \,. \tag{66}$$

A not so trivial operation is the composition of functions, which is described below. An useful tool to manipulate multivariate power series in this context is the so-called *radial derivative* (see [21]) which is defined as

$$Rf(x) = \nabla f(x) \cdot x = \sum_{i=1}^{d} \frac{\partial f}{\partial x_i} x_i \,.$$

Observe that R is a derivation in the algebra of differentiable functions and satisfies $Rf_k(f) = kf_k(x)$ for every homogeneous function of order k (Euler's identity). Therefore, the radial derivative of a power series (65) can be written as $Rf(x) = \sum_{k=0}^{\infty} kf_k(x)$. Finally, given a multivariate function $f(x)$ and a function $\phi(z)$ of one variable, we have that

$$R(\phi \circ f)(x) = \phi'(f(x)) Rf(x) \,.$$

If ϕ is an elementary function (see Remark A.2), this expression allows us to obtain a recurrence for the homogeneous terms g_k of the multivariate power series $\phi \circ f$. For example, given a series $f(x)$, we can compute $c(x) := \cos(f(x))$ and $s(x) := \sin(f(x))$ from the expressions $Rc(x) = -s(x)Rf(x)$ and $Rs(x) = c(x)Rf(x)$, where we used that $\cos' = -\sin$ and $\sin' = \cos$. Taking the homogeneous terms in these expressions, we obtain

$$c_k(x) = \frac{-1}{k} \sum_{j=1}^{k} j s_{k-j}(x) f_j(x) \,, \qquad s_k(x) = \frac{1}{k} \sum_{j=1}^{k} j c_{k-j}(x) a_j(x) \,, \tag{67}$$

which are equivalent to the recurrences in Lemma A.1 but involving operations with homogeneous polynomials.

Now we are able to describe the evaluation of $[F \circ \Phi_{<k}(s)]_k$ in Section 3.2.2 by means of Automatic Differentiation. As we mentioned, since we do not want to introduce explicitly the linear change of variables that diagonalizes the system, we consider instead $[C^{-1}F(C\Phi_{<k})]_k$ where C is the matrix of eigenvectors (this implies a little abuse of notation). Observe that the

vector field F associated to the ABC system demands to compose the functions $\cos(x)$, $\sin(x)$, $\cos(z)$ and $\sin(z)$ with Φ, so we require to evaluate the functions

$$\cos(\Pi_\sigma C\Phi(s)), \qquad \sin(\Pi_\sigma C\Phi(s)), \qquad \sigma = x, z, \tag{68}$$

where Π_σ is the projection of a vector function on the corresponding components. The process has several steps:

Step I. We first translate the equilibrium point to the origin (this is just a trivial modification of the vector field) and we compute the first order terms related to the problem. These are

$$\phi_{<2}(s) = s\,, \qquad \psi_{<2}(s) = 0\,, \qquad f_{<2}(s) = A_1 s\,, \qquad F_{<2}(s) = As\,.$$

From these objects, it is clear that the first order element of the parametrization is $\Phi_1(s) = (s, 0)^\top$ and the matrix of the differential $D\Phi_1(s)$ is straightforward. We initialize the functions (68) as

$$s_{\sigma,0} := \sin(\Pi_\sigma C\Phi_0(s)) = \sin(0) = 0\,, \qquad c_{\sigma,0} := \cos(\Pi_\sigma C\Phi_0(s))) = \cos(0) = 1\,,$$

for $\sigma = x, z$.

Step II. Assume that we have performed $k-1$ steps of the parametrization method, and we have to evaluate $[C^{-1}F(C\Phi_{<k}(s))]_k$. We first observe that we have already computed $[\cos(\Pi_\sigma C\Phi_{<k-1}(s))]_{k-1}$ and $[\sin(\Pi_\sigma C\Phi_{<k-1}(s))]_{k-1}$, without including the term $C\Phi_{k-1}$. Then, we first update the trigonometric functions as follows

$$[\cos(\Pi_\sigma C\Phi_{<k}(s))]_{k-1} = [\cos(\Pi_\sigma C\Phi_{<k-1}(s))]_{k-1} - s_{\sigma,0}\Pi_\sigma C\Phi_{k-1}(s)\,,$$

$$[\sin(\Pi_\sigma C\Phi_{<k}(s))]_{k-1} = [\sin(\Pi_\sigma C\Phi_{<k-1}(s))]_{k-1} + c_{\sigma,0}\Pi_\sigma C\Phi_{k-1}(s)\,,$$

for $\sigma = x, z$. Now, we can evaluate $[\cos(\Pi_\sigma C\Phi_{<k}(s))]_k$ and $[\sin(\Pi_\sigma C\Phi_{<k}(s))]_k$ using the recurrences (67). Next, we evaluate the vector field $[F(C\Phi_{<k}(s))]_k$ in a similar way using expression (66) and we obtain $[C^{-1}F(C\Phi_{<k}(s))]_k$ just multiplying the matrix C^{-1} and the vector $[F(C\Phi_{<k}(s))]_k$.

Step III. We solve the cohomological equations (24) and (25) to obtain $\phi_k(s)$ and $\psi_k(s)$. Notice that evaluating the right hand side of this expression requires $D\Phi_{<k}(s)$ and (66).

Step IV. We update the vector field $[C^{-1}F(C\Phi_{<k})]_k$ including the term $A\Phi_k(s)$ computed in Step III. Concretely we obtain

$$[C^{-1}F(C\Phi_{\leq k})]_k = [C^{-1}F(C\Phi_{<k})]_k + A\Phi_k(s)\,.$$

Step V. We compute $D\Phi_k(s)$, of degree $k-1$, by symbolic manipulation of the homogeneous terms in $\Phi_k(s)$. Then we update the matrix $D\Phi_{\leq k}(s) = D\Phi_{<k}(s) + D\Phi_k(s)$, which will be needed in the next iteration (Step III).

Step VI. We proceed inductively repeating the algorithm from Step II up to the requested order in the parametrization or normal form.

Finally, just to inform the reader, we would like to mention a very nice and straightforward application of a manipulator such as the one described above. If we implement the algebra of power series as a C++ data type, we can easily adapt the Taylor integrator described in Appendix A to run not in the field of real (or complex) numbers but in the ring of formal power series. Formally, this is equivalent to integrate simultaneously the variational equations up to order k of the vector field (see [2]).